MSc. Thesis

Joint development for a morphing wing skin

Adri Van Eemeren

Delft University of Technology

TU Delft

MSc. Thesis

Joint development for a morphing wing skin

by

Adri Van Eemeren

to obtain the degree of Master of Science
at the Delft University of Technology,
to be defended publicly on Tuesday August 24, 2021 at 14:00.

Student number: 4302494
Project duration: February, 2020 – August, 2021
Thesis committee:

Prof. C. A. Dransfeld,	TU Delft, Chair
Ir. J. Sinke,	TU Delft, Supervisor
Dr. O. K. Bergsma,	TU Delft, Examiner
Ir. H. van Goozen,	GKN Aerospace - Fokker Aerostructures B.V., Daily Supervisor

This thesis is confidential and cannot be made public until September 1, 2023.

TU Delft

Preface

This report shows my thesis for the MSc. Study Aerospace Structures and Materials at the Delft University of Technology. My thesis is part of the Morphing Tab development by GKN Aerospace - Fokker Aerostructures B.V. which is a possible Load alleviation solution as part of the MANTA - Clean Sky 2 project of the European Union. I investigated the connection of a flexible skin to a rigid structure. The research question is: What is the best method to connect a thin flexible skin element undergoing a peel-like motion to a rigid structure without disturbing the aerodynamic surface at the outside of the skin?

In my efforts to answer this question I have been supported by the Design Engineering Department of Fokker and especially by Hans van Goozen, who is my daily supervisor at Fokker. Also Wouter van der Eijk, who is the structural engineer of the department, has helped me throughout my thesis. At the TU delft, Jos Sinke, who is my thesis supervisor, guided me through the thesis in the best imaginable way. During my reporting phase I could not have wished for more help. I would like to thank Hans, Wouter and Jos for all they have contributed and for the friendly manner in which they did.

I would furthermore like to thanks everyone involved with the tests. The test set-up and samples were produced at Fokker and the tests have been performed at the DASML. The tests could not have gone as they have without the professional and patient help at both locations.

In advance I would like to address my appreciation for the committee members; Clemens Dransfeld, Jos Sinke, Otto Bergsma and Hans van Goozen, for reading and evaluating my thesis report and for giving me the opportunity to defend my thesis to them.

Finally I would like to thank my family and friends. Not only during my thesis but throughout my life and studies, I have been able to lean on their support.

Adri Van Eemeren
Delft, August 2021

Contents

List of Figures

List of Tables

List of Symbols and Abbreviations

DUT	Delft University of Technology
Fokker	GKN Aerospace - Fokker Aerostructures B.V.
MANTA	MovAbles for the Next generaTions Aircraft
ACARE	Advisory Council for Aviation Research and Innovation in Europe
PPS	Polyphenylene sulfide
MLA	Manoeuvre load alleviation
GLA	Gust load alleviation
q_m	Distributed load generated by the wing
q_c	Distributed load generated by the control surface
gal	Gallon
C-PPS	Carbon reinforces Polyphenylene sulfide
BVID	Barely Visible Impact Damage
FEM	Finite Element Method
S.C.	Stress Concentration
Log	Logarithmic regression
min	Minimum
max	Maximum
σ	Stress
y	vertical distance from neutral line
M	Moment
I	Moment of inertia
M_i	Internal moment
σ_{peak}	Peak stress
t	Skin thickness
d	Shaft diameter rivet
w	pitch distance
F_1	Out-of-plain load
$q2_{1,2,3,4,5,6}$	In-plain distributed load in skin layer 1,2,3,4,5,6
$a_{1,2,3,4,5,6}$	distance to middle of layer 1,2,3,4,5,6
F_{2_6}	In-plain load in outer skin layer (6)
σ_{s_b}	limit bearing stress of the skin material
A_{f_m}	cross-sectional surface of the fastener
F_o	Load in rivet direction
σ_{s_c}	limit compression stress of the skin material
$A_{s_{uh}}$	Surface area underneath the fastener head

τ_s	limit shear stress of the skin
$A_{s_{co}}$	skin shear surface at the edge of the fastener head
A	Edge distance
B	Pitch distance
C	Row distance
ϵ	Strain
DIC	Digital Image Correlation
SG	Strain gauge
$R_{1,2,3}$	Resistor 1,2,3
U_s	Voltage of the power source
U_m	Measured voltage
$\epsilon_{\%}$	Strain in percentage
E	Young's modulus
F	Machine force
f	Cycle count
S/N	Stress per cycle count
disp	Displacement

Abstract

Both GKN Aerospace - Fokker Aerostructures B.V. (Fokker) and Delft University of Technology (DUT) are partaking in a Clean Sky 2 program called MANTA. MANTA stands for: MovAbles in the Next generaTion Aircraft, and is a program created by the European Union in order to meet the 'ACARE Flightpath 2050 objectives' by achieving cleaner air travel. The MANTA program aims to reduce the fuel consumption by 3% to 5% using the knock on effects of smart usage of movables.

The contribution of Fokker in the MANTA program is the Morphing Tab concept. This is a newly introduced tab which will be located in the wingtip and must allow load alleviation during manoeuvres. By deflecting the tab in a smart manner, it will be able to generate an internal moment in the wing structure opposite to the internal moment generated by the lift. These internal moments counteract one another, reducing the peak stresses which can result in a lighter wing structure. This will have multiple aerodynamic beneficial knock-on effects such as the potential for a more slender wing.

The solution of Fokker to keep the drag introduced by the tab to a minimum, is to use a morphing tab rather than a conventional tab. The morphing tab has a continuous inboard skin surface which morphs in the section between the rigid winglet structure and the rigid tab. The continuous skin will add to the aerodynamic efficiency as airflow along the surface stays attached further along the wing chord and airflow leakage is largely avoided.

The morphing part of the winglet exists of multiple components. The component studied in this thesis is the flexible skin. More precisely, it is the attachment of the morphing skin to the non-morphing parts of the concept, the winglet and the tab. As the morphing skin is very thin, and the condition of use is an out-of-plain movement, a complex and rarely studied combination is formed. This has led to the following research question: *What is the best method to connect a thin flexible skin element undergoing a peel-like motion to a rigid structure without disturbing the aerodynamic surface at the outside of the skin?* Answering this question must lead to a solution for this specific situation as well as contribute to the body of knowledge to fill the current literature gap.

Based on the findings of the literature study, the analysis started with selecting a joining method. This process was performed by a trade-off in which six groups of joining methods (Integral Structure, Bonding, Welding, Mechanical Fastening, a Piano Hinge and a Flexible Hinge Element) have been compared. This resulted in the selection of Mechanical Fastening as the best joining method. Within this category, Rivets have been selected as the best suited solution for the Morphing Tab Connection.

Along with design guidelines, a comparison between the failure limits of the rivets and the loading conditions of the tab, led to the design of the riveted connection. A test had to be created in order to investigate whether the design is able to meet the requirements of the joint under the relevant loading conditions. No standardised test could be used as they did not create representative loading conditions. During the test, the stress and strain of the skin at the connection are measured via the machine output, Digital Image Correlation software and strain gauges. Additionally, video recordings are made of the test from the side in order to validate results.

Three main test conclusions can be made:

- The Aerodynamic Profile does not experience a significant effect of the Riveted connection. The required rotation angle and accuracy are achieved and the contour deformation is within the tolerance.
- The Static Failure is caused by skin bending without interference of the fasteners. The Static Failure Level is higher than the required minimum stress. Therefore, the Static Load Requirements are met.

- The rivets do not interfere on the skin behaviour during fatigue tests. The stiffness reduction due to the fatigue tests shows similar results with and without fasteners.

Overall this means that the Riveted connection meets all Aerodynamic and Structural Requirements. Besides this, no indication was apparent during the tests that another joining method would lead to better performance. Also, the riveted connection outperformed the other joining methods in the other Trade-off categories. The combination of these two facts warrant the overall conclusion of this thesis: A riveted connection is the best method to connect a thin flexible skin element undergoing a peel-like motion to a rigid structure without disturbing the aerodynamic surface at the outside of the skin. The connection design created in this thesis can be applied in further investigations in the Morphing Tab Concept.

1 Introduction

In pursuit of cleaner air travel, the European Union has created the Clean Sky 2 program. This program was created to contribute to the 'ACARE Flightpath 2050 objectives' of the European Union by funding research into different innovations, which have the potential to reduce the fuel consumption and noise of air travel [5]. MovAbles for the Next generaTion Aircraft (MANTA) is one of these projects within Clean Sky 2 and aims to reduce fuel consumption by 3% to 5% [20]. This must be realised through the development and demonstration of novel movable concepts. The fuel reduction may be realised by redesigning movables to reduce their drag or by finding a method to use them differently.

One project within MANTA is the use of a movable in the outer wing part to reduce fuel consumption [20]. GKN Aerospace - Fokker Aerostructures B.V. is developing a new control surface as part of that project. In the winglet, an aileron-like control surface must be able to create an opposite bending moment in the wing structure by generating a sideways oriented load. To limit the drag introduced by the control surface, Fokker has created a tab with a continuous morphing skin at the inboard of the winglet. The tab itself is rigid as well as the winglet, but in between these two the skin is not interrupted as it is in conventional tabs. The carbon fibre reinforced PPS skin will be morphing in this section. To allow this, the hinge behind the skin is also a morphing part. On the outboard section of the winglet, the skin is still sectioned in the conventional manner. The Morphing Winglet Tab Concept can be seen in Figure 1.1.

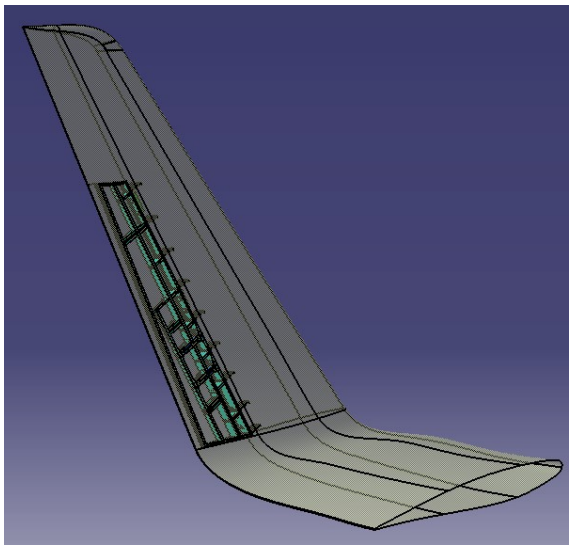

Figure 1.1: GKN Aerospace - Fokker Aerostructures B.V. Morphing Tab Concept in the winglet

In Chapter 2, the advantages of a tab will be discussed. Also, the application of the morphing

skin concept compared to a traditional tab will be shown to have a positive effect on the aerodynamic efficiency in Chapter 2. The development of this tab has been going on for multiple years now and the majority of the tab design is finalised. However, several aspects of the tab are still under development. One aspect of the design is the connection of the flexible skin to the rest of the structure. In Section 1.1 the reasons why the design of this connection is still pending, are explained.

1.1. Problem Statement

Fokker Aerostructures B.V. is very experienced in the production of wings, wing sections, aeroplane tails and control surfaces. Therefore, the design of the overall wingtip and flap is not overly new for the company. However, the load situation generated by a load alleviation system is new. To help clarify the load situation, the Delft University of Technology has been able to provide aerodynamic loads. This way, the MANTA team within Fokker has been able to design the solid parts of the winglet. The morphing parts have been lacking as they are new for Fokker.

There are two morphing components in the tab. The Flexible Skin and the Flexible Shear Element. The Flexible Shear Element is not part of this thesis. The Flexible Skin is the basis of this thesis. The skin itself is already designed, however the connection of this skin to the rest of the winglet is not. The problem is that in order to meet the requirements for morphing, the skin must be very thin and is loaded in a peel-like manner. The latter means that the skin is being bend away from the structure. The combination of the load and the small thickness is what makes it a difficult to design the joint. This will be elaborated upon in Chapter 2. In this thesis it will be investigated how to cope with the unique situation of the skin connection. The route towards such a solution starts with the research question formulated for this problem and the research objectives. The research question and objectives are given is Sections 1.1.1 and 1.1.2 respectively.

1.1.1. Research Question

For this thesis the following research question is constructed: *"What is the best method to connect a thin flexible skin element undergoing a peel-like motion to a rigid structure without disturbing the aerodynamic surface at the outside of the skin?"*

The research question is not tailored specifically to the application as it is desirable to find a solution which can be applied for the morphing tab as well as form a basis for similar applications. The research question is rather broad. In order to realise a well structured answer to the research question, four sub-questions have been constructed:

SRQ 1	*Are state-of-the-art joining methods available for peel dominated load situations?*
SRQ 2	*What makes a joint a good fit for a peel dominated load situation?*
SRQ 3	*How will the joining method be evaluated?*
SRQ 4	*Does the joining method meet all the requirements?*

1.1.2. Research Objectives

The research questions and sub-questions must be answered in order to realise the research objectives. The main research objective of this thesis is to: *"Contribute to the realisation of load alleviation by means of finding a way of connecting the morphing skin to the solid winglet structure"*. Achieving this goal and subsequently realising load alleviation would result in the potential to reduce the fuel consumption in air travel. Besides the commercial benefits of such reduction it also makes the airspace more clean. Next to realising the solution for this specific application, forming the basis for further development in similar applications is also desired. This is described in sub-objective one (SO 1). If this is successfully completed, it allows the realisation of similar designs without having to perform the same in-depth research. Other sub-objectives have been formulated as well. These are however more directed to intermediate goals which together fulfil the main objective:

SO 1	*Generate a basis of knowledge about the fastening of thin flexible skins under out-of-plain loading, upon which future research can be build.*

SO 2 *Determine the requirements which must be met in order to realise a successful design.*

SO 3 *Create a test which is able to determine the static and dynamic capabilities of morphing skin connections.*

SO 4 *Determine the static limit and the dynamic capabilities of the connection.*

1.2. Structure

The problem is described shortly and the research questions and objectives are formulated. To find a solution, a literature study has been performed and the most important findings of that study will be given in the Literature Summary [10]. This overview is presented in Chapter 2. From this literature six joining method categories have been deduced. Chapter 3 uses the knowledge from the literature to investigate three methods. By means of a Trade-off and Sensitivity Study, the best category and then the best connection is selected. Using design criteria and basic structural analysis, this connection method has been transformed in an initial design. This is discussed in Chapter 4. In order to evaluate the design, in Chapters 5 and 6, the test itself and measurement methods for the test are discussed respectively. The Test Design shows the design iterations and explains the test. The Measurements and Data Processing explains the different methods which have been applied for measuring the strain and stress in the samples and how this data is cleaned. These outcomes are discussed in Chapter 7, Results, which are then interpreted in the discussion which is Chapter 8. Subsequently, the conclusion can be found in Chapter 9 and recommendations for further investigation are given in Chapter 10. At last, the Bibliography is shown and additional information on the thesis can be found in Appendices A to C.

2

Literature Summary

In this chapter, the Literature Study that was previously performed for this thesis is summarised [10]. The summary starts with the concepts Load Alleviation and Morphing in Sections 2.1 and 2.2. Subsequently, The Morphing Winglet Tab Concept is discussed in Section 2.3 and the most important component for this thesis from the Tab, the Flexible Skin, is shown in Section 2.4. In Section 2.5, the requirements for the connection are discussed. The chapter is continued with Section 2.6 in which provides an overview of joining methods which may potentially form a solution and Analyses which must prove that in Section 2.7. Finally, the Literature Study is shortly concluded in Section 2.8.

2.1. Load Alleviation

Load alleviation is a method to cope with structural stress. Rather than designing a structure which is able to carry the ultimate load, load alleviation systems reduce the structural load by compensating it in some way. Load alleviation systems can be both passive and active. For active systems, there is Gust and Manoeuvre Load Alleviation possible. As the Morphing Tab Concept uses an active Manoeuvre Load Alleviation (MLA) system, the literature summary is limited to this method.

In an MLA system, the stress in the structure produced by a manoeuvre, is compensated by using the control surfaces. The control surfaces generate a force which compensates the internal bending moment of the wing [13]. Although the cumulative lift on the wing must be equal, the load is applied closer to the wing root which results in a lower bending moment at the root. Also, throughout the wing the bending moment is reduced. The opposite bending moment generated by the control surfaces must first be compensated before the bending moment will increase. The concept is shown in Figure 2.1. In this Figure q_m is the distributed lift load generated by the wing and q_c is the distributed load over the control surface for MLA in opposite direction to the lift. The negative lift created by the distributed load q_c control surfaces are compensated by a higher q_m.

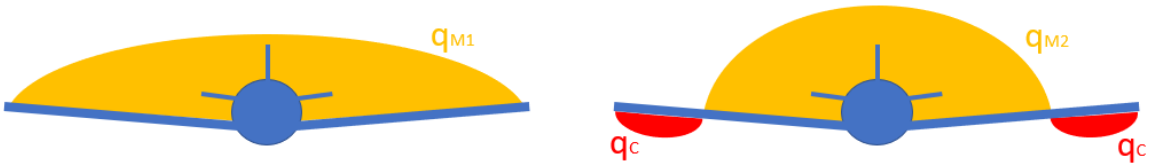

Figure 2.1: Changed lift distribution due to MLA

Systems like these have been tested and the effects are consistently positive. Wings which apply a MLA system are able to increase their wing span by 10% to 15% which results in a drag reduction of 8% to 13% compared to a wing with the same weight without a MLA system [3][17][24][38]. These statistics show the relevance of developments such as the Morphing Winglet Tab.

2.2. Morphing

In aviation at this moment, many control surfaces are used in order to adjust the wing to meet the requirements for different aspects of the flight envelope. The wing is designed for symmetric cruise flight and control surfaces such as flaps, slats and ailerons, are used for other flight conditions. These systems are not optimised, as for instance control surfaces must fit inside the wing profile during cruise flight and parasitic drag exists from gaps between the wings and the control surfaces. If a wing would be able to shift shape rather than extend some control surface, the aerodynamic profile would be closer to ideal. This shape shifting is called 'Morphing'.

Morphing as a concept has much variety. Incorporating the ailerons in the wing and adjusting the sweep angles of the wing are very different but both fall within morphing. Their effect will be very different as will be the technology required to realise these shape shifts. The effect will however be significant. Increasing the aerodynamic efficiency of an aeroplane will lead to fuel saving [28][29][32]. If the airfoil drag reduction is as little as 1% at a kerosene price of 0.70 $/gal, the US wide-body transport fleet alone would save 140 million dollar every year [2]. For medium-range transport aircraft, a fuel reduction is possible between 3% and 5% [2]. These statistics validate the impact of morphing applications, such as the Morphing Winglet Tab.

2.3. Morphing Winglet Tab Concept

GKN Aerospace - Fokker Aerostructures B.V. has created a morphing tab in the winglet which is supposed to deliver Manoeuvre Load Alleviation. This means that the concept uses the two technologies discussed in Section 2.1 and 2.2. The application of MLA and Morphing, are discussed in that order in this section.

Rather than using the already existing control surfaces for MLA, a new tab is added in the winglet. This has the potential to alleviate the bending moment in the wing structure without requiring a negative lift. As the morphing tab is located in the vertical winglet, the load generated by a tab in the winglet applies in horizontal direction. The use of this tab has been subjected to aero-elastic research [20] [18]. This research has shown that, at critical loads, the tab is able to reduce the positive and negative root bending moment by respectively 0.9% and 1.9% if the deflection angle of the tab is limited to 10^o [20] [18]. This is the limit used in the Morphing Winglet Tab. If this limit would be raised to 25^o, the positive root bending moment reduction would be maximum 2.2% and 4.8% for the negative bending direction [20] [18]. If the MLA system would use a combination of the tab and the conventional control surfaces with a tab deflection angle limit of 10^o, the maximum reduction of the positive root bending moment would be 9.5% [20] [18]. The conventional control surfaces would then also compensate the structural loads in a similar manner to the winglet tabs. The disadvantage of using these systems is that it can compromise their original function. Also using these control surfaces would lead to forces in vertical direction which might influence the intended lift. Therefore winglet tabs are more desirable. The reduction in structural loads, due to the alleviation, can have a significant influence on the aeroplane weight, which would subsequently reduce the fuel consumption.

To further reduce the fuel consumption of the aeroplane, the tab itself is designed to be as efficient as possible. A conventional control surface has a gap between the control surface and the main part of the wing. This gap is a cause for drag as it generates airflow separation and pressure leakage. Making the inboard skin of the winglet continuous would make the airflow more smooth and avoid pressure leakage. To make the skin continuous and have a control surface, the skin must be morphing. In the Winglet Tab Concept, this is the case between the two solid structures (the winglet and the tab) for 100 mm in chord direction. The tab has a length of 2220 mm which is therefore also the length of the morphing skin in spanwise direction. To accommodate the bending of this morphing skin section, also the hinge element of the tab is a morphing component. The outboard side of the winglet is still discontinuous and looks very similar to the surface of a conventional aileron. The latter two components are not further discussed in the literature as they are not relevant for the connection of the morphing skin to the solid structures. The skin is further elaborated upon in Section 2.4.

The Morphing Tab Concept is shown in Figure 2.2a. In this figure, the neutral position is shown in

the middle and the two maximum deflections are shown above and below. It can also be seen that the inboard skin is continuous and bend along with the tab deflection and that the outboard skin has a convectional design. In Figure 2.2a, also the flexible shear element is shown. Figure 2.2b indicates the location of the tab within the winglet.

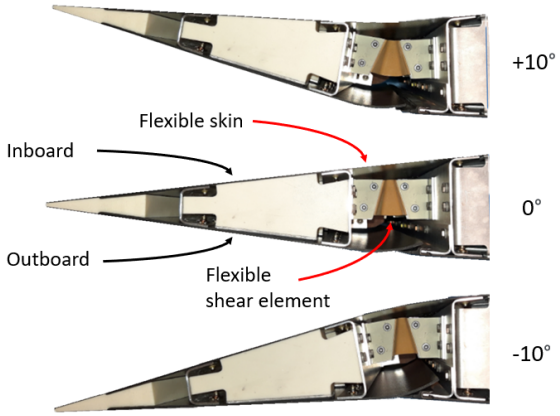

(a) Morphing Tab concept in positive, neutral and negative position [36]

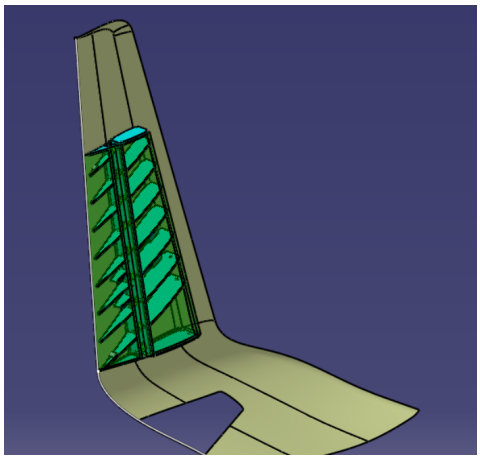

(b) Tab Location in wingtip [37]

Figure 2.2: Morphing winglet tab

2.4. Flexible Skin

The Flexible Skin is one of the two flexible elements of the Morphing Tab, as described in Section 2.3. It is the connection of this skin to the solid parts of the Winglet Tab which is the subject of this thesis. The skin is a six layer Carbon Fibre (5 Harness Satin T300JB Carbon Woven Prepreg) reinforced PPS composite [4] with lay-up: [$\pm$45,0/90,0/90,$\pm$45]. The skin lay-up is chosen because an orientation of $\pm 45^o$ in the outer layer can better handle high strains in span and chord direction than 0^o oriented skin layers. Also, the thickness which results from six layers could not be adjusted. Increasing the thickness would result in higher actuation forces and bending stresses. Decreasing the thickness would lead to lower buckling limits [22]. Some material properties of the laminate can be seen in Table 2.1

Table 2.1: Relevant material properties of the laminate [4]

Property	Laminate
Resin content per weight	43 %
Tensile Strength 0^o	752 MPa
Tensile Modulus 0^o	58.0 GPa
Tensile Strength 90^o	785 MPa
Tensile Modulus 90^o	56.0 GPa
Compression Strength 0^o	619 MPa
Compression Strength 90^o	609 MPa
In-plane Shear Strength $\pm 45^o$	130 MPa

This laminate has been tested using a four-point bending test. Both samples in pristine conditions as well as samples with Barely Visible Impact Damages (BVID) were subjected to the test. The relevant results and conclusions of this test will be discussed in this literature summary.

In order to investigate the failure of samples, the residual stiffness was calculated. If the residual stiffness dropped below 95%, the sample was considered failed. In order to investigate the failure damage propagation, B-scans were performed on the samples before, during and after the fatigue tests. The results of these tests indicated two failure modes. The first was damage propagation from the BVID. The second was matrix cracking due to bending failure. Also, the combination of these failures

occurred in some samples. Noteworthy is that damage propagation in samples under limited bending decreased. The predominant failure after this point was the bending induced matrix cracking.

The second result of the four-point bending test is the S/N-curve. This curve has been constructed for samples in pristine condition at the start of testing and samples with BVID. A distinction is made for both samples by using 90% and 95% residual stiffness as the failure level. The graph which shows the results from this study, can be seen in Figure 2.3. In this graph, the failure life is shown in number of cycles on the logarithmic x-axis. On the y-axis, the test amplitude is shown in both the deflection angle of the sample as well as the microstrain experienced during this deflection. It is unclear why the line representing the ”pristine starting condition, Failure level 95% residual stiffness” has a different slope than the others. It is recommended in the research [9] that this is investigated with more tests. If the results of the graph are interpreted for 10^o deflection angle, the skin should not fail before 1,000,000 cycles. This was the requirement.

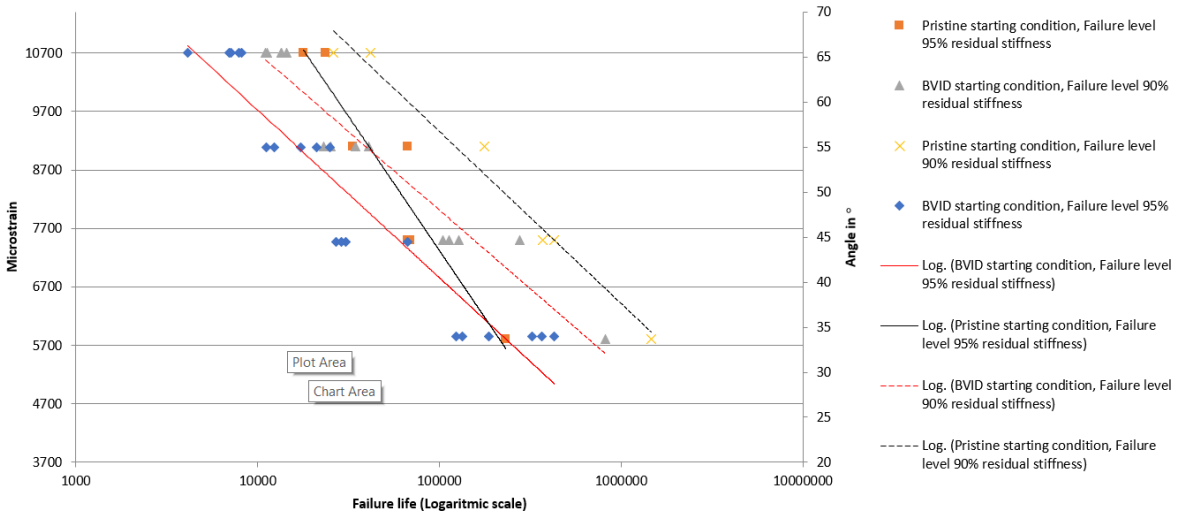

Figure 2.3: Failure life: Damaged vs. Undamaged, 95% vs. 90% residual strength [9]

The last result from the skin test is a potential fatigue limit. At high deflection angles, the skin material degraded throughout the whole fatigue test. At lower deflection angles, another effect could be seen. For samples, tested to a deflection angle of 34^o, the degradation of the material stagnated at about 90% residual stiffness. It is recommended that this is further investigated [9]. Especially for deflection angles below 34^o. This additional research has not yet been performed.

The results elaborated upon in this section, were the most important results of the skin bending tests. The test results of the connection may have to be compared with these results in order to analyse the effect of the fasteners on the skin. The next sections of the literature summary will take a look into the analysis of the connection. This starts with the Requirements in Section 2.5.

2.5. Requirements

The Requirements can be divided in three main categories: the Aerodynamic Profile Requirements, the Static Strength and Stiffness Requirements, and the Dynamic Requirements. The requirements in these categories are formulated as measurements of skin behaviour. This is because the purpose of the connection is to fixate the skin when it is morphing. Therefore, an overarching requirement could be formulated: the connection may not compromise the functionality of the skin. If the skin performs equally well when it is joint to the structure, the joining method does not interfere. The three categories or relevant requirements are discussed briefly in order to compare the skin behaviour when joint to the skin behaviour without connection.

2.5.1. Aerodynamic Profile Requirements

The Aerodynamic Profile Requirements are a set of specifications for the skin deformation and the tolerances to this deformation. This is summarised in Table 2.2 which is supported by Figure 2.4.

Aerodynamic profile requirements
Point A must be able to rotate between +10^o and -10^o
Point A must have a rotational accuracy of 0.5^o
Uniform bending (constant radius) between point O and A
The contour has a tolerance of 1 mm

Table 2.2: Aerodynamic profile requirements [35]

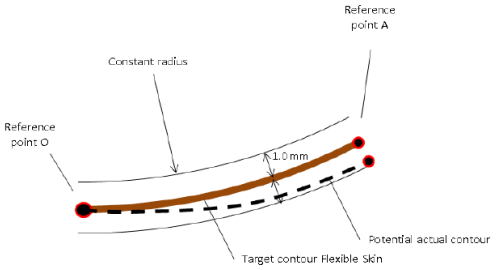

Figure 2.4: A table beside a figure[35]

2.5.2. Static Strength and Stiffness Requirements

For the Static Strength and stiffness Requirements, three load conditions have been indicated. For each of these load conditions, a combination of allowed damage and deformation is given. The three load conditions can be seen in Table 2.3. Table 2.4 will show the damage and deformation for each of these levels.

Table 2.3: Static load conditions [35]

Deflection angles	+10^0 to -10^0		0^0	
Static load	In-plane [N]	Shear [N]	In-plane [N]	Shear [N]
Nominal load conditions	± 1267	± 10	± 1267	± 15
Limit load condition	± 2533	± 10	± 2533	± 15
Ultimate load condition	± 3800	± 10	± 3800	± 15

Table 2.4: Static Strength and Stiffness requirements in the form of damage and deformation [35]

Static load	Allowed damage	Deformation
Nominal load conditions	No damage may occur	Contour limit of 1 mm
Limit load condition	Damage may occur but the tab must remain functional	No more contour limit
Ultimate load condition	Local damage may occur, tab may not separate form winglet	No more contour limit

2.5.3. Dynamic Strength and Stiffness Requirements

The morphing tab is used to alleviate the loads during manoeuvres. An assessment of the manoeuvres over the lifetime of the aeroplane, has resulted in the fatigue load spectrum [35]. This is based on the design life goal of 120,000 flight hours and the usage of the tab in a manoeuvre load alleviation system. The fatigue load spectrum indicates different fatigue life values for different conditions which is rather complex and may require a lot of tests. During the skin test, this was simplified and the goal was to reach a million cycles with a 10^o deflection up and down in order to safely test the entire spectrum at once [9]. This conservative method will be kept as simplification.

Additionally, the control speed is also discussed in the requirements. The tab must be able to rotate from the 0^o setting to the 10^o setting in both directions within 0.5 seconds [35].

2.5.4. Design Criteria

Next to all requirements mentioned in this section, there are design considerations. Some examples are the surface smoothness of the skin, the maintainability and the costs of the morphing tab. A reduced performance in these design considerations can however be acceptable if the benefits of the morphing tab are considerable. These design considerations are taken into account in the trade-off in Chapter 3. Not meeting the requirements is not acceptable as that would compromise the functionality and safety of the Morphing Tab Concept.

2.6. Joining Methods

The joining methods which are taken into account for the selection process are discussed in this section. The joining methods found in the Literature Study are divided in two groups. The first group that is investigated are the joining methods which are common in aerospace engineering. The second group are all other connections. These other connections, may be the less common connections within aerospace engineering or are connections which are used in other fields of engineering.

The connections must allow the aerodynamic surface to be smooth, which means that they cannot protrude outside the surface area on both sides and cannot counteract uniform bending of the skin. They must also be able to handle the load combination discussed in Section 2.5. During this phase of the analysis, the magnitude of those values is not considered yet, only that the connection must be able to handle both in-plane and out-of-plane loads.

These considerations have lead to many possible solutions among the common aerospace engineering connections. These solutions could be grouped in four categories: Mechanical fastening, Bonding, Welding and Integrated Assembly. These methods are schematically represented in Figures 2.5d, 2.5b, 2.5c and 2.5a respectively. Mechanical fastening are methods such as rivets and bolts in which the presence of a mechanical part obstructs the movement of the parts with respect to each other. Bonding is a method which uses an adhesive to hold two surface areas together. Many different types of adhesives can be used. The Welding category is relatively new for composites. The category exists of different methods which would melt the matrices of two thermoplastic composites in order to fuse them. Integrated assembly is not so much a joining method as it is a production method. In this method, the parts are produced as one big part rather than separately produced parts which are then connected. It is incorporated as a joining method as it would dissolve the need for a joining method.

During the investigation outside the field of aerospace engineering connections, the focus was placed on connections which would allow rotation to some extend while still fixing the skin to the structure. This has resulted in two methods. The first is a piano hinge which would run along the edges of the flexible skin. The core of this hinge does prevent displacement of the skin while allowing rotation and is shown schematically in Figure 2.5e. The second method is to incorporate a morphing element at the same location as the piano hinge would be located. The morphing element has been inspired on the Flexible Shear Element shown in Section 2.3. An element such as the Flexible Shear Element would allow an angular displacement. This displacement is limited and in other directions displacement is restrained completely. The Flexible element is represented in a schematic manner in Figure 2.5f.

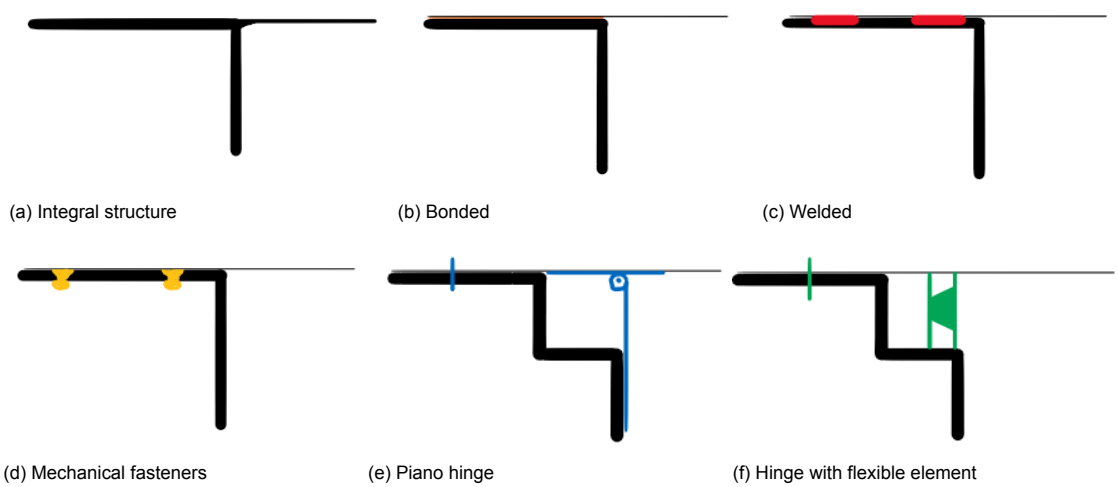

(a) Integral structure (b) Bonded (c) Welded

(d) Mechanical fasteners (e) Piano hinge (f) Hinge with flexible element

Figure 2.5: Joining methods investigated in the trade-off

These six options are only the top level Joining Methods. When a joining method is chosen, the precise connection within this category must be selected. To get a better understanding of these joining

methods, in Sections 2.6.1 to 2.6.6 they are discussed in more detail.

2.6.1. Integral Structure

The Integral Structure is not really a joining method but is incorporated in the six categories of joints as this would make a joining method obsolete. The flexible skin would be produced along with the structure and/or non-flexible skin [12][23][26]. This would mean that the skin and the component, with which it is simultaneously produced, must be made of the same material and have the same production method.

There are some issues with this method in general. First, requiring the same material is not desirable. Although it is probably feasible, because the other components are not morphing and are therefore less challenging. The second issue however, is more severe as the production in general is questionable. For instance, the rigid and flexible components will be made from a different amount of skin layers but the flexible part of the skin is to small for gradual layer drop-off. Lastly, having one large component in itself might be difficult. The reason for this, is that producing multiple components as one means that the component is much more complex. This is not desirable as it is a fairly new application. It would also complicate accessibility and replaceability.

The advantage of this method is that the component can be seen as one. Stress concentrations, additional to the ones generated by the shape, are absent. In addition, no extra material is present, resulting in no additional weight and material costs. Also aerodynamically, the 'connection' would not interfere with the flexible skin, unless ply drop-off would create local stiffness differences in the flexible skin.

2.6.2. Bonded Connection

The Bonded connection category can be divided in two groups: adhesive bonding and solvent bonding. The most common of these two methods is the adhesive bonding [30]. In this method, two adherents can be connected via an adhesive. No requirements for the adherent material come with this method as many structural adhesives have been developed which can connect a wide variety of materials. For solvent bonding, the materials are not connected via an adhesive. The connection is made by softening the thermoplastic matrix material of the composite using a solvent. By compressing the softened components together, and giving the material the time to solidify again, the joint is created. This however requires the matrix material of the two parts to be the same thermoplastic.

When adhesive bonding would be the selected joining method, a choice must be made for the bonding type. Adhesive bonding would have the advantage of being a very mature technology. The adhesive might on the other hand be an origin of stress concentrations. This can be caused by the potentially different stiffness and because the adhesive only connects the contact surfaces of the adhesives. Solvent bonding creates a connection which exists of one material and the matrix material of both adherents becomes one. This method is much less mature.

2.6.3. Welded Connection

Thermoplastic welding is one of the greatest advantages of high performing thermoplastics. The reshaping possibilities of thermoplastics allow the material between two surfaces to be heated and subsequently merged as if they are one. For carbon reinforced materials with thermoplastic matrix material, this means that two composites can be made into one. However, as no fibres transfer from one part to the other part, the connection does not yield to the same strength compared to the original parts. Still the matrix material is merged as if the parts are one, which is the best result for a joint regarding its strength.

A requirement of this method is that the matrix material of both welded components is of the same material. This requires the structure to be of the same thermoplastic material as the skin. If this method would be selected, a selection must be made from several thermoplastic welding methods. The selection between these methods can be based on criteria such as one-sided access and whether or not the method requires physical contact. A few examples of thermoplastic welding techniques are: ultrasonic welding, friction welding, vibration welding, hot plate welding, resistance welding and induction welding [31].

2.6.4. Mechanical Fasteners

Mechanical fastening is a very elaborate group as it exists of a high variety of methods. A few examples are: bolts, nails, spring clips and rivets [30]. Some of these components are permanent and others can be removed. The principle behind mechanical fastening is that a mechanical object links two parts together. By then tightening that mechanical object, the two parts cannot be separated without damaging one of the components. The type of mechanical object and the method of tightening that part, is the main difference between the different mechanical fasteners. For instance, a rivet is deformed in order to tighten, whereas for bolts a second part is clamped against the tread of the bold by means of turning until the friction prevents the bolt from loosening.

2.6.5. Piano Hinge

The Piano Hinge is a method which is not commonly used in aerospace engineering. At least not as a structural aeroplane element. It is for instance used in the hinges of solar panels of satellites [16]. The principle behind a piano hinge is much similar to the hinges of a common indoor door. The core connects the two hinge plates to prevent the plates from separating but allows rotation. The hing must be located at the original corner of the spar. Therefore, the spar must be slightly altered. Also, the skin must still be connected to the hinge and to the spar in a second spot but the loading situation at that point does not contain peel anymore.

2.6.6. Flexible Element Hinge

The second alternative connection uses a flexible element much like the Flexible Shear Element of the Morphing tab. This can be seen in Figure 2.6. At the wide end of the flexible element the stiffness is lower than on the narrow end. This way the displacement and rotation are controlled. As for the Piano Hinge, this also comes with an additional challenge for the spar and for the other connections.

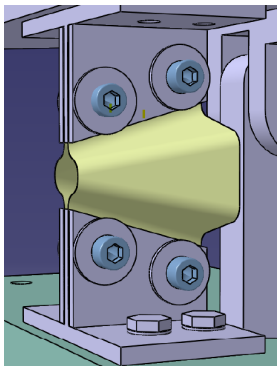

Figure 2.6: Flexible Shear element [7]

If this method would be selected, the optimisation of this flexible element might warrant a research of itself. It is very complex to allow the right amount of lateral and angular strain in the element and still make sure that the element is sufficiently strong and able to carry the loads. This is proven by the research in the Flexible Shear Element [7].

2.7. Analysis methods

As the potential joining methods are now discussed, the analysis to determine which is more suited can start. Several analyses are required in the process of determining an answer to the research question. This starts with the selection of a joining method. Subsequently, an initial design must be created on the basis of an optimisation analysis. Eventually, this design is tested and the results must be validated and verified.

For the joining method selection, the common approach is to perform a weighted trade-off [6][11][25]. In this analysis, first relevant criteria are selected and their relative importance to the solution is graded. The second step of the analysis is to review every researched element on each criterion on the basis of elementary research and literature. This judgement is not performed with respect to one another

but rather by predetermined guidelines. If this is done for every criterion and all criteria have a weight assigned to them, a multiplication of these values indicate the absolute value of every element of research. If these absolute values are summed per researched joining method, the connection with the highest overall value is assumed to be the best initial design. This analysis is executed in Chapter 3.

For the optimisation of the initial design, several methods can be applied. However, methods such as Finite Element Method (FEM) analysis, require more work than simple structural analysis and design guidelines. The latter two therefore allow design iteration better. Also, they generate more of an understanding than the 'black-box' which a FEM analysis is. The basic structural analysis starts with the static analysis. For the static analysis [8][22], the structural integrity can be calculated by means of stress and strain values in certain loading cases. Ensuring that the peak stresses and strains do not exceed the failure levels, is the basis of this analysis. When this basis is generated dynamic, analysis can be added. The dynamic analysis [27], introduces the effects of inertia and fatigue. This makes precise calculations much harder. It is important to be conservative enough, especially since the out-of-plane loading on thin composites is a topic with little tailored literature. To support the design based on the basic structural analysis, design guidelines are used [1]. These design guidelines are a set of suggestions which are based on a wide array of analyses and tests in previous projects. The implementation of these analyses are shown in Chapter 4.

For the testing, validation and verification, multiple standardised tests have been investigated. These tests however did not represent the loading situation sufficiently. Therefore, a new test is created for both the static and dynamic tests. These have been described in Chapter 5. The measurements in these tests as well as the verification and validation have been described in Chapter 6.

2.8. Literature Conclusion

The first part of the literature has created an understanding of the importance of the Morphing Tab Concept. It also provided some insight in the operational use of such a system. Subsequently, the tab itself is shown and the skin is discussed. This shows to what knowledge this thesis should contribute. The last four sections of this chapter formed the basis of the analyses in the remaining part of this thesis. This starts with the selection of the Joining Method in Chapter 3.

3

Joining Method Selection

In this chapter, the joining method which will be designed and analysed as a component for the Winglet Tab is selected. This selection will be performed based on the joining methods shown in Section 2.6. First, the Trade-off weight factors and scoring guide are explained. Then, the Trade-off itself is shown. To finalise this chapter, one joining method will be selected from the category which performed best in the Trade-off.

3.1. Trade-off Weight Factors and Scoring Guide

The Trade-off will be performed using 17 criteria which have been divided in seven main categories. To assign a weight factor to every criterion, these categories are first weighted. This is based on their relative importance. At category level, this process is re-iterated. This method is used because this avoids that a category with lesser importance but with multiple criteria becomes disproportionately important.

From the seven categories, three directly influence the functionality of the tab. These categories are the Aerodynamics, Static Strength and Dynamic Strength. If performance is lacking in any of these three categories, the joining method should not be selected. As these variables are critical, they have been assigned the highest score. As the scoring system runs from 1 to 5, they have been assigned the highest weight factor of 5. Next, three categories have been assigned a weight factor of 3; Mass, Manufacturing and Maintenance. These categories have been assigned a lower weight factor than the first category because they do not directly influence the functionality of the concept. They do have an effect on the ease of use and efficiency. The last category is Cost and is assigned the value 1. Money is important as it drives business and therefore Cost should always be taken into consideration. But it has been given a low weight factor as it is not very important in a research and development project. An additional argument to assign a low weight factor to Cost is that technology might become less expensive overtime. Also, a significant improvement in fuel consumption would warrant a more expensive solution. Therefore, Cost is taken into consideration but is assigned with a low weight factor. The reasons behind the division within each category are shown below, including the scoring guide. The scoring guide indicates per criterion how points must be attributed.

Aerodynamics

The category Aerodynamics is divided in two criteria, connection and shape of the skin. The weight division slightly favoured the shape of the skin as the induced drag due to premature airflow separation is rather big. Disturbing the airflow with small inconsistencies due to the presence of a connection, is estimated to have a smaller effect than the effect of a disturbed shape.

Static Strength

In this category, the ultimate strength has been assigned a higher weight factor than the morphability. This is because meeting the ultimate strength requirements are an absolute must. The weight difference between the two criteria is however only one as the morphability is also very important. The morphability

Table 3.1: Weight factors and scoring for the Aerodynamic category

Criterion	Weight	Score	Reason
Connection	2	5	No interruption in surface
		4	Interruption in surface, completely flush
		3	Interruption in surface, indent of < 0.5 mm
		2	Interruption of surface, step of < 0,5 mm
		1	Worse scenarios
Shape of skin	3	5	No effect of skin form
		4	Local stiffening, effects barely observable
		3	Local flattening, no overall shape change
		2	Overall effect, within requirements
		1	Worse scenarios

is an indication of the required load for the skin to be deformed. Important is that the skin is still able to resist against deformation due to the aerodynamic loads.

Table 3.2: Weight factors and scoring for the Static Strength category

Criterion	Weight	Score	Reason
Ultimate strength	3	5	No stress concentrations, connection and material properties equal
		4	S.C., connection able to carry loads both in-plain and out-of-plain
		3	S.C., connection primarily able to carry load either in-plain or out-of plain
		3	S.C., connection only able to carry load either in-plain or out-of plain
		1	Worse scenarios
Morphability	2	5	No change to stiffness
		4	Stiffer, within properties (more actuation force)
		3	Less stiff, within properties (less resistant against aerodynamic forces)
		2	Stiffness change, close to property margin
		1	Worse scenarios

Dynamic Strength
For the dynamic strength, different fatigue performances are evaluated. The division of the dynamic strength weight factor is based on the resistance of a connection for different expected fatigue regimes. A low amplitude combined with a high frequency is mainly to be expected in the case of Gust Load Alleviation (GLA) [13]. A high amplitude combined with a low frequency is more likely a consequence of Manoeuvre Load Alleviation (MLA) [13]. Achieving MLA is the overarching project goal, whereas GLA is only a long term desire.

Mass
In the aerospace industry, mass is always an important factor as weight introduces a snowball effect. However, it is relatively unimportant where the mass is added within this tab. This is because wing bending moment is unaffected by a different location of weight addition within the winglet. As the winglet is vertical, the location on the wingspan is the same. Therefore, the weight factor has been evenly divided among the connection and the structure.

Manufacturability
Being unable to manufacture a certain connection would make the selection of that joining method useless. This is true for both the test as well as for the operational use. However, producing a single

Table 3.3: Weight factors and scoring for the Dynamic Strength category

Criterion	Weight	Score	Reason
Low amplitude, high frequency	1	5	No Stress Concentrations.
		4	S.C., no apparent problems with fatigue at high frequency.
		3	S.C., not generally selected for fatigue at high frequency.
		2	S.C., Apparent problems with fatigue at high frequency.
		1	Worse scenarios
High amplitude, low frequency	2	5	No Stress Concentrations.
		4	S.C., no apparent problems with fatigue at high amplitudes.
		3	S.C., not generally selected for fatigue at high amplitudes.
		2	S.C., Apparent problems with fatigue at high amplitudes.
		1	Worse scenarios
Combined fatigue regime	2	5	Both 5, no specific reasons for problems with combined fatigue
		4	Both min. 4, no specific reasons for problems with combined fatigue
		3	Both min. 3, no specific reasons for problems with combined fatigue
		2	Specific problems with combined loading
		1	Worse scenarios

Table 3.4: Weight factors and scoring for the Mass category

Criterion	Weight	Score	Reason
Connection	1.5	5	No added mass in the connection
		4	Connection mass < 10% of flexible skin mass
		3	Connection mass < 40% of flexible skin mass
		2	Connection mass < 70% of flexible skin mass
		1	Worse scenarios
Structure	1.5	5	No mass introduction in structure
		4	Increase in material mass
		3	Structure redesign, heavier
		2	Material change and structure redesign, heavier
		1	Worse scenarios

test sample which is difficult to produce is less of a problem than producing that same sample in high volume. Being able to find a solution which can be up-scaled is therefore the focus. Operation has therefore been attributed a higher weight factor than manufacturability for the test. There is no clear distinction in importance between the Connection and the Structure. Therefore, the weight for these criteria have been divided evenly.

Maintainability
The reasoning within maintenance is the same as the one for manufacturing. However, the maintenance of the test criterion is not subdivided. No subdivision is made because no real maintenance is needed for the test in the same way as it would be when the tab is in use.

Cost
Only the material costs are investigated for costs. This is done to ensure the mutual exclusiveness of the Trade-off criteria. Manufacturing costs of a difficult to manufacture product would otherwise score low in both cost and manufacturing criteria. Material costs are not directly or indirectly included in another criterion.

3.2. Trade-off Table

The Trade-off is performed using the criteria, weight factors and scoring guides discussed in Section 3.1 on the joining methods shown in Section 2.6. The Trade-off is shown in Table 3.8. The motivations

Table 3.5: Weight factors and scoring for the Manufacturability category

Criterion	Weight	Score	Reason
Test	1		
Connection	0.5	5	Easy manufacturable for small numbers
		4	Manufacturable for small numbers
		3	Already difficult, even for small numbers
		2	Production of a single part barely possible
		1	Worse scenarios
Structure	0.5	5	Easy manufacturable for small numbers
		4	Manufacturable for small numbers
		3	Already difficult, even for small numbers
		2	Production of a single part barely possible
		1	Worse scenarios
Operation	2		
Connection	1	5	Easy manufacturable for large numbers
		4	Manufacturable for large numbers
		3	Labour intensive production, doable for large numbers
		2	Too complex for large numbers, possible improvement by manufacturing engineering
		1	Worse scenarios
Structure	1	5	Easy manufacturable for large numbers
		4	Manufacturable for large numbers
		3	Labour intensive production, doable for large numbers
		2	Too complex for large numbers, possible improvement by manufacturing engineering
		1	Worse scenarios

for assigning certain scores per joining method for each criterion can be seen in Appendix A.

The joining method with the highest accumulated score of all weighted criteria is the Mechanical Fastener. It can however also be seen that the Welded structure is ranked as a second choice with a margin of only four points on a total of 125. Therefore, the sensitivity of the selection is discussed in Section 3.3.

3.3. Sensitivity Study

The sensitivity study must investigate how solid the selection of Mechanical Fastening is. The margin between Mechanical Fastening and Welding is only 4 points. A deduction of 5 points for the Mechanical Fasteners or a gain of 5 points for Welding would be sufficient to change the outcome of the selection. This is very sensitive as this is only 4% of the total score of 125. Also, individual criterion weight factors of two and three are used 6 times in total. If the scores of two criteria deviate as little as one point, the weighted difference would be five and the selection could change.

The second aspect of the sensitivity study is to check how solid the scores are. If the scores are all determined objectively, the selection may still be relatively solid. However, when the reasons for the scores are investigated in the scoring guides, it must be concluded that this is not the case. Especially the Reasons given at scores for Static and Dynamic Strength are open to interpretation and lack reference values. These reference values would allow a quantified selection of a score. This is however not applied in the Trade-off as no suitable method for quantification was found. Therefore, the scores are selected based on literature study. This is open for interpretation and scores could therefore deviate. A reasonable assumption is that there might be one point margin on the current scores for the Static and Dynamic Strength criteria and potentially in some other categories as well. The overall scores could

Table 3.6: Weight factors and scoring for the Maintainability category

Criterion	Weight	Score	Reason
Test	1	5	No maintenance required, does not obstruct access to parts behind the skin for maintenance
		4	Maintenance required, does not obstruct access to parts behind the skin for maintenance
		3	No maintenance required, does obstruct access to parts behind the skin for maintenance
		2	Maintenance required, does obstruct access to parts behind the skin for maintenance
		1	Worse scenarios
Operation	2		
Accessibility	1	5	No maintenance required, does not obstruct access to parts behind the skin for maintenance
		4	Maintenance required, does not obstruct access to parts behind the skin for maintenance
		3	No maintenance required, does obstruct access to parts behind the skin for maintenance
		2	Maintenance required, does obstruct access to parts behind the skin for maintenance
		1	Worse scenarios
Replaceability	1	5	Easily replaceable
		4	Difficult to replace, no effect on other parts
		3	Effect on other parts limited
		2	Effect on other parts extensive
		1	Worse scenarios

Table 3.7: Weight factors and scoring for the Cost category

Criterion	Weight	Score	Reason
Material cost	1	5	No additional material cost for the connection
		4	Insignificant additional material cost for the connection
		3	Additional material cost for the connection is significant
		2	Expensive material required to make the joining method feasible
		1	Worse scenarios

reasonably not deviate more than 10 points. Integral Structure, Bonded, Welded and Mechanical Fastened would fall within that margin. However the most likely candidates are Welded and Mechanical Fastened joints.

Testing all four or even two joining methods would become very complex and demands more resources, such as test time. This is beyond the scope of this thesis. Therefore, still one method is selected to be used in the continuation of the thesis. Besides the overall score, the category scores can be observed in the Trade-off Table 3.8. It can be seen that a mechanical fastened joint does not perform best in the three main categories (Aerodynamics, Static Strength and Dynamic Strength) but does not score bad on any category. All other joining methods score low in at least one category. If a joining method is selected with a low scoring category, a solution must be found for that problem. This also requires research. As there is no good reason to change to another joining method and Mechanical Fasteners do not have a low scoring category, the selection is not changed. The other methods may be a subject of further investigation. However, if the Mechanical Fastened joining method proves to perform very well in the categories Aerodynamics, Static Strength and Dynamic Strength during the tests in this thesis, they show that the Trade-off did not overestimate the joining method. Then, there would not be a good reason to doubt the Mechanical Fasteners.

3.4. Select Mechanical Fastener Type

As result of the Trade-off the mechanical fastener is chosen to be the joining method used in this research. There are different types of mechanical fasteners such as bolts, rivets , high-locks, etc. To be able to move to the design stage, the type of mechanical fastener must be determined. To select what type of mechanical fastener should be used no elaborate analysis is required, as the effect will be minimal as long as the selected method is able to meet all the requirements which have led to the Trade-off scores. Some of these requirements are:

- Flush with the aerodynamic surface.
- Sufficiently strong for the application.
- Installed with one-sided access from the aerodynamic surface.
- Aerospace proven and off-the-shelf available.
- Sufficiently wide at the top against pull-out

Rivets are one of the most commonly used mechanical fasteners in aerospace engineering. They are very versatile and meet the requirements for the mechanical fasteners. Also, at the production facilities of GKN Aerospace - Fokker Aerostructures B.V. Papendrecht, they are very familiar with rivets. This has led to the selection of Rivets as Mechanical Fasteners for the joint. In Chapter 4, design guidelines and basic structural analysis are used to determine the rivet model and specifications and the initial joint design.

Table 3.8: Trade-off for the joining method selection.

Criteria	Weight factor	Integral structure		Bonded		Welded		Mechanically fastened		Piano hinge		Flexible element	
		Score	Reason	Score	Reason	Score	Reason	Score	Reason	Score	Reason	Score	Reason
Aerodynamics	5												
Connection	2	5	I-A-1	4	B-A-1	4	W-A-1	4	R-A-1	4	P-A-1	4	F-A-1
Shape of skin	3	5	I-A-2	5	B-A-2	5	W-A-2	5	R-A-2	4	P-A-2	4	F-A-2
Static strength	5												
Ultimate strength	3	5	I-S-1	3	B-S-1	5	W-S-1	4	R-S-1	4	P-S-1	3	F-S-1
Morphability	2	5	I-S-2	5	B-S-2	5	W-S-2	5	R-S-2	4	P-S-2	4	F-S-2
Dynamic strength	5												
Low A, High f	1	5	I-D-1	4	B-D-1	5	W-D-1	4	R-D-1	4	P-D-1	4	F-D-1
High A, Low f	2	5	I-D-2	4	B-D-2	5	W-D-2	4	R-D-2	4	P-D-2	3	F-D-2
Combination	2	5	I-D-3	4	B-S-3	5	W-D-3	4	R-D-3	4	P-D-3	3	F-D-3
Mass	3												
Connection	1.5	5	I-W-1	4	B-W-1	5	W-W-1	4	R-W-1	3	P-W-1	2	F-W-1
Structure	1.5	4	I-W-2	5	B-W-2	4	W-W-2	5	R-W-2	3	P-W-2	3	F-W-2
Manufacturability	3												
Test	1												
Connection	0.5	3	I-Mn-1.1	5	B-Mn-1.1	4	W-Mn-1.1	5	R-Mn-1.1	4	P-Mn-1.1	2	F-Mn-1.1
Structure	0.5	3	I-Mn-1.2	5	B-Mn-1.2	4	W-Mn-1.2	5	R-Mn-1.2	4	P-Mn-1.2	4	F-Mn-1.2
Operation	2												
Connection	1	2	I-Mn-2.1	5	B-Mn-2.1	4	W-Mn-2.1	5	R-Mn-2.1	3	P-Mn-2.1	2	F-Mn-2.1
Structure	1	2	I-Mn-2.2	5	B-Mn-2.2	3	W-Mn-2.2	5	R-Mn-2.1	4	P-Mn-2.2	4	F-Mn-2.2
Maintainability	3												
Test	1	3	I-Mi-1	4	B-Mi-1	4	W-A-1	5	R-Mi-1	4	P-Mi-1	3	F-Mi-1
Operation	2												
Accessibility	1	1	I-Mi-2.1	2	B-Mi-2.1	2	W-A-2	5	R-Mi-2.1	4	P-Mi-2.1	2	F-Mi-2.1
Replaceability	1	1	I-Mi-2.2	2	B-Mi-2.2	2	W-A-2	5	R-Mi-2.1	4	P-Mi-2.2	3	F-Mi-2.2
Cost	1												
Material cost	1	3	I-C-1	4	B-C-1	3	W-C-1	4	R-C-1	3	P-C-1	3	F-C-1
Weighted score	Max. total:125	103.5		102.5		108.5		112.5		95		80.5	

4

Riveted Joint

As the outcome of the joining method selection in Chapter 3 was that a riveted joint is the best method of forming the connection between the skin and the structure. The riveted connection is further analysed. In this chapter, the basic rivet design is performed to select the type of rivet. These rivets are subsequently structurally analysed for the heaviest loaded part of the tab. Finally, using this structural analysis, it is shown in this chapter what a riveted connection would look like.

4.1. Basic Rivet Design

To select the type and size of the rivet which is best suited to start the structural analysis with, the first section of this chapter addresses some basic design guidelines for riveted connections.

4.1.1. Countersunk Angle

For carbon fibre reinforced composites, the design guidelines stipulate that a countersunk angle (Fig. 4.1) of 100^o is standard practice. However, increasing the countersunk angle is a method of creating more material underneath the fastener head. This increases the failure limits of failure methods which depend on the material under the fastener head, such as pull-out. This is especially useful for thin skins such as the ones used in this application. Therefore, the rivets used have a countersink head of 130°.

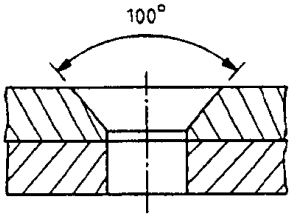

Figure 4.1: Countersunk angle [34]

4.1.2. Countersunk Depth Limit

For structural components in fibre reinforces composites with a countersunk fastener, there is a design guideline for the amount of material underneath the countersink head. This requirement stems from the ability of the material to avoid fastener pull-out. As can be seen in Figure 4.2, the requirement is to have at least a third of the thickness of the material with a minimum of 0.4 mm, as residual material underneath the countersunk. In case of the skin used for the morphing tab, the skin thickness is 1.86 mm. This means that the countersunk can only be 1.24 mm deep as this is two thirds of the thickness. This design guideline excludes fasteners with deeper countersink heads.

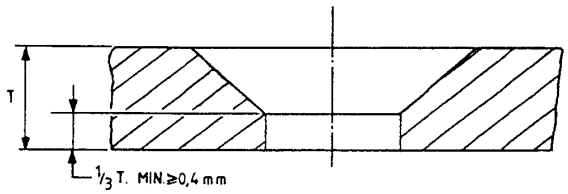

Figure 4.2: Countersunk rivet depth limit [34]

4.1.3. Fastener length

When the length of a fastener is determined, the grip length, shown in Figure 4.3, is the main driver. The grip length is the combination of the material thickness of the joined parts. For the morphing skin, this would be the flexible skin and the structure to which it is attached. A rivet must thus be selected such that a grip length is available which can contain the skin and the structure thickness.

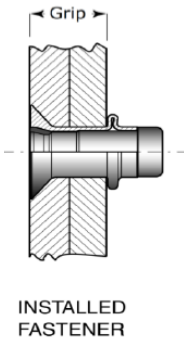

Figure 4.3: Grip length [14]

4.1.4. Selected Rivets for Structural Analysis

The available options for rivets which match these requirements at the manufacturing location within Fokker Aerostructures B.V. are EN6122-rivets which are shown in Figure 4.4.

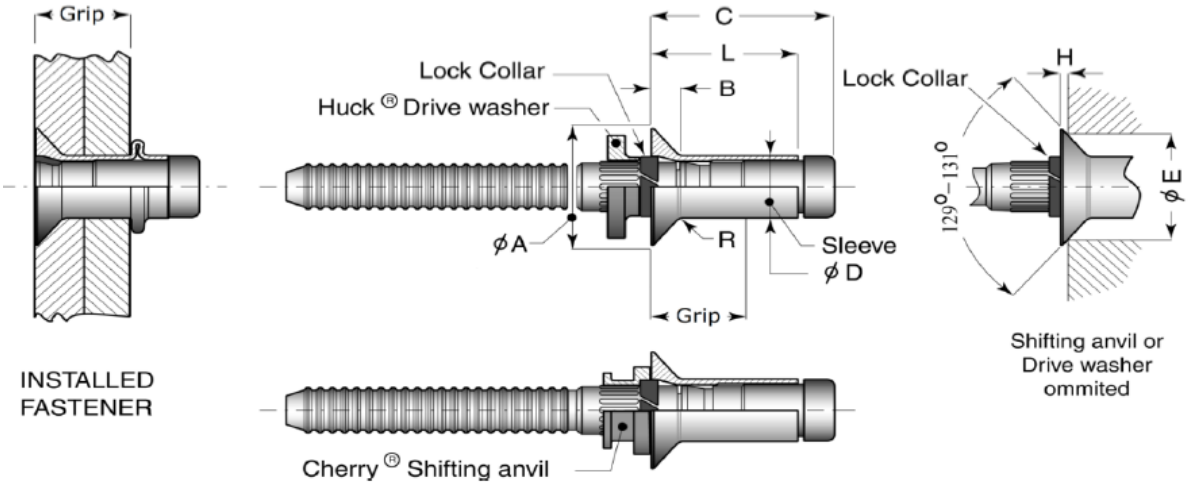

Figure 4.4: The selected rivet: EN6122 [14]

Three sizes are considered for the EN6122-rivet. These are shown in Table 4.1. The sizing is performed in Section 4.2.

Table 4.1: Specifications of three sizes of EN6122-rivets [1]

Rivet type	Material -	⌀A mm	⌀ D mm	B mm	Min. grip mm	Max. grip mm	Angle °
EN6122C05	Cres	4.14	7.52	0.99	3.71	24.36	129-131
EN6122C06	Cres	5.03	8.81	1.09	3.56	30.56	129-131
EN6122C07	Cres	5.74	9.47	1.09	3.56	30.56	129-131

4.2. Structural Analysis

In this section of the rivet design, an analysis will be performed which must indicate the sizing of the fasteners and the connection in general. The main requirement of the connection is that it may not be the critical structural element. Therefore, the connection must be at least as strong as the surrounding components. The structural behaviour of the skin is taken as a benchmark for the design of the connection. The non-flexible elements can be strengthened and therefore the Flexible Skin is the critical component. Next to the skin there is also the Flexible Shear Element as a morphing component. It is possible that this component is more critical. This must be investigated when it is fully developed. The Flexible Shear Element is not directly linked to the connection and is still in an earlier stage of development. Therefore, the Flexible Skin is selected as the critical component for now. This approach may be somewhat conservative and leaves potential for optimisation once the Flexible Shear Element is fully developed.

The combination of tension or compression with shear loading result in an internal bending moment in the skin. As a system requirement of the tab, the amount of shear carried by the skin is limited to 10% of the overall shear load of the tab [35], the main failure mode is calculated to be buckling [35]. The selected skin is a six layer 5 Harness Satin T300JB Carbon Woven PPS composite with lay-up [$\pm$45,0/90,$\pm$ 45,$\pm$ 45,0/90,$\pm$ 45] [4]. At the buckling limit of this skin, the outer layers of the skin are experiencing 350 MPa of in-plain stress in the 0^o direction [35]. At this point, local failure of the skin cannot be excluded and the skin may buckle. The 350 MPa in-plain stress is therefore taken as the failure level of the skin. If the connection is able to cope with this situation, it will not be the critical structural element.

In Section 4.2.1 the maximum pitch between fasteners is calculated by means of analysing the amount of load which one fastener can carry.

4.2.1. Connection Stress and Loads

In this section the conversion is made from the peak stress in the outer layers of the flexible skin at the buckling limit to the loads experienced by the fasteners. The first step in this process is shown in Equation 4.1. The conversion from this peak stress to the internal bending moment is performed assuming pure bending [22]. This assumption is made because the stress on top and at the bottom, in the buckling analysis, have perfect inverse values (350 MPa tension and 350 MPa compression) [35]. This indicates that the order of magnitude of other affects such as in-plane tension, is much lower. In case those other effects would be present, this assumption is conservative as the peak stress will be attributed entirely to the moment. This will lead to a safe design, although it might leave room for optimisation.

$$\begin{aligned} \sigma &= \frac{M \cdot y}{I} \\ M &= \frac{\sigma \cdot I}{y} \\ M_i &= \frac{\sigma_{peak} \frac{w \cdot t^3}{12}}{\frac{t}{2}} \\ M_i &= \frac{\sigma_{peak} \cdot t^2}{6} w \end{aligned} \tag{4.1}$$

Equation 4.1 starts with the formula for pure bending for isotropic and homogeneous materials. This

assumption does not match the reality completely but allows a simple and effective approach to the reality. Equation 4.1 gives the stress (σ) at the location of vertical distance y from the neutral line, for moment M on a part with moment of inertia I. Subsequently, the equation is transformed and filled in for this specific situation. The values shown in Equation 4.1 can be found in Figure 4.5. The value M_i stands for the internal bending moment which would cause the peak stresses (σ_{peak}) for a skin with thickness t and a fastener with diameter d. The only value not mentioned in the figure is value w. This is the width of the sample and is kept as a variable for now.

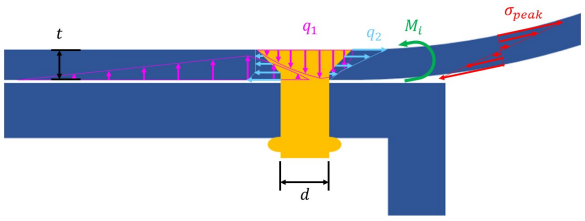

Figure 4.5: Bending stress to internal bending moment to reaction loads in a fastened structure

As the internal bending moment is derived from Equation 4.1, the next step in the analysis of the failure levels of the fasteners can be taken. This starts with the assumption that the entire moment is taken by the first row of fasteners. This assumption is made in order to simplify the analysis and eliminate the unknown aspect of the design.

The internal bending moment will be transferred in the fastener in multiple ways. This leads to a complex situation which can be seen in Figure 4.5. In order to analyse the structural ability of the fasteners in this situation, this complex situation is split into two parts. The first part of this dissection is the load on the fastener in the out-of-plain direction of the skin. When the skin is bend upwards, it will pull on the rivet head and lever on the structure behind the rivet. This effect is shown in Figure 4.6a. When the skin would bend downward, the skin will bend around the corner of the structure. This would still result in a tension force on the rivet as the skin is levered over the corner. The second part of the load dissection is the load in skin direction. The inside surface of the hole in the skin will press against the outer surface of the fastener. This effect can be seen in Figure 4.7a. The ratio between these two effects is dependent on the specific load situation, the bending profile and some other aspects which makes a precise calculation very complex. Therefore, both individual load cases are calculated as if the other load case does not carry any load. To do these calculations, the situation is simplified as much as possible.

The out-of-plain load case can be approached by replacing the distributed loads by two forces. The rivet is pretensioned, because of which the whole rivet head will experience loading. This distributed load may be slightly skewed, but the load which replaces the distributed load in this analysis will apply in the shaft of the rivet. The distributed load on the structure will be different and is dependent on the pretension and stiffness of the skin. As the skin is morphing, it is rather flexible. The load distribution is expected to apply fairly close to the fastener. Also, the distributed load will be skewed to the fastener. Replacing this load distribution by one load would require the load to apply closely behind the fastener. The transition from distributed to point loads can be seen in Figure 4.6. The closer the two loads apply, the higher they will be as the moment arm decreases. In order to maintain conservative with the calculation, the distance between the loads is kept small and set equal to the diameter of the rivet. The subsequent calculation of the skin is shown in Equation 4.2.

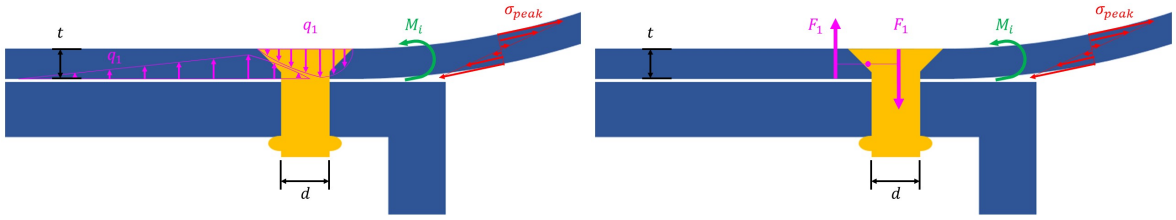

(a) Reaction loads of fastener and structure out-of-plain.

(b) Simplified reaction loads of fastener and structure out-of-plain.

Figure 4.6: Out-of-plain reaction loads

$$
\begin{aligned}
2 \cdot F_1 \frac{d}{2} &= M \\
F_1 \cdot d &= \frac{\sigma_{peak} \cdot w \cdot t^2}{6} \\
F_1 &= \frac{\sigma_{peak} \cdot t^2}{6 \cdot d} w
\end{aligned}
\tag{4.2}
$$

To investigate the loads on the fastener in skin direction, the load distribution is simplified from a continuous changing load distribution to a load distribution per skin layer. This transition is represented in Figure 4.6. The conversion between the actual and the simplified loading situation is performed by investigating the pressure from the skin on the outside of the fastener at every layer. The result of this is shown in Equation 4.3.

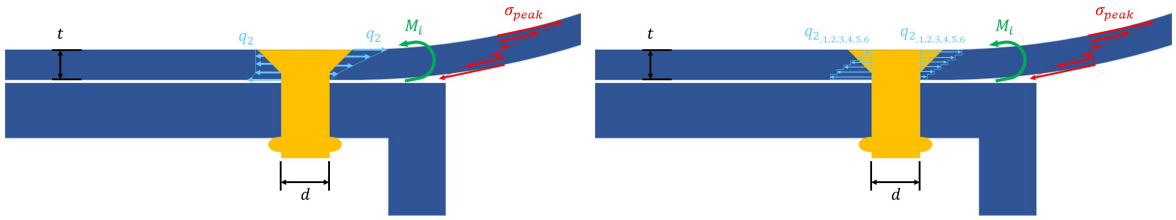

(a) Reaction loads of fastener in-plain.

(b) Simplified reaction loads of fastener in-plain.

Figure 4.7: In-plain reaction loads

$$
\begin{aligned}
2\left(\frac{t}{6}q_{2_1}\cdot a_1+\frac{t}{6}q_{2_2}\cdot a_2+\frac{t}{6}q_{2_3}\cdot a_3+\frac{t}{6}q_{2_4}\cdot a_4+\frac{t}{6}q_{2_5}\cdot a_5+\frac{t}{6}q_{2_6}\cdot a_6\right)&=M\\
2\left(\frac{t}{6}q_{2_1}\frac{t}{12}+2\frac{t}{6}q_{2_1}\frac{3t}{12}+3\frac{t}{6}q_{2_1}\frac{5t}{12}+4\frac{t}{6}q_{2_1}\frac{7t}{12}+5\frac{t}{6}q_{2_1}\frac{9t}{12}+6\frac{t}{6}q_{2_1}\frac{11t}{12}\right)&=M\\
\frac{161\cdot F_{2_1}\cdot t}{6}&=M\\
\frac{161\cdot F_{2_6}\cdot t}{36}&=M\\
\frac{161\cdot F_{2_6}\cdot t}{36}&=\frac{\sigma_{peak}\cdot w\cdot t^2}{6}\\
F_{2_6}&=\frac{6\cdot\sigma_{peak}\cdot w\cdot t}{161}\\
F_{2_6}&=\frac{6\cdot\sigma_{peak}\cdot w\cdot t}{161}
\end{aligned}
\tag{4.3}
$$

F_1 and F_{2_6} from Equations 4.2 and 4.3, are the loads which the fastener will encounter at the moment the skin would experience ultimate loading. The load is written as a function skin width. The next step is to investigate the failure loads of the rivets. By coupling the required loads and the failure levels of the skin, the pitch distance between the rivets can be determined. The common failure types of fasteners under this kind of loads are:

1. Rivet Failure in tension
2. Fastener shear failure
3. Hole bearing failure
4. Pull through due to skin shearing
5. Pull through due to compression failure under rivet head

The first two failures do not have to be calculated. Commercial fasteners are sold with maximum shear and tensile load properties. These loads are several magnitudes of order higher than for the latter three failure modes, as can be seen in Appendix B. Therefore, they do not have to be further analysed for the pitch distance. Failure will therefore be dependent on one of the three latter failure modes. These three failure modes are respectively analysed using Equations 4.4, 4.5 and 4.6.

$$
\begin{aligned}
\sigma_{s_b}&=\frac{F_i}{A_{f_m}}\\
F_i&=\sigma_{s_b}\cdot t\cdot d\\
F_{i_6}&=\sigma_{s_b}\cdot\frac{t}{6}\cdot d
\end{aligned}
\tag{4.4}
$$

In Equation 4.4, (F_i) stand for the out-of-plain skin loads. Equation 4.4 calculates the maximum load in skin direction by analysing the bearing limit. The bearing stress (σ_{s_b}) is calculated by dividing the load over the thickness (t) times the fastener diameter (d) which together form the cross-sectional surface of the fastener (A_{f_m}). A bearing load is introduced by an in-plain load on the fastener which pushes the fastener in the skin. To effectively analyse bearing damage for the load situation of the flexible tab, the bearing limit for the outer layer is compared to the applied load in the outer layer. The outer layer is analysed as the in-plane load is much higher there than in the rest of the skin. This can be done by replacing the thickness (t) in Equation 4.4 by the thickness of only one layer (t/6) and then compare it to the applied load shown in Equation 4.3. The calculation can be found in Appendix A. This results in a maximum pitch distance between two fasteners which can be seen in Table 4.2.

$$\sigma_{s_c} = \frac{F_o}{A_{s_{uh}}} \qquad F_o = \sigma_{s_c} \cdot \pi \left(D^2 - d^2\right) \tag{4.5}$$

$$\tau_s = \frac{F_o}{A_{s_{co}}} \qquad F_o = \tau_s \cdot \pi \cdot D \cdot t \tag{4.6}$$

In Equations 4.5 and 4.6 two types of pull-through are analysed. These analyses will both lead to a maximum load in the direction of the fastener (F_o). The first pull-through failure occurs due to failure of the material underneath the fastener head. This analysis is comparable to a bearing failure analysis. To analyse pull-through failure due to failure of the material underneath the fastener head, the load on the fastener is calculated by multiplying the compression limit of the skin material (σ_{s_c}) with the surface underneath the fastener head ($A_{s_{uh}}$). This surface therefore is equal to the surface area of the fastener head with diameter D minus the area taken by the fastener shaft with diameter d. The second pull-through failure mechanism is pull-through due to the shear failure of the skin at the edge of the fastener head. To analyse this, the maximum shear stress of the skin (τ_s) is analysed for the shear surface at the edge of the fastener head ($A_{s_{co}}$) which is the cross sectional surface of the skin at the circumference of the rivet head. This surface is dependent on the skin thickness (t) and the rivet head diameter D. These calculations can be found in Appendix B. By dividing the applied loads with the maximum failure loads, the amount of fasteners per set length can be calculated or the maximum pitch distances can be found. These can be seen in Table 4.2.

Table 4.2: Maximum pitch distance to meet structural requirement per failure type, for three rivet sizes

Rivet type	Fastener bearing mm	Pull-out shear mm	Pull-out bearing mm	⌀ d mm	⌀ D mm
EN6122C05	27	100	104	4.14	7.52
EN6122C06	32	142	167	5.03	8.81
EN6122C07	37	174	207	5.74	9.47

Table 4.2 shows the maximum pitch distances per failure method. The smallest pitch distance determines the final distance as any larger value would lead to failure by another failure mode. The final pitch distance per fastener can be seen in Table 4.3.

Table 4.3: Overall maximum pitch distance for three rivet sizes

Rivet type	Overall maximum pitch distance mm
EN6122C05	27
EN6122C06	32
EN6122C07	37

The difference between the maximum pitch distances per failure mode is rather big as can be seen in Table 4.2. Also, the calculations have been conservative. Especially in the start of the calculations, where the internal moment is assumed to be taken entirely by in-plain and out-of-plain loading. If in reality, the load in in-plain direction is very small, fastener bearing would not occur and the most sensitive failure mode becomes pull-out shear. As the maximum pitch distance for that failure is more than three times larger than the currently selected one, the design would be overly conservative. A test may indicate the extend in which this is the case.

Besides the maximum pitch distance, there is also a requirement for the minimum pitch distance as well as some other requirements for the location of fasteners with respect to each other and the material. These are discussed in Section 4.2.2.

4.2.2. Edge, Row and Pitch Distance

As the maximum pitch distance is known, the other requirements for the location of fasteners with respect to each other and the material must be checked. Based on many analyses such as net section failure and stress concentrations within carbon fibre reinforced composites, design guideline have been

created for the location of the fasteners with respect to the edges of the material and to each other. These are shown in Figure 4.8. The distance between the edge of the material and the fastener is called the Edge distance (A). The spacing between two rivets in sideways direction and in length direction are called Pitch (B) and Row distances (C) respectively.

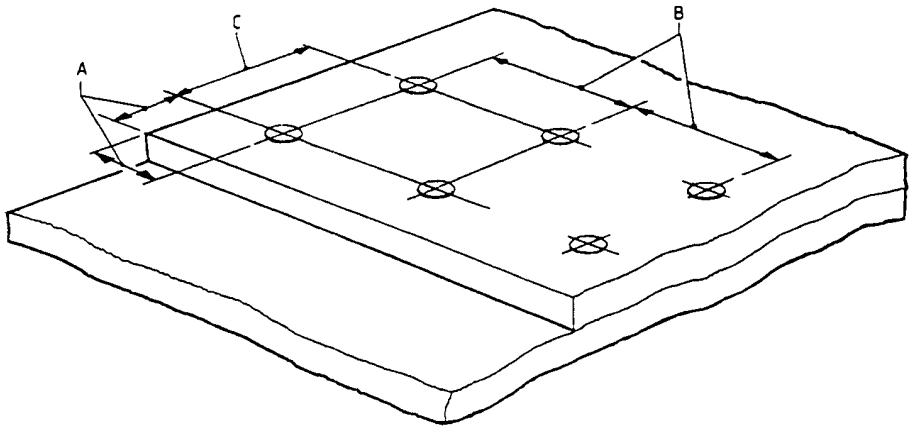

Figure 4.8: Edge (A), pitch (B) and row (C) distances [34]

Table 4.4: Edge (A), Pitch (B) and Row (C) distances w.r.t. nominal diameter (D) for fibre-reinforced material [34]

Rivet type	Edge distance (A) mm	Pitch distance (B) mm	Row distance (C) mm	⌀ d mm	⌀ D mm
Countersunk holes	3d	5d	4d		
EN6122C05	12.4	20.7	16.6	4.14	7.52
EN6122C06	15.1	25.15	20.1	5.03	8.81
EN6122C07	17.2	28.7	23.0	5.74	9.47

5

Test Design

In Chapter 3 the selection procedure showed that, based on a Trade-off, a riveted connection is the most promising connection for morphing tab application. Subsequently, in Chapter 4, the rivet joint was designed based on the applied ultimate loading. The joint was designed based on a simplified static analysis. In order to determine the static and dynamic behaviour in a non-simplified manner, a realistic test must be performed. In this chapter, that test is elaborated upon. First the test samples based on the previous analysis are discussed. Secondly, the test itself is presented along with the test procedure. The design iterations of the test design and test procedure are also shown.

5.1. Test Samples

From previous tests on the skin itself, skin material was available with a width of 100 mm and a length of 220 mm. These skin sections were therefore selected as the basis for the samples. Based on the minimum and maximum pitch distance between two rivets, found in Chapter 4, the amount of fasteners for this 100 mm wide section is analysed. The maximum amount of fasteners which can be implemented on these 100 mm of skin is determined by the minimum pitch and edge distance shown in Table 4.3. Based on the number of times the pitch distance fits in the sample width, minus twice the edge distance, the maximum amount is determined. The result is a maximum of four fasteners using the smallest rivets and three fasteners using the two larger ones.

Three sample lay-outs are created for the test. To investigate the effect of the fastener size, two rivet sizes are tested. To determine which two sizes are selected, the failure levels for different failure modes are investigated. Failure modes which damage the fasteners were much stronger than the failure modes related to the skin. This can be seen in Table B.4. Table 4.2 shows the difference in pitch distance for the skin related failures for the three rivet sizes. When the difference between pitch distances for the different failure modes is small, the design is efficient. This is the case for the smallest size. The largest rivet size has the largest scatter in pitch distances and is therefore excluded as a rivet. The smallest and medium rivets (EN6122C05 and EN6122C06) will be used for the samples. Besides the rivet size, another sample variation is created. As explained in Section 4.2.1, the maximum pitch length is based on a conservative analysis. In order to analyse the extend of the conservatism, a test will be performed with fewer rivets than indicated by the analysis. For the smallest rivet size, rather than the indicated four required rivets, three rivets will be applied. Testing more variations might lead to a better optimisation, however, it would significantly complicate the study and put a strain on the time and resources for this thesis. Therefore, the tests are limited to the three lay-outs discussed above. Based on the differences between the results for these three lay-outs, trends may be observed.

The sample skins will be mounted on an aluminium plate (the support plate) which represents the solid structure underneath the flexible skin in the tab design. Where the second fastener row would be, the skin will be clamped by another aluminium piece (the upper clamp). On the other side the skin will also be clamped. This is because these sections of the sample are the subject of the investigation. The test lay-outs can be seen in Figure 5.1. The samples shown in Figures 5.1a and 5.1c use respectively

three and four EN6122C05-06H rivets. Figure 5.1b shows the sample which uses three of the larger EN6122C06-07H rivets.

5.2. Test set-up and procedures

In this section, the test itself is discussed. This starts with the initial design and test procedure. Subsequently, two design iterations are explained.

5.2.1. Initial test

The initial test design can be seen in Figure 5.2. In this figure, two clamping plates can be observed at the bottom and top of the set-up. These plates are clamped in a 250 kN fatigue bench of Zwick Roell GmbH & Co. KG. The upper cross-head of the fatigue bench maintains in place, and the lower cross-head moved up or down to create bending in the flexible skin. This cross-head displacement has a range of 150 mm due to the limitations of the test machine.

Table 5.1: Legend for test set-up drawings in Figures 5.2 and 5.5

Label	Part	State
A	Upper cross-head mount	Rigid
B	Lower cross-head mount	Rigid
C	Upper clamp	Rigid
D	Lower clamp / L-arm	Rigid
E	Double hinged arm	Rigid
F	Upper hinge	Hinging
G	Lower hinge	Hinging
H	Flexible Skin	Flexible
I	Support plate	Rigid
J	Rivets	Rigid

The test procedure is as follows. The cross-head mounts (A and B) is placed in the machine. The sample is clamped in the upper clamp which symbolises the second fastener row. The other end of the flexible skin (H) is clamped as well in part D. If the test must simulate an outward bend, the lower cross-head mount is moved down. For inwards bending, the lower cross-head mount is moved up. In case of a fatigue test, where the sample is bent in two directions, the lower cross-head is displaced maximum 75 mm in both directions. The flow chart of the test procedure for the tests is shown in Figure 5.3.

The initial test design has a problem. In Figure 5.4 the progression of a static test can be seen. Figure 5.4a shows the sample in unloaded condition. This corresponds to the set-up shown in Figure 5.2. In order to bend the skin section away from the fixed part, the bottom cross-head is pulled down. Figure 5.4b shows the test for small deflection angles. In this part of the test, the skin is bend uniformly. However, when the cross-head displacement is further increased, the bending is no longer uniform. The radius is no longer constant as can be seen in Figure 5.4c. This is caused by a change in applied load. When the double hinged part of the test set-up is in its initial position, the majority of the load applied by the bench is applied as a moment on the end of the skin. When this part becomes increasingly vertical, the applied load does no longer largely create a moment but will also pull in the direction of the skin. This leads to a high local bent at the lower clamp. The result of continuing the test with this set-up is shown in Figure 5.4d. Both Figures 5.4c and 5.4d indicate that this test is not valid. The fasteners are not loaded in a representative manner and the resulting failure is therefore not indicative for the connection in the morphing tab. This necessitates a redesign of the test set-up.

5.2.2. Design iteration 1: adjusted test set-up

Using the same components as the initial set-up, the test can be adapted so that also in the high bending regime, the load is largely applied perpendicular to the skin section at the fasteners. The majority of the input load of the machine will therefore be experienced by the skin as a bending moment. This is a much more representative test compared to the initial test. The redesigned test set-up can be obtained by mounting the samples in a horizontal manner on the upper cross-head. This set-up is shown in

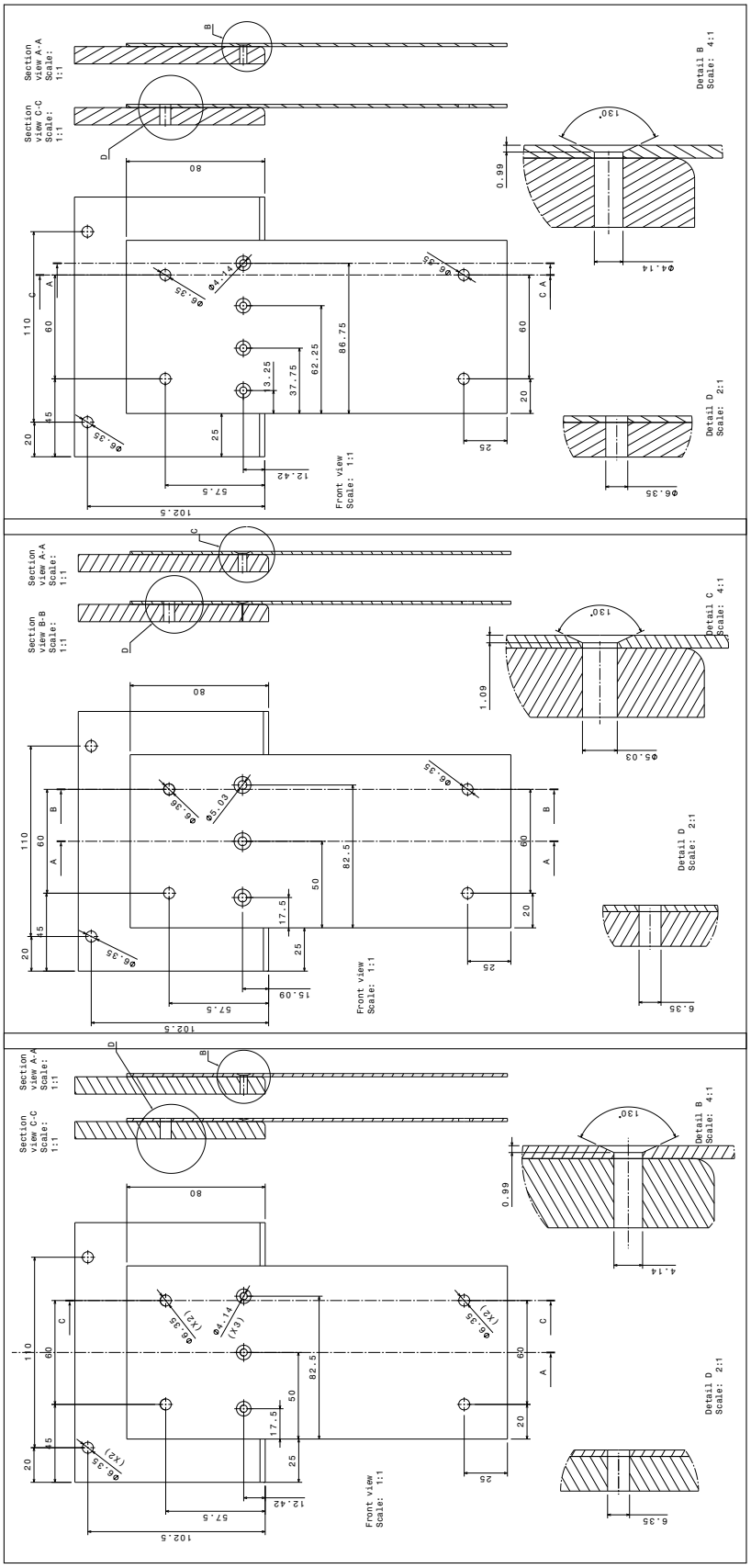

(a) Lay-out 1: three small rivets '3x05' (b) Lay-out 2: three large rivets '3x06' (c) Lay-out 3: four small rivets '4x05'

Figure 5.1: Test samples lay-outs

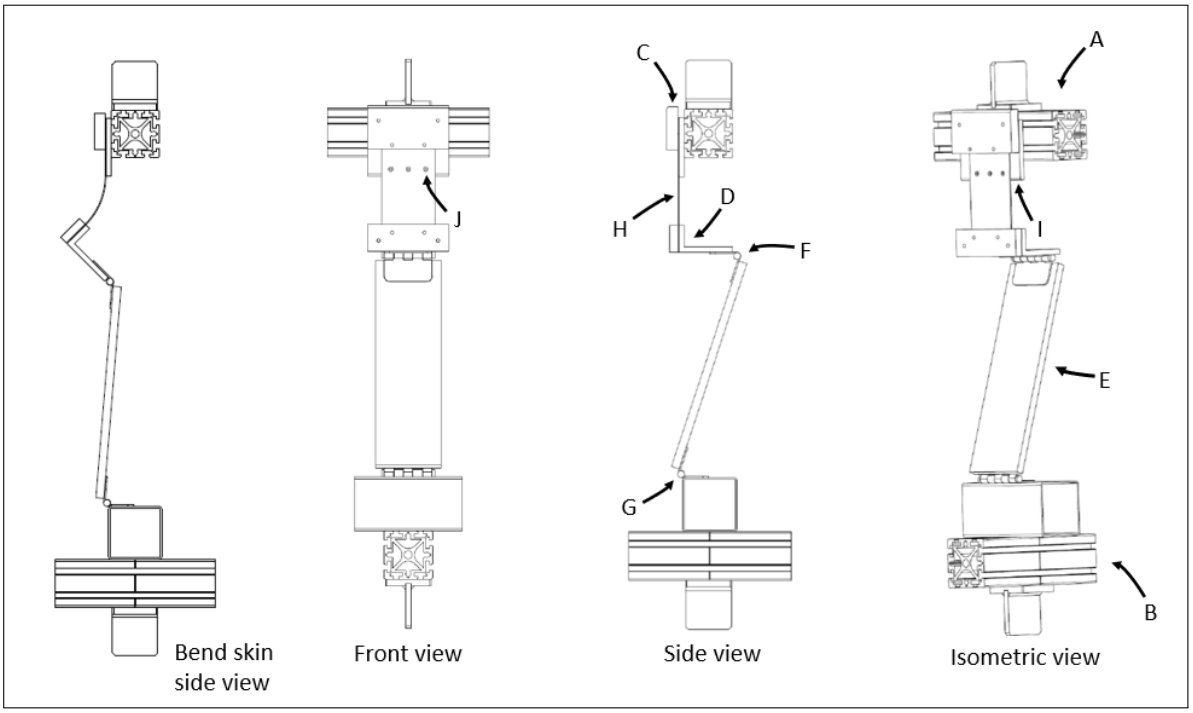

Figure 5.2: Original test design

Figure 5.5.

The test procedure of this test set-up is not changed except for upwards bending of the skin. In the previous set-up, this was achieved by moving the lower cross-head down. For small deflection angles this can still be done with this set-up. But for deflections which require more than 75 mm downwards cross-head displacement, the procedure is changed. The upper clamp (C), the flexible skin (H) and the Support plate (I) are then flipped upside-down. The cross-head displacement is then performed upwards to simulate the upwards skin bending. Examples of the upwards and downwards bend can be seen in Figure 5.6. Figures 5.6c and 5.6d show an inverted clamp compared to figures 5.6a and 5.6b.

The positions shown in Figures 5.6b and 5.6d are the positions in the maximum machine deflection. It is clear that the samples have not failed due to this deflection. Both the failure loads and the failure mode can give insights in the structural behaviour of the connection. To investigate the failure loads and modes, the samples have to fail. In order to do so, the deflection must be increased. To achieve this, not the machine hardware but the test procedure will be altered. Next to this test procedure update, the strain measurements are also updated. These changes are discussed in Section 5.2.3.

5.2.3. Design iteration 2: adjusted test procedure

As mentioned in Section 5.2.2 to achieve failure in a manner which would represent a loading situation similar to the one experienced in the morphing tab, the bending deflection must be increased. This can be done without altering the parts of the test set-up. If the static test is performed, the upper cross-head is fixed, subsequently the lower cross-head is moved up in increments of 5 mm. When the cross-head has travelled for 150 mm, the range limit is reached. Then the entire test set-up is lowered in the machine by 150 mm. The result of doing this, is that the deflection of the sample is not changed but that the 150 mm machine range can be used again. The test can proceed as before by moving the lower cross-head up in 5 mm increments. This can be reiterated until failure occurs. The adjusted test procedure can be seen in the flow chart in Figure 5.7

Another change in the test procedure is the addition of two measurement methods. The strain levels on the outer surface of the skin will be measured by both strain gauges and a DIC system. These

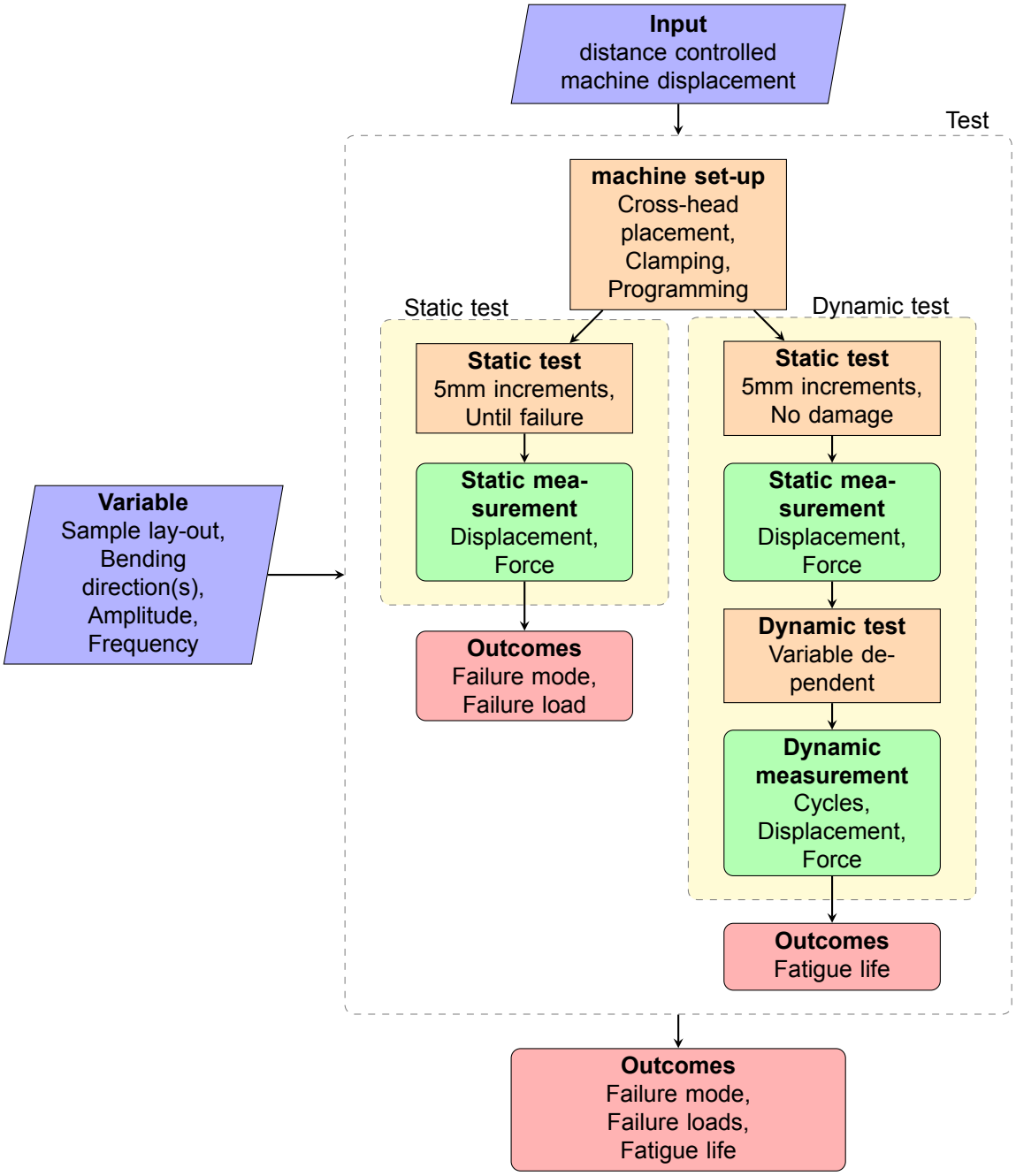

Figure 5.3: Flow chart of the initial test

measurements give an insight in the strain across the surface. They can also be part of the verification and validation of the test results.

This design iteration has been applied after the dynamic test have been performed. Therefore, the iteration only applies to the static test. The measurement data of the dynamic test will be compared with the data gathered by the new measurements. The static test after a dynamic test run will for instance be performed once again using the updated test model to get an insight in the strain across the surface of the skin.

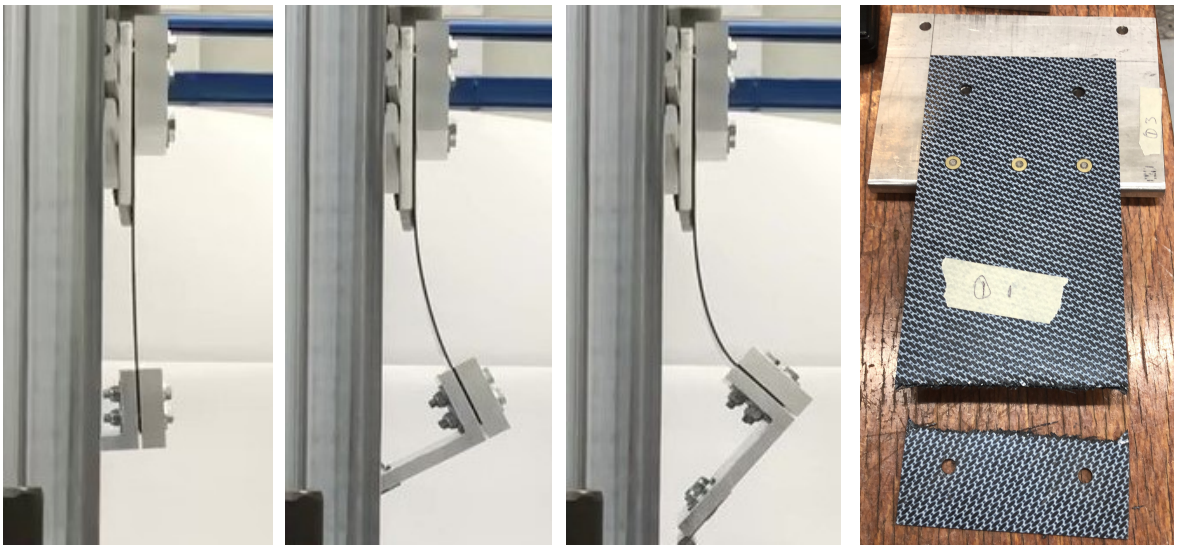

(a) Start of the test (b) Even bending of skin (c) Local bending of skin (d) Broken at lower clamp

Figure 5.4: Initial test

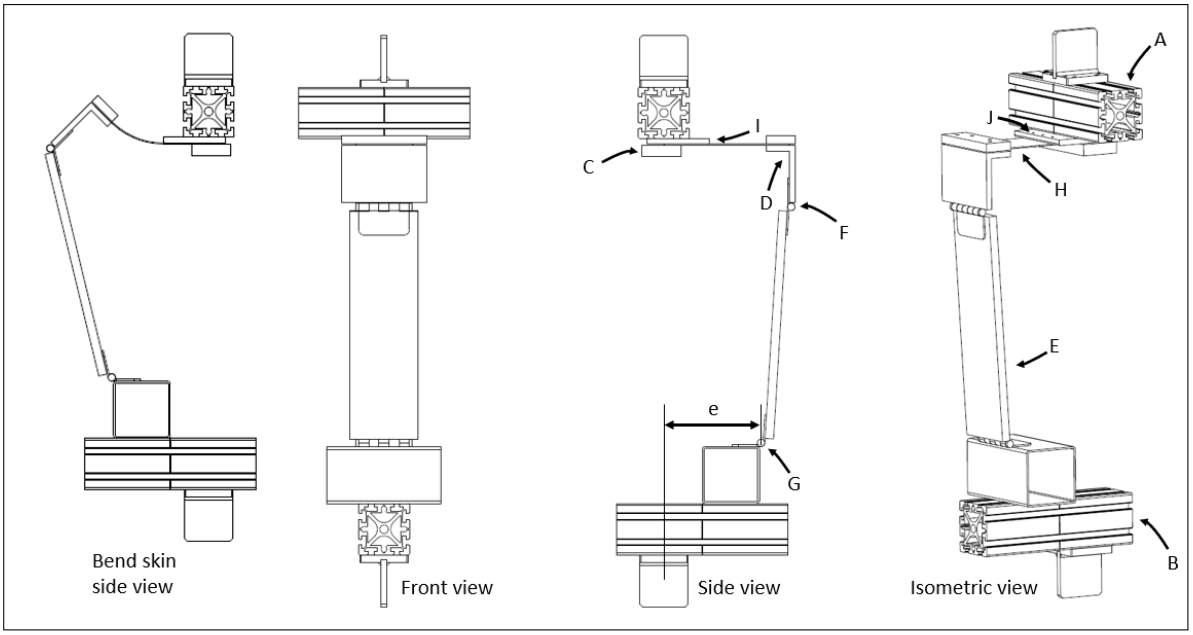

Figure 5.5: Adjusted test design

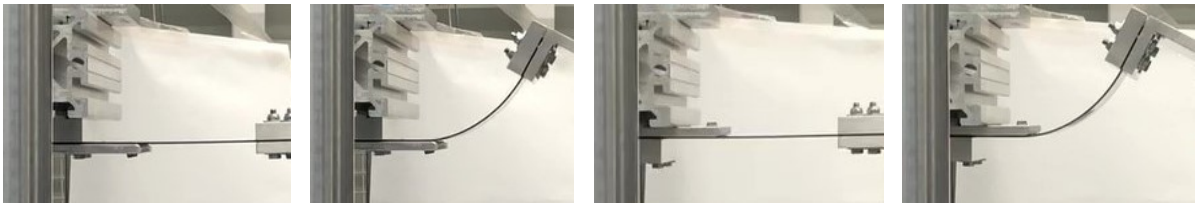

(a) Start position upwards (b) Bend position upwards (c) Start position downwards (d) bend position downwards

Figure 5.6: Adjusted test design, Upwards vs downwards test. The test shown in Figures c and d have upside-down samples compared to the test shown in Figures a and b.

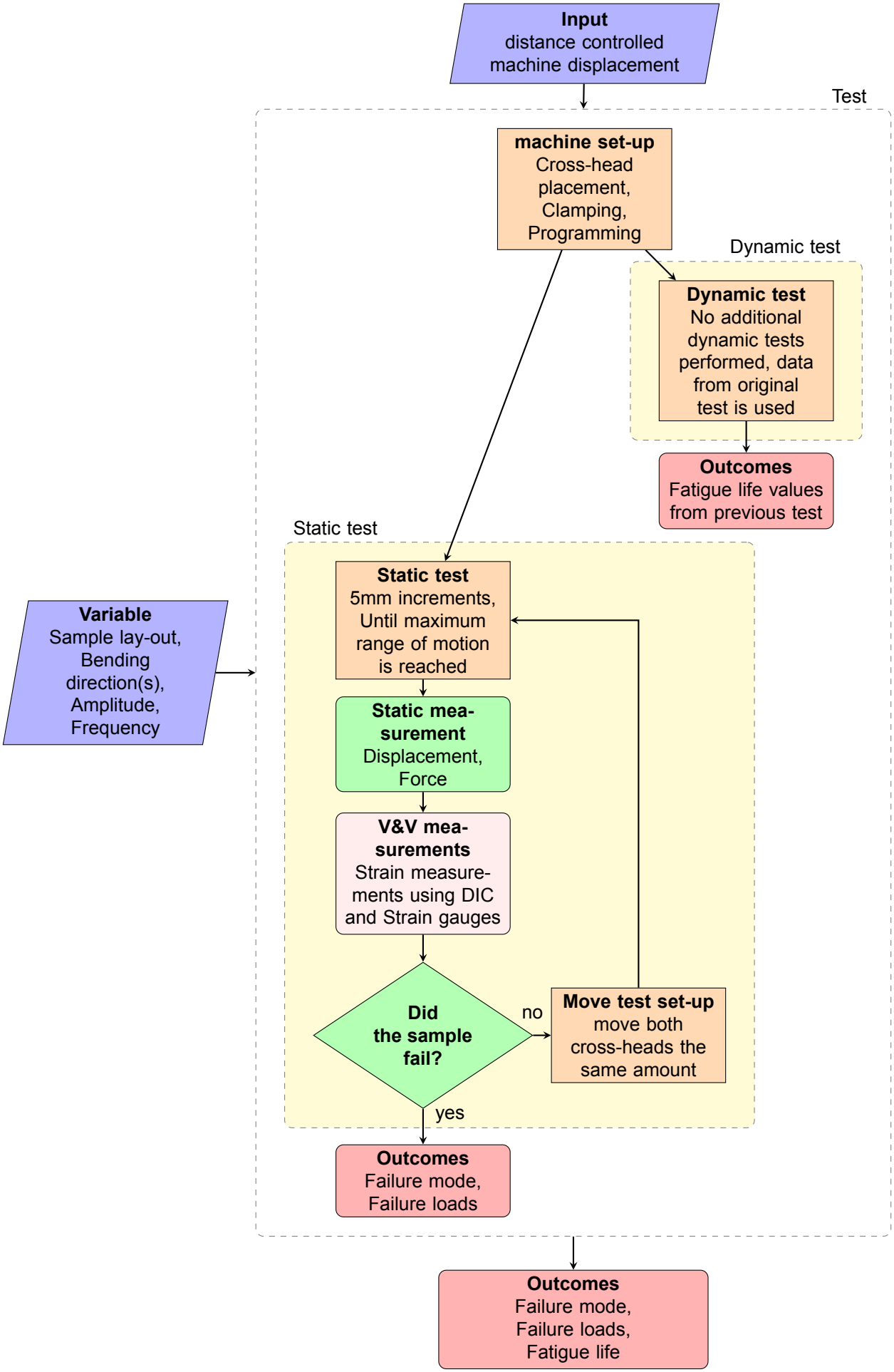

Figure 5.7: Flow chart of the adjusted test

6

Measurements and Data Processing

To generate results from the test, designed in Chapter 5, measurements must be performed. The joint can be analysed by these measurements as the requirements can than be checked. As test data for the skin is available, the test results in this thesis will be compared to the results of the four-point bending test of the skin. To check the requirements, the following outcomes are desired from the test:

- Stress in the outer layer of the flexible skin
- Strain in the outer layer of the flexible skin
- Deflection angle of the flexible skin
- Contour deviations of the flexible skin
- Cycle count for the dynamic test
- Failure mode

To obtain these outcomes, five measurement methods are applied in the test. These measurements as well as the processing of the measurement data are explained in Sections 6.1 to 6.5. The combination of these measurement methods also forms the validation and verification of the thesis.

6.1. Measurement A: Machine Force and Displacement Input

The first measurement is the test machine input. The lower cross-head is incrementally moved up with 5 mm each time. This is performed as a displacement controlled input. This control input is measured continuously. Also, the force required in order to realise this displacement is measured. This is performed by a load cell in the upper cross head of the test machine.

Based on the kinematics of the test set-up, the load path of the machine input load can be traced. This way the load at the connection can be calculated. In Figure 6.1 the relation between the angular deflection of the skin α_i and the machine displacement d_i can be seen. This relation however assumes a perfect circular bending of the skin. This assumption must be verified by Measurement E, explained in Section 6.5.

In this figure, the part between point (0,0) and A is the flexible skin. The rest is rigid which can be seen in Figure 5.5 and Table 5.1. The connection between point B and C in Figure 6.1 is a double hinged arm. The load on and displacement of the bottom of that double hinged arm determines the stress and strain in the sample. The mathematics of this measurement method can be seen in Equations 6.1 to 6.5.

The fist Equation (6.1) starts with the assumption that the skin radius is perfectly circular. This must be verified by Measurement E. However, when this is the case, the relation between a skin section (l) which is 100 mm, the radius of the circle (r) and the deflection angle (α) can be constructed as shown in Equation 6.1.

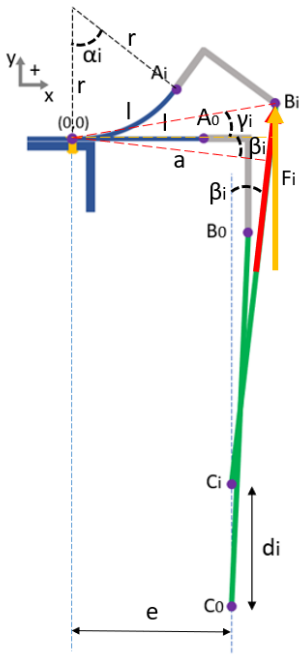

Figure 6.1: Force and displacement of cross-head as input. Stress, strain and deflection as output.

$$\begin{aligned} l &= 2\pi \cdot r \cdot \frac{\alpha}{2\pi} \\ l &= r \cdot \alpha \\ 100 &= r \cdot \alpha \\ r &= \frac{100}{\alpha} \end{aligned} \tag{6.1}$$

From Equation 6.1 and by taking the centerline of the riveted joint of the skin as the (0,0) point, the coordinates of point A can be determined. In Figure 6.1 it can be seen that point A is the end of the curved skin section. In Equation 6.2, X_{A_i} and Y_{A_i} indicate the X and Y value of point A.

$$\begin{aligned} X_{A_i} &= r \cdot sin(\alpha) = \frac{100 \cdot sin(\alpha)}{\alpha} \\ Y_{A_i} &= r - r \cdot cos(\alpha) = r(1 - cos(\alpha)) = \frac{100}{\alpha}(1 - cos(\alpha)) \end{aligned} \tag{6.2}$$

Equation 6.3 shows the X and Y coordinate calculations for point B in Figure 6.1. Point B is at the end of the L-shaped clamp. The short side of the clamp is 50 mm and the long side is 100 mm. The short side of the clamp is tangent to the curvature at point A, meaning that it is under angle α with respect to the x-axis.

$$\begin{aligned} X_{B_i} &= X_{A_i} + 50 \cdot cos(\alpha) + 100 \cdot sin(\alpha) = \left(100 + \frac{100}{\alpha}\right) sin(\alpha) + 50 \cdot cos(\alpha) \\ Y_{B_i} &= Y_{A_i} + 50 \cdot sin(\alpha) - 100 \cdot cos(\alpha) = \frac{100}{\alpha} + 50 \cdot sin(\alpha) - \left(\frac{100}{\alpha} + 100\right) cos(\alpha) \end{aligned} \tag{6.3}$$

Point C in Figure 6.1 shows the location of the lower cross-head of the test set-up. Point B and C are connected via the 400 mm long double hinged arm. As the cross-head only moves in y-direction, the X coordinate (X_{C_i}) is constant for every deflection angle (α). This constant x coordinate is set at

140 mm and defined as by e. This is 10 mm of the l-arm in starting position which makes sure that β_0 is larger than zero. The force at the start situation is therefore already pointed slightly outwards. There are two methods to calculate the Y coordinate (Y_{C_i}). The first one (Method 1) with respect to point B. The second one (Method 2) with respect to the the starting Y coordinate (Y_{C_0}) and in terms of the displacement of the cross-head (d). These are shown in Equation 6.4.

$$
\begin{aligned}
X_{C_i} &= X_{C_0} = e = 100 + 50 - 10 = 140 \\
&Method 1 \\
Y_{C_i} &= Y_{B_i} - \sqrt{400^2 - (X_{B_i} - X_{C_i})^2} \\
Y_{C_i} &= \frac{100}{\alpha} + 50 \cdot sin(\alpha) - \left(\frac{100}{\alpha} + 100\right) cos(\alpha) - \\
&\quad \sqrt{400^2 - \left(\left(100 + \frac{100}{\alpha}\right) sin(\alpha) + 50 \cdot cos(\alpha) - 140\right)^2} \\
&Method 2 \\
Y_{C_i} &= Y_{C_0} - d = -100 - \sqrt{400^2 - 10^2} + d = -10\left(10 + \sqrt{1599}\right) + d
\end{aligned}
\tag{6.4}
$$

By equating the two methods to determine the Y coordinate (Y_{C_i}) from Equation 6.4, a relation can be formulated between the machine displacement (d) and the skin deflection angle (α). This relation is shown in Equation 6.5.

$$
\begin{aligned}
d = &10\left(10 + \sqrt{1599}\right) + \frac{100}{\alpha} + 50 \cdot sin(\alpha) - \left(\frac{100}{\alpha} + 100\right) cos(\alpha) - \\
&\sqrt{400^2 - \left(\left(100 + \frac{100}{\alpha}\right) sin(\alpha) + 50 \cdot cos(\alpha) - 140\right)^2}
\end{aligned}
\tag{6.5}
$$

By solving Equation 6.5 for α, a deflection angle can be determined for every input displacement by the machine. By knowing the kinematics of the test set-up at every displacement input and by knowing the required force by the machine to get the set-up in this position, the internal moment at the connection can be determined. In the double hinged arm between point B and C in Figure 6.1, the forces can only be in the direction of the double hinged arm due to the double hinged structure. The force in the arm is therefore equal to the input force of the machine (F_i) divided by the cosine of the angle of the arm with respect to a vertical line (β_i). This force times the smallest distance from the arm to the connection (a) is equal to the internal moment at the centerline of the joint. This distance is the perpendicular distance from the arm to the connection. The resulting equation of this reasoning can be seen in Equation 6.6. However one more variable is used in the transformation of the equation. That last variable is γ_i, which indicates the angle between a the a line from point (0,0) to B_i and a horizontal line.

$$
\begin{aligned}
M_i &= a \cdot F \\
&= \sqrt{X_{B_i}^2 + Y_{B_i}^2} \cdot cos(\beta_i + \gamma_i) \cdot \frac{F_i}{cos(\beta_i)} \\
&= \sqrt{X_{B_i}^2 + Y_{B_i}^2} \cdot cos\left(tan^{-1}\left(sin^{-1}\left(\frac{X_{B_i - 140}}{400}\right) + \frac{Y_{B_i}}{X_{B_i}}\right)\right) \cdot \frac{F_i}{cos\left(sin^{-1}\left(\left(\frac{X_{B_i - 140}}{400}\right)\right)\right)}
\end{aligned}
\tag{6.6}
$$

In Chapter 4, during the structural analysis of the rivets, Equation (4.1) was formulated to relate the internal moment to the peak stress at the outer layers of the skin. By inserting this equation in Equation 6.6, the peak stress (σ_{peak}) can be shown as a function of X_{B_i} and Y_{B_i}. This results in Equation 6.7.

$$\frac{\sigma_{peak} \cdot 1.86^2 \cdot 100}{6} = \frac{\sqrt{X_{B_i}^2 + Y_{B_i}^2} \cdot cos\left(tan^{-1}\left(\frac{Y_{B_i}}{X_{B_i}}\right) + sin^{-1}\left(\frac{X_{B_i-140}}{400}\right)\right) \cdot F_i}{cos\left(sin^{-1}\left(\left(\frac{X_{B_i-140}}{400}\right)\right)\right)}$$
$$\sigma_{peak} = \frac{F_i \cdot \sqrt{X_{B_i}^2 + Y_{B_i}^2} \cdot cos\left(tan^{-1}\left(\frac{Y_{B_i}}{X_{B_i}}\right) + sin^{-1}\left(\frac{X_{B_i-140}}{400}\right)\right)}{57.66 \cdot cos\left(sin^{-1}\left(\left(\frac{X_{B_i-140}}{400}\right)\right)\right)} \tag{6.7}$$

As shown in Equation 6.3, X_{B_i} and Y_{B_i} are only dependent on α. Subsequently, in Equation 6.5, α has been shown to dependent on only the displacement of the lower cross-head (d). Therefore, it can be concluded that the peak stress in the outer layer of the skin is determined by the displacement of the lower cross-head. The calculation is performed by inserting Equations 6.3 and 6.5 in Equation 6.7. Solving this for the all displacement values d encountered in the test, gives the stress values required for the test results. From this the peak stress in the outer layer can be found.

By knowing the stress in the outer layer of the skin and the Young's-modulus (E), which is material dependent, the elongation in the outer layers of the skin can also be calculated as shown in Equation 6.8.

$$\sigma = E \cdot \epsilon$$
$$\epsilon = \frac{\sigma_{peak}}{E_6} \tag{6.8}$$

The main reason for using Measurement A, explained in this section, is that it is very reliable and the data was available during all tests. In order to make the data generated in this manner useful, data cleaning is performed. The test machine is rather precise but is intended for loads up to 250 kN while the applied loads in this test did not exceed 250 N. The load cell, measuring the applied force, had some problems with determining the zero load situation. During the cleaning, the noise from these measurements was cleaned out of the data. This is done by taking the relative machine input force per cycle rather than the absolute force. The difference between the cleaned data and the raw data is shown in Figure 6.2 for a fatigue test. The blue line is the continuous force measurement along the cycles. The yellow and orange line at respectively the top and bottom of this blue line indicate the maximum and minimum measurements. These measurements are absolute with respect to a fluctuating zero force. The green top line and purple bottom line are the maximum and minimum measurements in the cleaned data.

The zero force point was a problem with the static tests as well. Here also the relative force has been used rather than the absolute value indicated by the test machine.

6.2. Measurement B: Machine Displacement Input

The second method is very similar to the first method. The method is based on the same theories and mathematics. Therefore, Equations 6.1 to 6.5 are also applicable to this method.

The deviation in the method starts after these equations. The second method does not consider the force in order to calculate the infernal moment from which the stress and strain are calculated. Equation 6.5 indicates the link between the machine displacement and the angular deflection. This angular deflection is the basis of the strain calculation in this method. The strain (ϵ) is calculated according to Equation 6.9.

$$\epsilon = \frac{t/2}{r} \tag{6.9}$$

By multiplying the strain of Equation 6.9 with the Young's Modulus the strain can be calculated. The result of the multiplication can be seen in Equation 6.10.

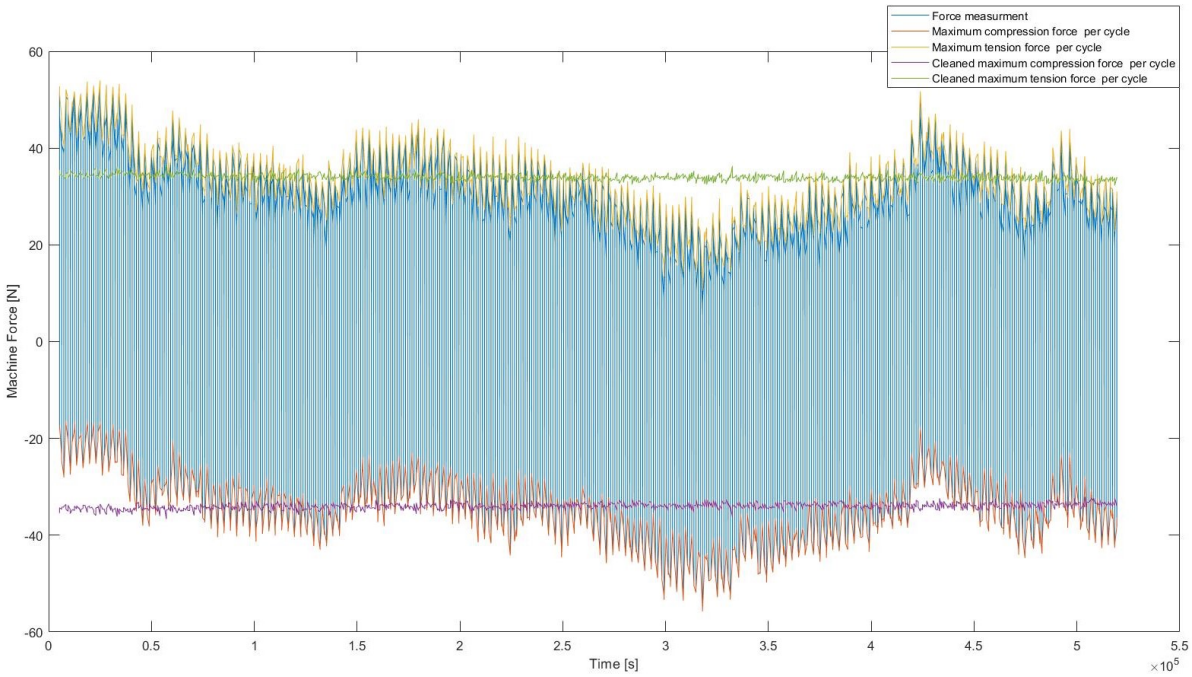

Figure 6.2: Noise cleaning example, Fatigue test

$$\sigma = \frac{t/2}{r} \cdot E \tag{6.10}$$

In comparison to Measurement A, Measurement B is not subjected to noise as much. The measurements in Measurement A, are an order of magnitude 1000 lower than the machine limit of 250 kN [21]. Measurement B does not use the force measurement. Both measurements use the displacement. The tests use the entire operating range of the machine displacement. Therefore, proportionately there is much less noise in the displacement measurement. As measurement B only uses this displacement, there is not much less noise in this measurements as well.

6.3. Measurement C: Digital Image Correlation

The third measurement is Digital Image Correlation (DIC). In Figure 6.3a the set-up is shown as it was used during the tests. By using two cameras which have been calibrated, the location of a spot on a sample can be determined in three dimensions as shown in Figure 6.3b. In Figure 6.3c an example of a set of photographs taken by the two cameras can be seen. By comparing the location of the set of speckles with the location of that same set of speckles of the previous pictures, the displacement of those speckles can be determined. The relative displacements of speckles indicates strain. If this is done over the entire surface area, a vector field of deformation can be created from which a strain field can be constructed. This is shown in Figure 6.3d.

In Sections 6.1 and 6.2, two measurement systems were discussed which calculate the strain and stress from the origin of the deflection. The DIC system measures the displacement of the speckles and calculates the strain from the relative displacement. This is a more direct measurement. This is a big advantage as this is not dependent on assumptions. Another big advantage of this system is that it gives insight on the entire surface area captured by the two cameras. This gives insight in the behaviour around the fasteners which the first two methods cannot give.

The limitations of this measurement method is the fact that it is relatively difficult to perform this analysis for large data sets. This is because of two reasons. The first reason is that the DIC system is independent from the test machine. The system must be controlled separately and get an input to

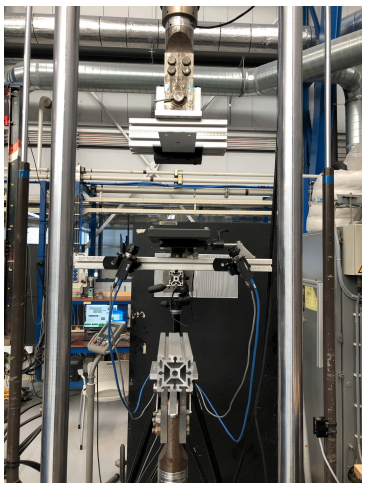

(a) DIC set-up during test

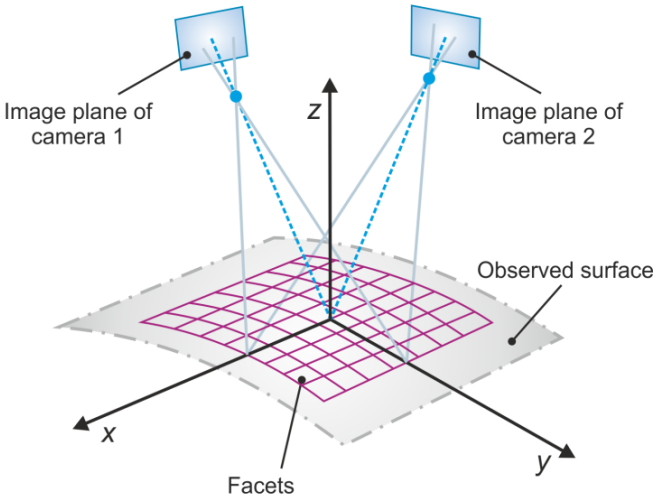

(b) Two camera principle [15]

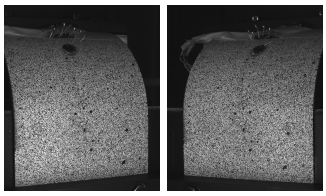

(c) View from cameras

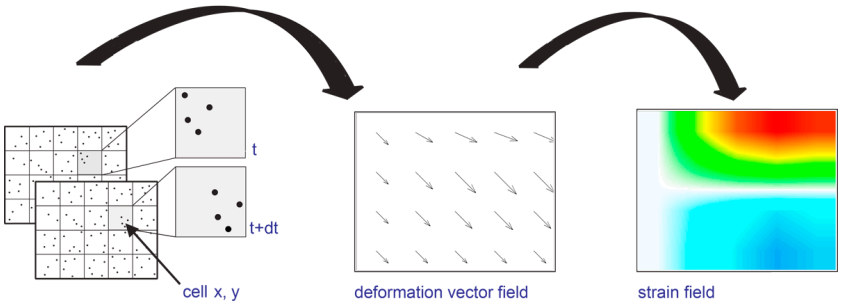

(d) Strain determination principle [19]

Figure 6.3: DIC measurement method

take the pictures for the analysis. This leads to two data sets, of which one is a collection of photographs, which must be coupled. This is a fairly labour intensive process. It is impossible to combine this with a fatigue analysis which makes up to 250.000 cycles and runs for multiple days. The second reason is that even when it would be possible, the resources required for this analysis would be disproportionate to its advantages. The required memory for that vast amount of photographs would be enormous. Also, the processing power required for the analysis of such a vast amount of data would be excessive. Mainly because the advantages which were mentioned before are only relevant for some measurements, the behaviour around the fasteners will not continuously change. Therefore, it is a very informative measurement system as an addition to the previously discussed methods.

To process the DIC data, good documentation is required. This way the data can be processed and merged with other measurement methods later. Furthermore, the analysis exists of selecting the relevant area for investigation and so on. This is all performed inside the DIC system. The system than interprets the photographs in an internal system. There is no control over the way the system produces the results and thus no data processing. To interpret the results and show relevant findings, the results must be linked to other data by means of the documentation. This however is not really data processing.

6.4. Measurement D: Strain Gauges

measurement Method D uses strain gauges to determine the strain at some locations on the outer surface of the samples. Most samples had a set of three strain gauges on the top surface and bottom surfaces of the sample. Two of such triplet strain gauges can be seen in Figure 6.4b. These triplets combine a strain gauge under +45°, 0°and -45°. One such triplet gives an insight of the strain in these

three directions on one location. In Figure 6.4a a sample is shown with eight triplet strain gauges. It also had triplet strain gauge at the bottom surface. The reason for the high amount of strain gauges is to investigate the strain at multiple locations such as the around the rivets and along the length of the samples. This can validate the DIC system. The strain gauges themselves change in resistance by increasing strain. This can be measured by integrating the strain gauge in a Keithley quarter bridge set-up, shown in Figure 6.4c.

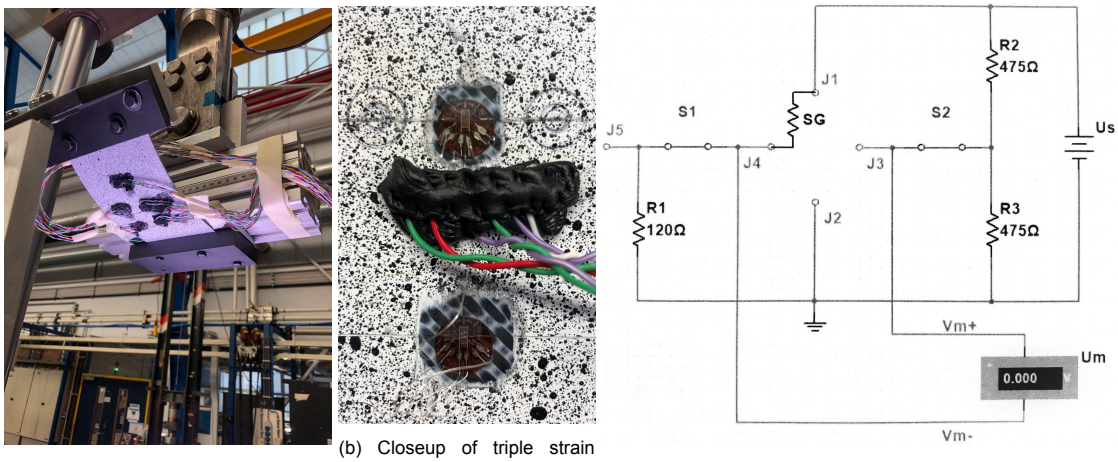

(a) Strain gauges on test sample

(b) Closeup of triple strain gauge (+45°, 0°, -45°)

(c) Keithley quarter bridge [33]

Figure 6.4: Strain gauges method for surface strain measurement

In Figure 6.4c, the system is powered by source U_s. The voltage measurement over the bridge is U_m and the bridge itself exists of three resistors (R_1, R_2 and R_3) and a strain gauge (SG). If the resistors have the values R_1 = 120Ω and R_2=R_3=475Ω and the gauge factor of the strain gauge is k = 2, the equation for the strain in percent $\epsilon_{\%}$ becomes very simple [33]. This is shown in Equation 6.11.

$$\epsilon_{\%} \approx -200 \cdot \frac{U_m}{U_s} \tag{6.11}$$

Strain gauges have the advantage of being very simple and reliable [39]. Also, the system at the DUT is able to link with the test machine which allows the strain gauge data to link with the test machine data. Therefore, this system is able to deliver measurements at the surface which can also be used during fatigue tests. The disadvantage in comparison to the DIC method is that strain gauges are local measurements. Multiple strain gauges indicate the strain at multiple locations, but it is not able to give a strain field as for instance a DIC system can. Also, applying strain gauges is rather labour intensive and the complexity of 24 strain gauges, as can be seen in Figure 6.4a, in enormous. All parts are very fragile which works poorly with the limited space available on the sample. However, the strain gauges are able to verify the results from the DIC system. These are the only two measurement methods which give insight in the strain at multiple locations on the surface of the samples.

6.5. Measurement E: Photographic comparison

The last of the five measuring methods is the usage of photographic and video imaging. This is the least specific measurement. By filming and photographing the samples, it is possible to investigate a sample on a specific moment without performing measurements at that time. Figure 6.5a is an example of a frame selected from a video. Using this image, it is possible to show the kinematics of the test set-up. For instance the straight lines drawn indicate the deflection angle and the curved line is a circle section, with which the skin bending can be compared to evaluate homogeneous bending. Besides the two highlighted measurements, this photograph can support the kinematic assumptions made in measurement methods 1 and 2 from Section 6.1 and 6.2.

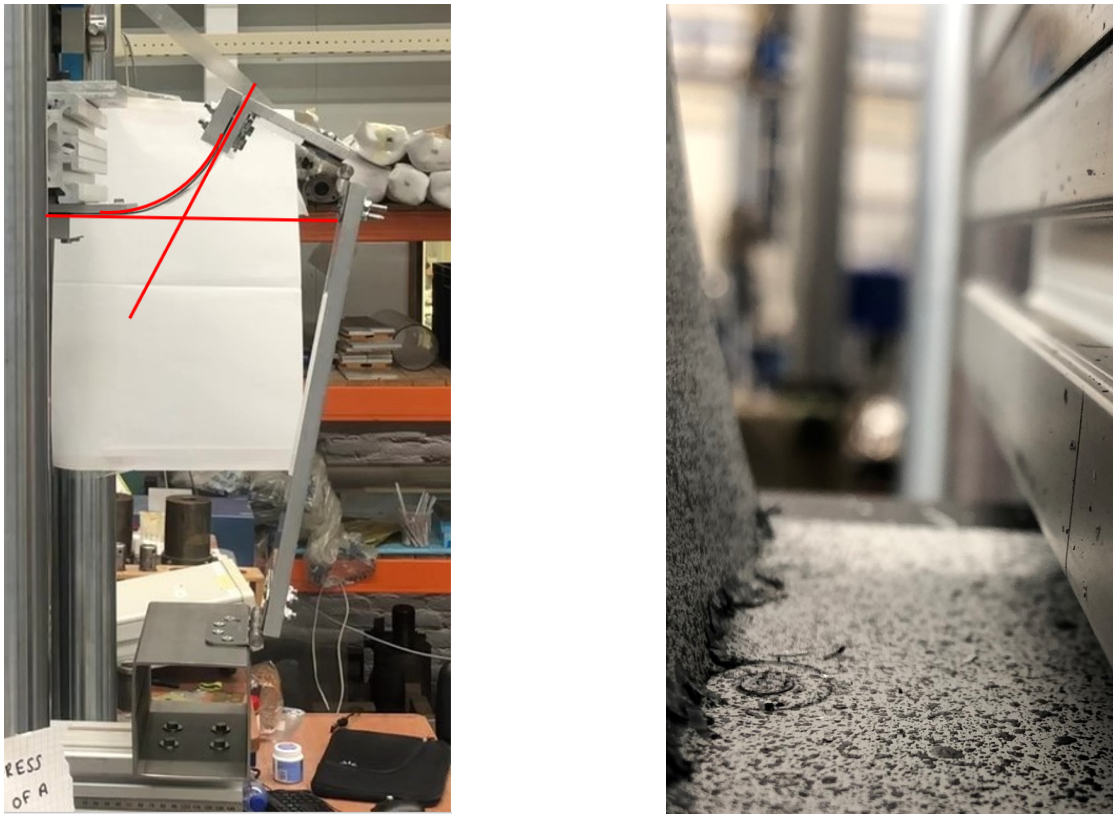

(a) Photograph from the side allows deflection angle and curvature analysis

(b) Photograph of a failed sample for failure analysis

Figure 6.5: Examples of photographic contribution to analyses

In Figure 6.5b an example is given of a photograph taken to analyse the failure mode. From such photograph, the location of the failed upper skin can be seen. In the example in Figure 6.5b the fracture is shown just in front of but also touching the rivet heads.

Other examples of this analysis method is video recording of a failure. This can later be watched again or even be analysed frame by frame. Video and photographic material allow to verify some things which come to the attention later in the analysis.

7

Results

The goals of the tests were to give an insight in the kinematics, the stress and the failure of the skin and the connection. The connection is not meant to influence the functionality of the skin and should not be critical. In order to investigate those goals, both static and dynamic tests are performed. This chapter will show the results in that order.

7.1. Static Test Results

The first section of this chapter discusses the static tests. Three sample lay-outs were tested during the tests. For each lay-out, three samples were produced, which led to a total of nine test samples. During the test design, one sample broke in a non-representative measurement which led to the first design iteration. This was described in Chapter 5. For the remaining tests, eight samples were available. Each of these samples has been statically tested multiple times. One reason for testing a sample multiple times, is to compare static test results before and after a fatigue test. Also, samples have been tested before and after the second design iteration. Before this iteration, the range of the test machine was 150 mm which was insufficient to fail the samples. During these tests, the measurements were limited to fatigue bench displacement and force as well as video material of the sample (Measurement Methods A, B and E). This way, no information could be gathered about the strain distribution across the surface. In the second iteration, the machine range was increased by adjusting the test procedure and the measurements were complemented with strain gauges and DIC as discussed in Chapter 6. Samples were tested before and after this iteration to obtain knowledge from the other measurement systems and some samples were tested until failure.

The combination of eight samples with multiple tests per sample and several measurement methods has led to a large amount of data from which results are produced. The graph in Figure 7.1 is purposely shown without context and legend as it is only intended as a basic example of the data. What can be seen in this figure is that many tests have been performed within the lower cross-head displacement regime from 0 mm to 150 mm. The tests which have been tested beyond this point were tested until failure which occurred between 250 mm and 270 mm displacement of the lower cross-head.

First the strain will be discussed as a result. Subsequently, the stress is elaborated on. These results must form an indication on the kinematic and structural behaviour of the skin and joint. The static test results will be closed by discussing the failure mode of the four samples which were tested until failure.

7.1.1. Strain

In four out of the five measurement methods discussed in Chapter 6, the strain is calculated using the deformation measurements. Only Measurement Method A calculates the stress in the outer layer and by dividing by the Young's modulus (E), the strains are achieved. Figures 7.2, 7.3a and 7.3b show examples of these measurements.

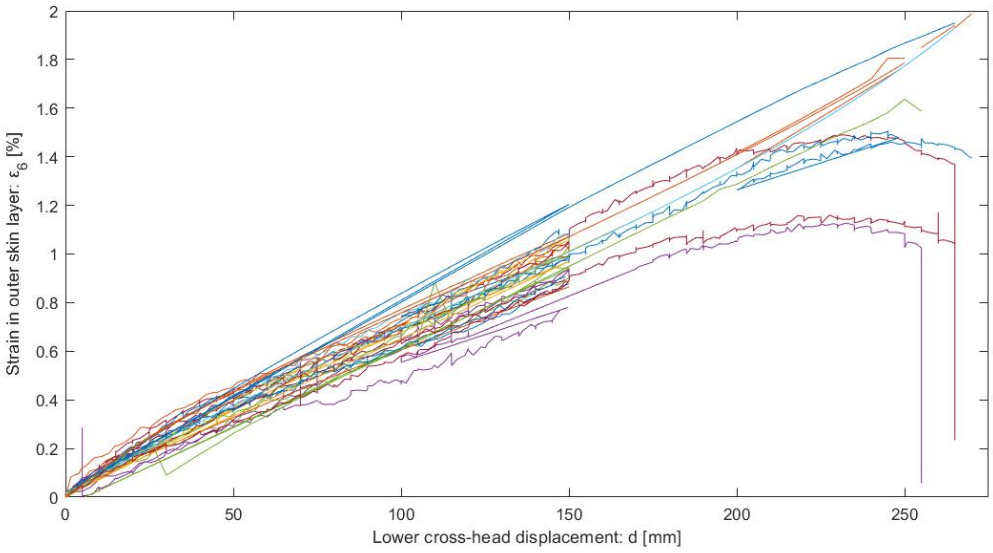

Figure 7.1: Strain of all tests using Measurement Methods A, B and D

The graph in Figure 7.2 has the machine lower cross-head displacement on the horizontal axis ranging from 0 mm to 275 mm. This represents the input variable of the static test. On the vertical axis, the strain in the outer skin layer is shown in percentage. The sample shown in this graph is 'C 4x05 3', which is the third sample of lay-out three. The samples and their respective lay-outs can be seen in Table 5.1. Sample 'C 4x05 3' has been tested three times. Also, three different measurement methods are represented in the graph. Table 7.2 is created to elaborate on the details of the codes found in the legend of Figure 7.2, to clarify which combination of sample test and measurement method is indicated by a line in the graph.

Table 7.1: Sample code explanation

Sample code	Lay-out(Figure 5.1)	Sample
A 3x05 2	1	2
A 3x05 3	1	3
B 3x06 1	2	1
B 3x06 2	2	2
B 3x06 3	2	3
C 4x05 1	3	1
C 4x05 2	3	2
C 4x05 3	3	3

In the graph in Figure 7.2, the solid lines represent measurements which have been performed using Measurement Method A, explained in Section 6.1. Measurement Method A deducts the stress in the sample from the input load and displacement, and divides this stress by the Young's modulus to find the strain. The dashed lines in the graph show the measurement explained in Section 6.2 (Measurement Method B). This method measures the input machine displacement and calculates the theoretical strain. The last group of measurements shown in the graph use Measurement Method D, which are strain gauges. These measurements are discussed in Section 6.4 and are presented in the graph by the dotted lines. This information is also shown in Table 7.2.

The results in Figure 7.2 show that the measurement systems are rather consistent. Across the three different tests and three measurement methods the scatter of the data does not exceed 0.1% strain up until the cross-head displacement of 200 mm. This scatter can be caused by measurement noise. Until 200 mm cross-head displacement, the scatter is sufficiently compact to determine the trend

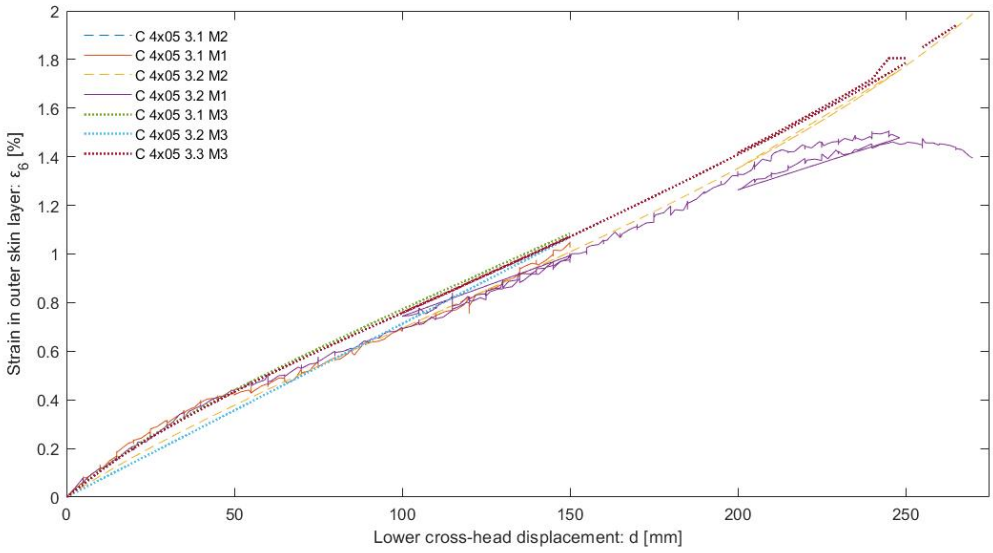

Figure 7.2: Strain C 4x05 3, Measurement Methods A, B and D

Table 7.2: Legend support for Figure 7.2

Legend code	Lay-out (Figure 5.1)	Sample	Test	Measurement Method	Section	Lines
C 4x05 3.1 M2	3	3	1	B: displacement	6.2	dashed
C 4x05 3.1 M1	3	3	1	A: force and disp.	6.1	solid
C 4x05 3.2 M2	3	3	3	B: displacement	6.2	dashed
C 4x05 3.2 M1	3	3	3	A: force and disp.	6.1	solid
C 4x05 3.2 M3	3	3	2	D: strain gauges	6.4	dotted
C 4x05 3.2 M3	3	3	2	D: strain gauges	6.4	dotted
C 4x05 3.3 M3	3	3	3	D: strain gauges	6.4	dotted

and magnitude of the measurements. However, from the 200 mm point on the x-axis one measurement method separates from the others. This is Measurement Method A, which does not calculate the strain from deformation. It converts stress into strain by means of the Young's modulus. A potential explanation for this deflection will be discussed in Chapter 8.

Two other measurement methods were used: DIC and Strain Gauges. These should be able to confirm which measurement is correct. In Figure 7.3 the results of the two other measurement methods are shown for the same sample (C 4x05 3). Both sub-figures present their measurements at the moment just before failure of the sample and thus correspond to a lower cross-head displacement (d) of 270 mm. Figure 7.3a presents the DIC measurement and Figure 7.3b represents the validation measurement by means of a photograph of the test. The contour of the sample cannot be seen in the latter Figure but it does indicate the deflection angle of the skin.

The DIC results show more than just a strain value at one location, as for instance the results in Figure 7.2 show. It displays a strain field which gives an insight in the strain progress. Even in the case of Figure 7.3a where only a partial strain field is shown due to the presence of the strain gauges. The Figure shows a gradient for the strain levels in the skin length direction. The strain is quite evenly divided over the bend surface but increases when approaching the edge of the plate on which the skin is mounted. At this edge, the strain is highest. As indicated by the colour bar legend, the strain at this point measures about 20,000 microstrain. This is very similar to the data represented by the two upper lines in Figure 7.2. The strain beyond the fastener row is close to zero.

The angular deflection shown in Figure 7.3b is in direct relation with the strain as shown in Section 6.1 and 6.2 as long as the bending is circular. Rather than calculating the angular deflection, the frame from a video recording allows a direct measurement of the angular deflection. Images such as shown in Figure 7.3b have been checked for different stages of the test and have validated the strain measurements represented by the upper two curves in Figure 7.2.

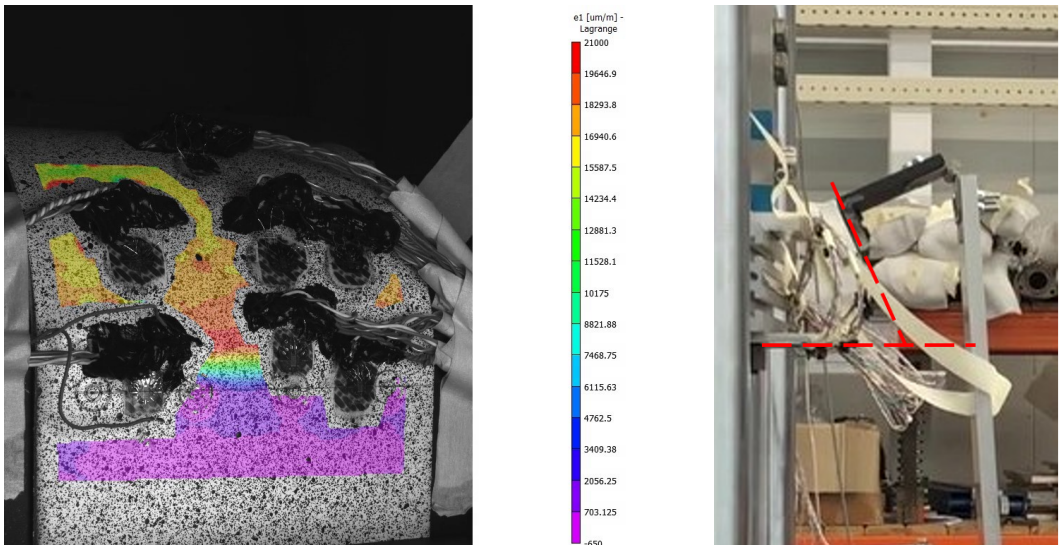

(a) Strain C 4x05 3, measurement method C

(b) Angular deflection C 4x05 3, measurement method E

Figure 7.3: Strain in C 4x05 3 via DIC and Angular deflection

The static results shown in Figures 7.2 and 7.3 are representative for the other results. Table 7.3 shows measurement data of the other tests. In Appendix C, the graphical representation of these tests can be observed in a similar manner as in the above figures. By displaying them as such, it is possible to see trends whereas a table only gives interval values.

In addition to these results, the last set of results are two strain fields of skin sections which are not interrupted by strain gauges. These strain fields give more insight in the behaviour of the skin as a whole. Both samples in Figure 7.4 are bend by a cross-head displacement (d) of 150 mm.

In Figure 7.4a, a sample with three of the smallest rivets has been shown while it is bend down. It can be seen that, similar to the earlier discussed DIC image, the strain near the support plate is increasing. What is new in this image is that the behaviour in front and behind the fasteners is different than the behaviour between the fasteners. The strain between the fasteners is more evenly distributed. Strain peaks can be observed in front of the fasteners. In Figure C.2a in Appendix C the other measurement methods of this sample have been presented. At the same bending situation, the strain measurement is about 1%. The local peak strain of 1.3% presented by Figure 7.4a is significantly above that.

In Figure 7.4b, a sample is shown when it is bend in the other direction, away from the structural plate. This corresponds to an upwards tab setting. The sample shown here is one with three of the larger fasteners. The DIC analysis does not show the outside surface of the skin as this was impossible for the camera set-up. In the upwards tab setting, the skin is not bent over the edge of the support plate but away from the plate. The fasteners must directly cope with the loads. The DIC image in Figure 7.4b, shows a similar strain distribution compared to the same section in Figure 7.4a. The strain of the sample in Figure 7.4a is only slightly higher than the strain of the sample in Figure 7.4b. The difference is about 1000 microstrain. This can be seen by comparing the strain at the same location on the samples. Just below the strain gauges (which are both placed at the same distance from the rivets and placed in the centre of the sample), the strain for sample 'A 3x05 3' is between 9500 and 10,375 microstrain as it is indicated by yellow. The strain at this location for sample 'B 3x06 2' is between 8450 and 9100 microstrain as it is indicated by orange on its own scale. A possible explanation for the difference is discussed in Chapter 8.

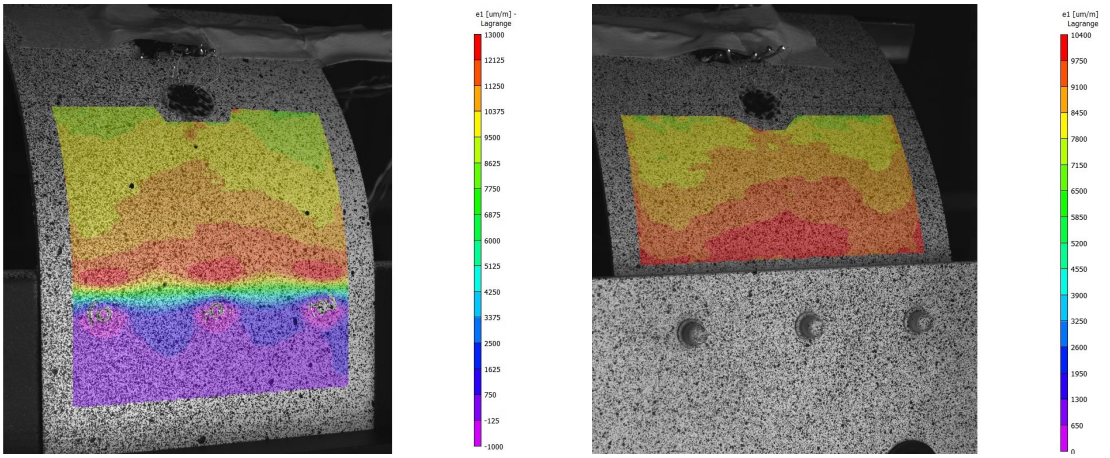

(a) Downwards bend A 3x05 3

(b) Upwards bend B 3x06 2

Figure 7.4: Upwards and downwards DIC Measurements

The DIC measurement confirms that Measurement Method A indicates a wrong strain above a cross-head displacement of 200 mm. The strain results from the other measurements (B, C, D and E) are therefore considered when discussing strain results further more. The well established conversion between stress and strain by means of factoring the Young's modulus must therefore be discussed. This is done in Chapter 8.

7.1.2. Stress

Stress is something which cannot be measured directly. The most common method is to measure deformation and calculate the strain. This strain can be converted in stress by means of multiplication with the Young's modulus. This is the method used in four of the five measurements in this thesis. The other measurement method, uses the applied load of the test machine and calculate the stress at the joint. This method is explained in Section 6.1. The method is also used to measure the strain in Section 7.1.2. Therefore, the only difference between the results of the strain and the stress measurements is the Young's modulus (E) of 58 GPa [4] times the sinus of 45^o because of the fibre direction in the outer layer of the skin. The Young's modulus is further discussed in Chapter 8.

The results of the stress measurements are therefore congruent to the results of the strain measurements. This can be seen by comparing the graph in Figure 7.5 to the graph in Figure 7.2.

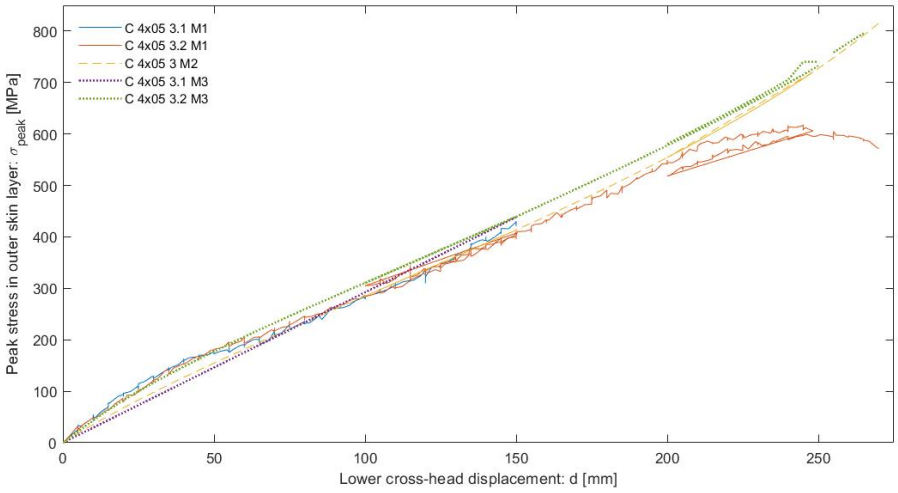

Figure 7.5: Stress C 4x05 3, Measurement Methods A, B and D

In Section 7.1.1, no conclusion has been drawn or potential causes enlightened as this is something for the next two chapters. It was however apparent that the Measurement Method A is similar to the other measurements until failure loads are approached. Above a cross-head displacement of 200 mm, the measurement methods deviate. All measurements can be used below 200 mm above this value, Measurement Method A should be used to avoid the conversion between stress and strain by means of the Young's modulus as this seemed to be the problem in the strain measurements. For completion, also Measurement Methods B and D are shown in the graphs. The data from the DIC and the video material is not discussed separately in this section as it does not contribute to unique results.

The graph in Figure 7.6, shows that the required ultimate load can be reached. This was set to be 350 MPa of load in the outer surface layer of the skin and is indicated by the green line. By any measurement method and for any sample, this load is reached without failure.

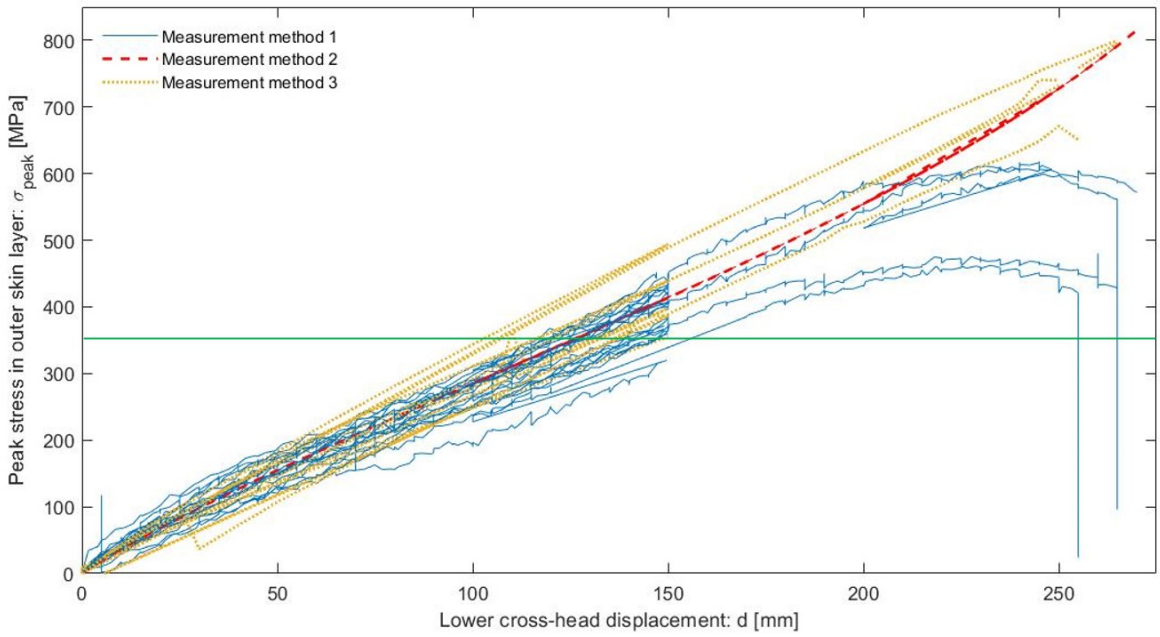

Figure 7.6: Stress measurements using Measurement Methods A, B and D

In Figure 7.7 a graph is shown which presents the stress measurements of the first measurement method for all samples from 0 mm to 150 mm. The data is divided between upwards bend and downwards bent samples, which are respectively indicated by yellow x-signs and blue o-signs. When this data is fit with a linear model, it can be seen that the upwards bent samples experienced less stress compared to the downwards bent samples. In Chapter 8, the reason for this difference is discussed.

Additional stress and strain data are shown in detail in Appendix C. However, the most important data is given in Tables 7.3 and 7.4. Table 7.3 provides the average stress and strain values at 50 mm, 100 mm and 150 mm of lower cross-head displacement. Table 7.4 gives information on the failures. The strain values are the average values of Measurement Methods B and D and the different tests per sample. The stress values are the averages of the different tests per sample measured by Measurement Method A. The machine displacement is an output of the test machine and the deflection angle is calculated using the method described in Measurement Method A and B.

7.1.3. Failure Mode

In this section, two samples are shown once they are failed. In Figure 7.8, the failure is shown for a sample which is bent in a situation representative of a downwards tab bend. Figure 7.9 shows a failure for the opposite bending situation. Both samples are represented by a picture to indicate their position when they failed, a close-up from the surface and a close-up from the side which may potentially indicate the origin of failure.

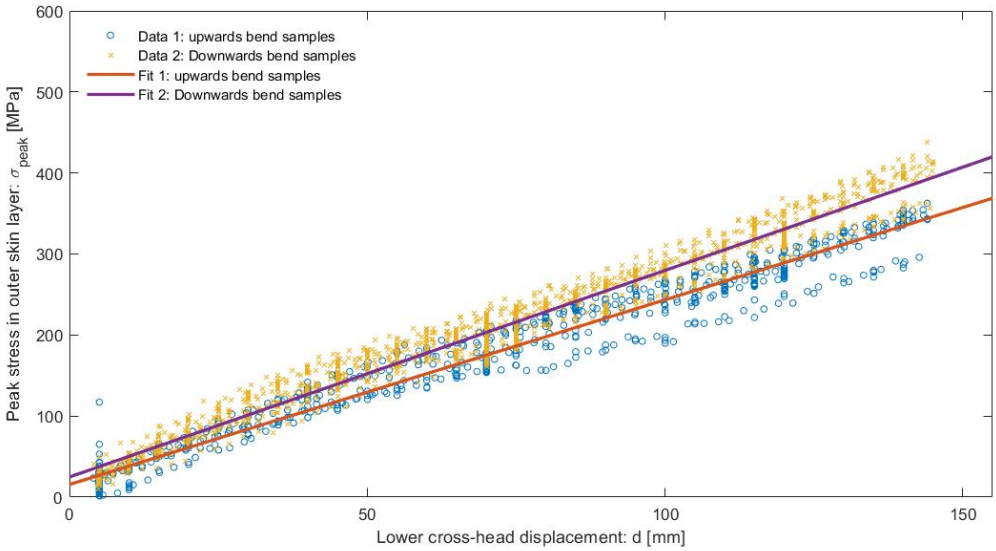

Figure 7.7: Stress in upwards vs downwards bending tests

Table 7.3: Average stress and strain of values of all test samples

Machine displacement (d)	50 mm		100 mm		150 mm	
Deflection angle (α)	23^o		42^o		62^o	
Sample code	ϵ_{ave} [%]	σ_{ave} [MPa]	ϵ_{ave} [%]	σ_{ave} [MPa]	ϵ_{ave} [%]	σ_{ave} [MPa]
A 3x05 2	0.3772	164.56	0.6954	282.17	1.0085	408.84
A 3x05 3	0.3772	146.68	0.6947	282.84	1.0083	427.76
B 3x06 1	0.3772	157.00	0.6939	269.15	1.0084	371.87
B 3x06 2	0.3766	159.10	0.6949	265.89	1.0084	435.05
B 3x06 3	0.3800	123.28	0.6949	212.60	1.0067	319.90
C 4x05 1	0.3764	154.47	0.6960	263.94	1.0069	387.21
C 4x05 2	0.3783	127.75	0.6947	249.24	1.0090	389.11
C 4x05 1	0.3773	177.90	0.6946	285.45	1.0083	413.91

Table 7.4: Failure values of failed samples

Sample code	Machine displacement (d) [mm]	Deflection angle (α) [°]	Average stress (ϵ_{ave}) [%]	Average strain (σ_{ave}) [MPa]
A 3x05 2	265	119	1.931	561
B 3x06 3	255	109	1.824	420
C 4x05 2	265	119	1.922	427
C 4x05 1	270	123	1.980	572

Additional information on the failure is that the failure was preceded by cracking noises. The first observations of cracking sounds occurred at about 170 mm of cross-head displacement. With increasing deformation of the sample, the frequency of the cracks increased as did the volume of the cracks. Yet, no visible damage could be detected. All failures eventually occurred in the following sequence of events. The cross-head was moved with the usual increments of 5 mm. At some point the cracking occurred semi-continuous. Even when the cross-head was kept stationary the cracks continued. No damage could be seen on the sample. The cracking intensified and suddenly, the sample snapped. The damage occurred on the outer plies of the skin. The middle plies kept the sample together but the structural rigidity was obviously compromised.

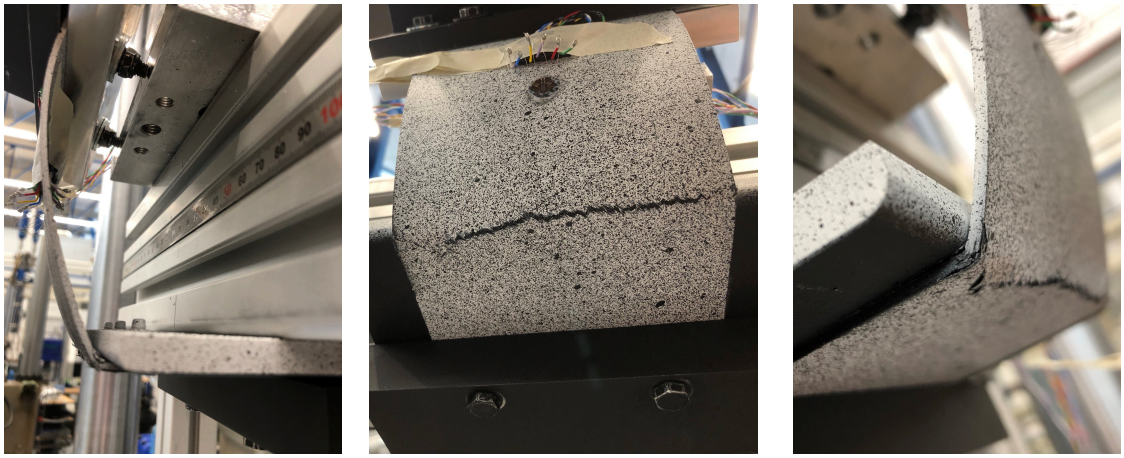

(a) Side view (b) Skin fracture close-up surface (c) Skin fracture close-up side

Figure 7.8: Downwards bend failure

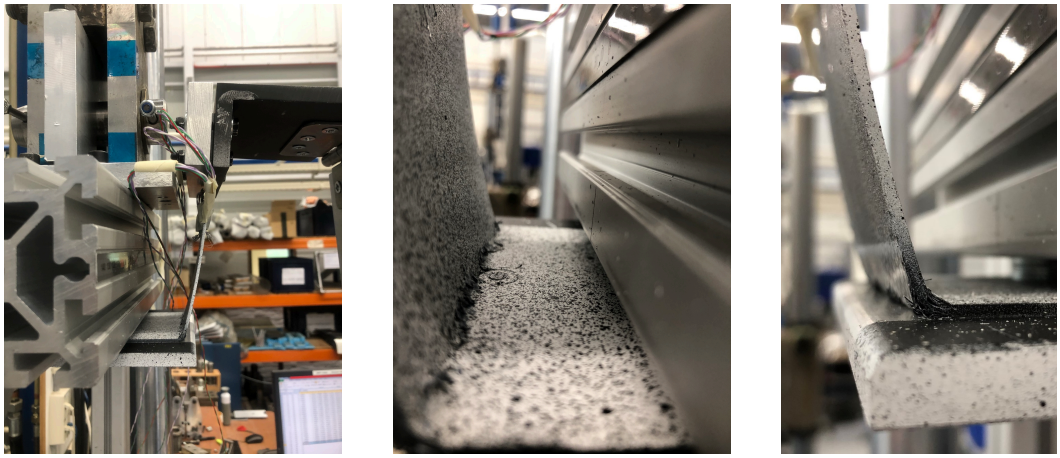

(a) Side view (b) Skin fracture close-up surface (c) Skin fracture close-up side

Figure 7.9: Upwards bend failure

7.2. Fatigue Test Results

The skin has been subjected to extensive fatigue testing. The goal of the dynamic tests the joint is to indicate that the connection does not contribute to a decrease in fatigue life. In order to investigate this, machine loads and displacements are used as measurement methods as well as the video imaging. Measurement Methods A, B and E, discussed in Chapter 6 are thus available. DIC and Strain gauges have not been applied to the fatigue tests as explained in Chapter 6.

Due to the time required to perform a dynamic test and the limited resources, such as machine time, only three dynamic tests have been performed. These three dynamic test have all been performed on the same machine but were tested with different amplitudes in order to gather as much information as possible. This is sufficient to compare the tested connection to the skin dynamic tests. It will however not be possible to create an entire S/N-graph for the joint. As the test have been performed slightly different for each sample, in this section the tests themselves are described and the results are shown for the three dynamic tests separately.

7.2.1. Fatigue A 3x05 3

The first fatigue test is performed using a test sample with three small fasteners. The sample is coded 'A 3x05 3' and details on the sample can be found in Table 7.1. For this fatigue test, the initial test set-up was used shown in Figure 5.2. This test allowed two way bending which was closest to the

usage of the connection in real life. The skin was clamped in the neutral (0°) position with the machine displacement in the middle of its range. This allowed the machine to reach a deflection angle of 22^o in both directions. This deflection angle corresponds to a strain of 0.35% and a peak stress in the outer layer of 150 MPa. Although this is a limited load situation, the situation is representative for the usage. One cycle exists of moving from the 0^o position to the maximum deflection on one side. Then moving from that position all the way to the other maximum deflection and then back to the zero position.

The data of this fatigue test can be seen in Figure 7.10. On the x-axis of the graph the amount of cycles is given. On the y-axis, the force required for the sample to be bend in the maximum deflection angle is given in N. The raw result of the fatigue test is given by the blue line. As described in Chapter 6, the zero level of this force output has noise of about 25 N which is within the noise spectrum of the machine [21]. This is because this machine is able to perform fatigue tests with up to 250 kN of load. The data could be cleaned by investigating the relative load within a cycle rather than the load with respect to the zero setting which experiences the noise. This is showed a very consistent result. In Figure 7.10 the transition can be seen between the data before and after cleaning. The blue line indicates the fatigue data. The orange and yellow line respectively show the maximum and minimum load per cycle. After cleaning the data from noise the maximum and minimum are indicated by the red and green line respectively.

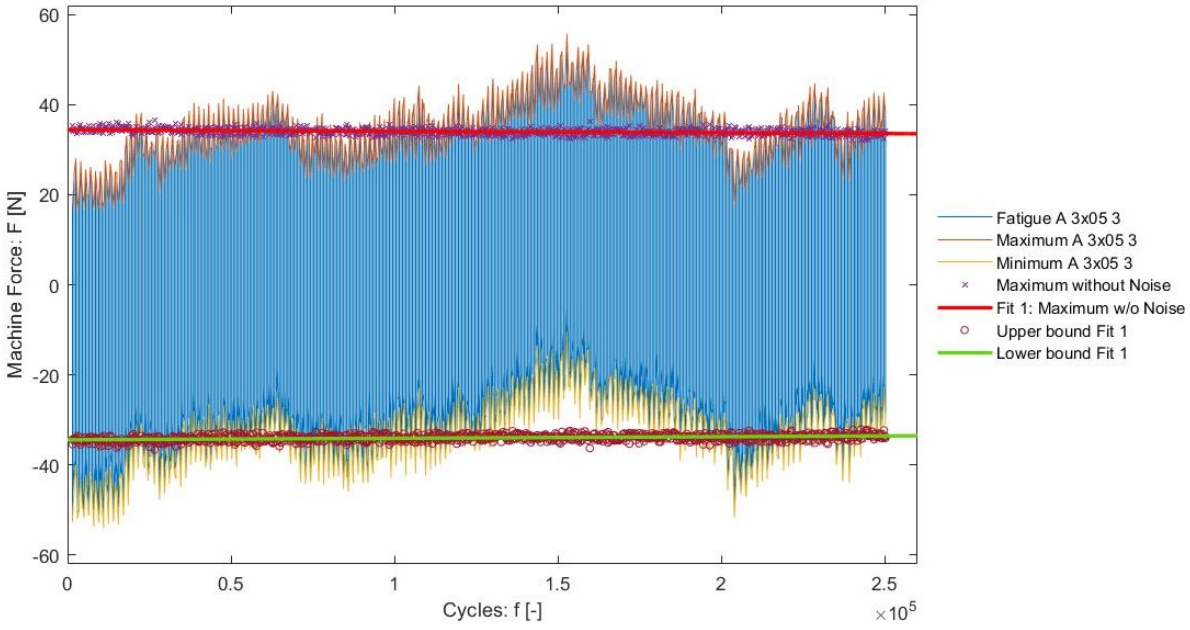

Figure 7.10: Fatigue test data of Sample A 3x05 3

The formula of the fit is shown in Equation 7.1. In this Equation, the first term represents the initial force required for the skin to be bend in the 22^o position. The second term, which is dependent on the cycle count (f) shows the degradation of this load per cycle.

$$F = 34.427 - 3.4351 \cdot 10^{-6} \cdot f \tag{7.1}$$

Equation 7.1 can be used to determine the amount of cycles it takes for a certain degradation to occur. Assuming, a stiffness degradation of 5% constitutes failure, similar to the skin, the formula can be used as shown in Equation 7.2. From this equation it can be deducted that more than half a million cycles are required for a stiffness degradation of 5%.

$$
\begin{aligned}
F &= 34.427 - 3.4351 \cdot 10^{-6} \cdot f \\
0.95 \cdot 34.427 &= 34.427 - 3.4351 \cdot 10^{-6} \cdot f \\
f &= \frac{0.05 \cdot 34.427}{3.4351 \cdot 10^{-6}} \\
f &= 5.0109 \cdot 10^{5}
\end{aligned}
\tag{7.2}
$$

7.2.2. Fatigue B 3x06 1

In order to test the sample to higher deflection angles, the test set-up in this and the next fatigue test have changed compared to the previous discussed fatigue test. In essence, the fatigue tests on samples 'B 3x06 1' and 'C 4x05 1' are one-sided fatigue tests with an amplitude of 150 mm with a frequency of 2 Hz. The test set-up is shown in Figure 5.5. In the 150 mm displacement position the skin at the connection experiences a strain of about 1% and a stress of about 400 MPa in the outer layer of the lay-up. The deflection angle of the skin is 62^o in that situation.

The difference between test of sample 'B 3x06 1'and the test of sample 'C 4x05 1' is that during the 'B 3x06 1' test the sample started with upwards bending. After about 5000 cycles, the sample was turned over to be tested for downwards testing. After about 23000 cycles the sample was put back in it's original position. In the test of 'C 4x05 1' the sample has been tested with a downwards bend for the entire test. The other difference is the sample that was used. The details of the samples can be found in Table 7.1 but the difference comes down to three larger versus four smaller fasteners.

The lay-out of the graph is the same as in the first test. Also, the same data processing has been performed in this test. Which has resulted in the graph shown in Figure 7.11.

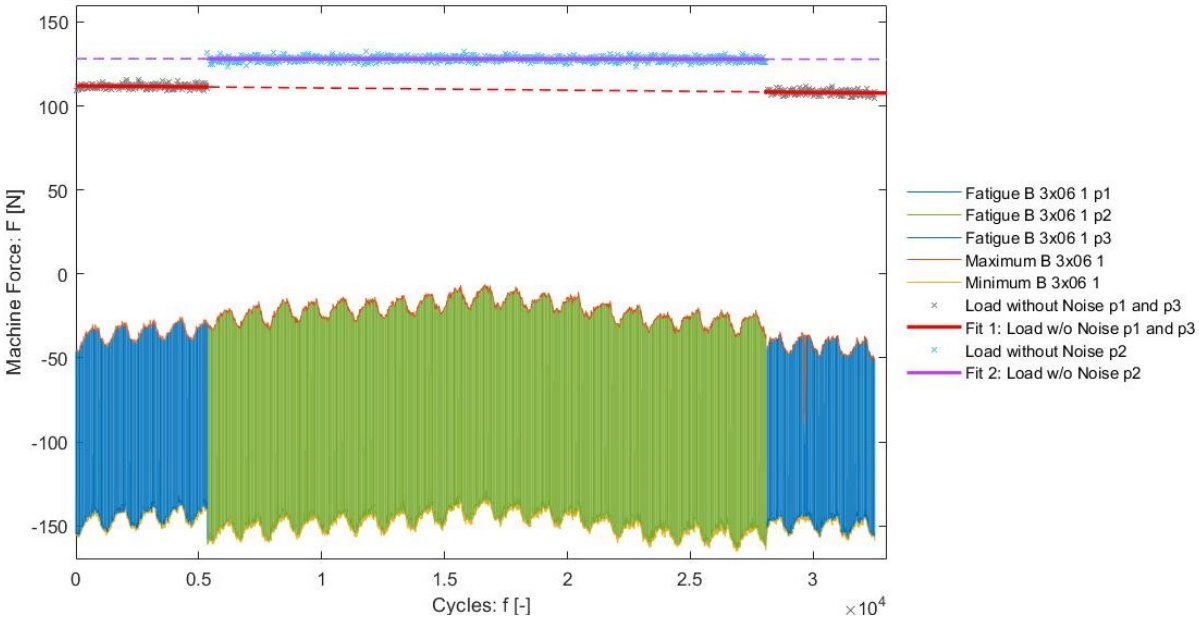

Figure 7.11: Fatigue test data of Sample 3x06 1

Due to the two loading situations and the significant difference in stiffness between these two bending directions, two data sets have been generated. One to measure the degradation in the upwards bending direction and one for the degradation in the downwards bending direction. Both these graphs have been fitted with a linear model. This has resulted in Equation 7.3 for the upwards bend and Equation 7.4 for the downwards bending data.

$$F_1 = 112.0245 - 1.3204 \cdot 10^{-4} \cdot f_1 \tag{7.3}$$

$$F_2 = 128.1210 - 8.6526 \cdot 10^{-6} \cdot f_2 \tag{7.4}$$

Similar to the method of the first fatigue test, this test is evaluated for 5% stiffness reduction. This is shown in Equations 7.5 and 7.6. The result is 42,000 and 740,000 cycles respectively. In Section 8 this large difference will be discussed. Overall the smallest cycle count will be critical and therefore the fatigue limit is 42,000 cycles.

$$\begin{aligned} F_1 &= 112.0245 - 1.3204 \cdot 10^{-4} \cdot f_1 \\ 0.95 \cdot 112.0245 &= 112.0245 - 1.3204 \cdot 10^{-6} \cdot f_1 \\ f_1 &= \frac{0.05 \cdot 112.0245}{1.3204 \cdot 10^{-6}} \\ f_1 &= 4.2422 \cdot 10^4 \end{aligned} \tag{7.5}$$

$$\begin{aligned} F_2 &= 128.1210 - 8.6526 \cdot 10^{-6} \cdot f_2 \\ 0.95 \cdot 128.1210 &= 128.1210 - 8.6526 \cdot 10^{-6} \cdot f_2 \\ f_2 &= \frac{0.05 \cdot 128.1210}{8.6526 \cdot 10^{-6}} \\ f_2 &= 7.4036 \cdot 10^5 \end{aligned} \tag{7.6}$$

7.2.3. Fatigue C 4x05 1

The explanation of this fatigue test is given in the previous section (7.2.2). This results in the graph shown in Figure 7.12.

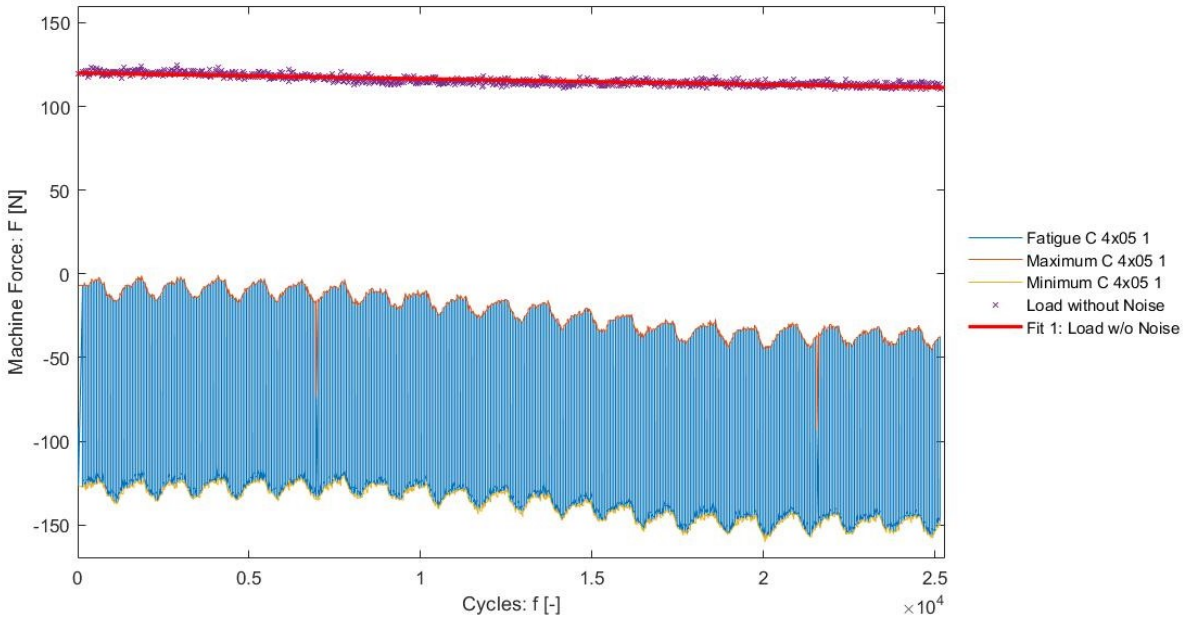

Figure 7.12: Fatigue test data of Sample C 4x05 1

The fit which represents the data gathered from this test and processed for the null load variation, can be represented by Equation 7.7.

$$F = 119.9210 - 3.3935 \cdot 10^{-4} \cdot f \tag{7.7}$$

To evaluate the sample for 5% stiffness degradation, Equation 7.8 is constructed. The result of this equation is that this degradation already occurs after about 17,500 cycles. The test has run beyond that amount of cycles and no other failure has occurred besides the stiffness loss. In Chapter 8, this data shall be discussed.

$$\begin{aligned} F &= 119.9210 - 3.3935 \cdot 10^{-4} \cdot f \\ 0.95 \cdot 119.9210 &= 119.9210 - 3.3935 \cdot 10^{-4} \cdot f \\ f &= \frac{0.05 \cdot 119.9210}{3.3935 \cdot 10^{-4}} \\ f &= 1.7669 \cdot 10^{4} \end{aligned} \tag{7.8}$$

8

Discussion

In this section, the results shown in Chapter 7 is discussed. In this chapter, the order from Chapter 7 is maintained. This means that the static tests is discussed first with the strain, stress and failure modes in that order. A sub-section (Sec. 8.1.1) is added in the beginning of the Static Test Result section. In this subsection, the Young's modulus will be discussed as it is the basis of some discrepancies in the stress and strain results. The chapter will then discuss the fatigue results which are subdivided in the three dynamic tests.

8.1. Static Test Results

8.1.1. Young's Modulus

The Young's modulus is a mechanical property which represents the resistance of material against deformation by means of elongation [22] which is material dependent. Based on the material properties report of the test samples, the Young's modulus is equal to 58.0 GPa [4]. In Section 7.1.1, multiple measurement methods for the strain are shown. One of these method calculated the stress in the sample based on the input force of the machine. To obtain the strain, the Young's modulus could be used as this represents the relation between stress and strain. The strain calculated by this method matched the other strain measurements well until a displacement of about 200 mm. From this point on the strain indicated via this measurement, gradually diverged from the linear relation measured by the other methods.

The shape of the deviating curve was very similar to a general stress-strain curve. The first part of the curve is linear, after which the material properties degrade and more strain can be produced at less stress. This effect increases and eventually the material fails. The high similarity in shape became the leading reason to expect damage to be the cause of the deviation.

During the test, a form of cracking was noticed from about 170 mm machine displacement. This is discussed in Section 7.1.3. This cracking intensified as the sound was noticed more frequently and louder with further deformation of the skin. The cracking itself may indicate material damage. The intensifying cracking sounds may indicate that the material degradation does not only continue with further deflection but even accelerates.

In order to investigate the effect of the damage which is expected due to these observations, the Young's modulus degradation is investigated. This is presented in Figure 8.1. The graph contains measurements using Measurement Method B for all samples. On the x-axis, the lower cross-head displacement is shown. No values before a displacement of 80 mm are shown because in this part no material damage occurred, which is also the case for the data between 80 mm and 170 mm. On the y-axis, the residual relative Young's modulus is shown. The blue dots are measurement point in which the stress is measured and divided by the correct strain. The red line is a quadratic polynomial fit of this data. It can clearly be seen that the fit is relatively flat in the beginning at about 100% of the original value. When the material is degrading, the Young's modulus goes down as well. At the point of failure

(255 mm to 270 mm), the residual Young's modulus is only about 70% of its original value of 58 GPa which is approximately 40 GPa.

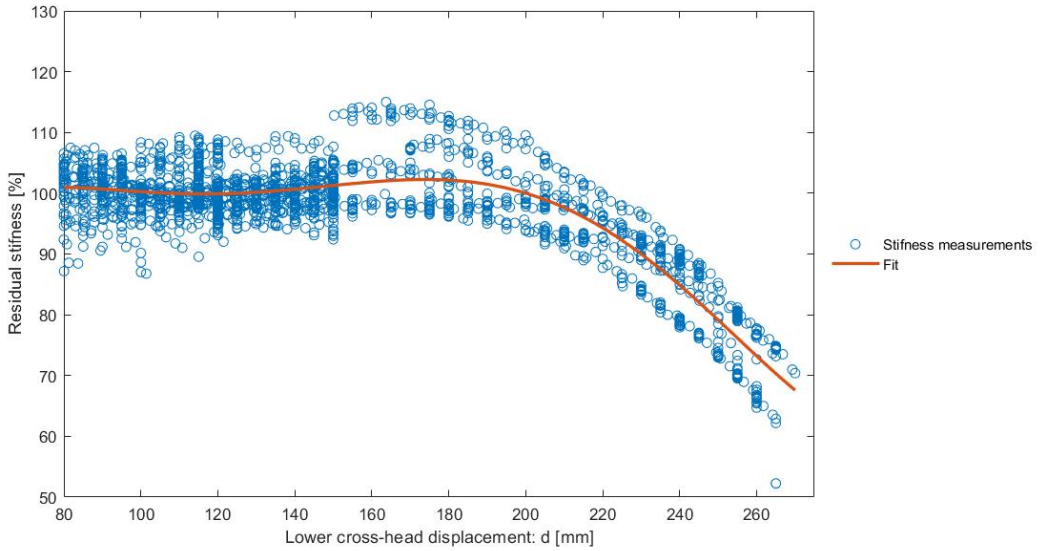

Figure 8.1: Young's modulus degradation

The material degradation indicates that the conversion between stress and strain using a constant Young's modulus does not give accurate results for deflections larger than 200 mm. There has not been a sufficient amount of tests to establish accurate values for the Young's modulus once material degradation has started. Therefore, the Young's modulus for conversion between stress and strain values from a displacement of 200 mm cannot be used. This means that for strain measurements the four measurement methods which indicated a linear trend are considered accurate. For the stress values at a displacement of more than 200 mm, only the method which uses the input force does not use the Young's modulus and is therefore accurate.

8.1.2. Strain

In Section 8.1.1, the strain results have shown the degradation of the sample material. In this section, the effect of the fasteners on the bending profile is discussed based on the strain results. Subsequently, the DIC results are used to discuss local strain differences. Finally, the difference between upwards and downwards bending is discussed.

Morphing skin bend

The second measurement method only uses the machine displacement as a measurement and theoretically approaches what the deflection angle of the skin and the strain in the skin will be in case of perfect circular bending. When this method is compared the strain measurements by the strain gauges, they seem to match fairly close. The average strain on the skin measured by the strain gauges also match the expected strain values. This indicates continuous bending as the method using the assumption seems to match other measurement methods. However, the DIC measurements shows that the strain over the surface is not uniform. Uniform bending would lead to a uniform strain field. Therefore, it can be reasoned that the skin bend does not have local bending to such extend that the tab setting is changed, but that the morphing skin is not curved perfectly uniform. The requirement is that the skin contour should not deviate for more than 1 mm from the the intended circular bend at nominal load as explained in Chapter 2. The DIC results at nominal load does not indicate an entirely uniform strain distribution. It is difficult to calculate how much the skin contour deviates from the intended circular bend using DIC. Therefore, the last measurement method is used, which is the video material from the side of the test. If the skin in video at nominal load is compared to a circle element, no clear deviation is visible. The effect of local bending does increase above nominal load, but that is allowed. These results indicate that the rivets do not interfere with the functionality of the tab in nominal load conditions.

Fastener surrounding

When investigating the close surroundings of the fasteners by means of DIC, it sometimes shows local strain peaks. This can be seen in Figure 8.2. What also can be observed, is that these peaks are only one colour gradient different to other sections in width direction. This indicates that the peaks are not very severe and the stress/strain concentration factors are limited. This could indicate that fasteners do not have a high impact on the resistance of the skin to static loading.

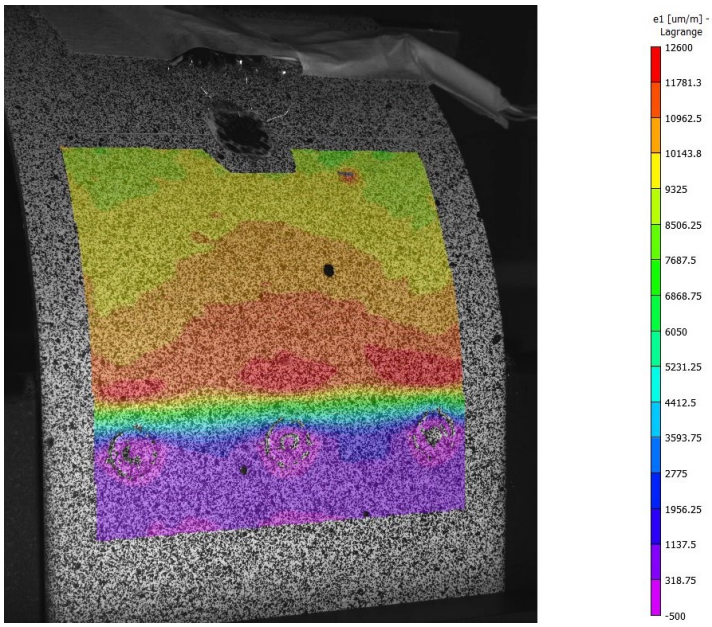

Figure 8.2: Local strain peaks surrounding the fasteners

The colour code on the fasteners themselves and the skin between and behind the fasteners indicates that no significant strain can be measured there. This implies that the fasteners have no in-plain deformation, which implies that the fasteners are sufficient in numbers to prevent large local deformation behind or in between the fasteners.

Upwards vs. downwards bending

In Chapter 7, Figure 7.7 was shown. This figure indicates a difference in strain between upwards and downwards bending of the skin. When upwards bending is induced by a certain amount of cross-head displacement, less strain was measured compared to downwards bending with the same cross-heard displacement. This is caused by the fact that the bending direction determines the length of the skin which is able to morph. In Figure 8.3, the green lines indicate the location at which bending is possible for both upwards and downwards bending. It can be seen that for upwards bending, this is at the edge of the fastener whereas for downwards bending this location is at the edge of the supporting structure. This is the case at both ends of the flexible skin. The difference in length of the skin which is able to bend is therefore twice the edge distance minus the head diameter of the rivet. This distance is dependent on the rivet diameter. Equation 6.1 shows the relation between the skin length and the bending radius. The effect of this bending radius on the strain is shown in Equation 6.9. The combination of these relations explain the difference in strain for the two bending directions.

The effect of this different strain can be seen in samples which have been tested in two directions. This can be seen by the large scatter between measurements 'C 4x05 2.1' and 'C 4x05 2.2' in Figure C.7a. The effect can also be observed in Figure 7.11. For the same cross-head deflection, more load is required for downwards bending compared to upwards bending. This is because the strain and the required input force are linked. This is explained in Section 6.1.

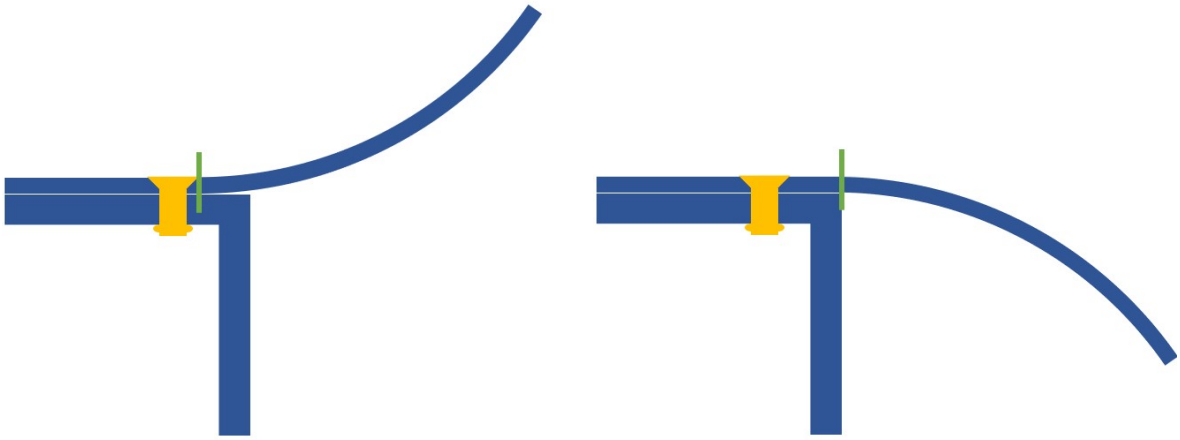

(a) Upwards bend (b) Downwards bend

Figure 8.3: The cause of the difference between upwards and downwards bending: different length of bend skin

8.1.3. Stress

The discussion on the Young's modulus in the beginning of this chapter, explains the difference is stress measurements between the measurement methods. The different measurements function well for the linear part of the stress-strain curve. Above 200 mm lower cross-head displacement, the measurement which uses the machine force input is the most accurate.

The stress results for static testing are positive as the failure levels are sufficiently high to meet the structural skin buckling requirement. No failures were observed below 350 MPa of stress in the outer skin layers as is shown in Figure 7.6. Statically the samples meet the structural stress requirements.

8.1.4. Failure Mode

The combination of failure characteristics shown in 7.1.3, confirms that it is the skin which has failed and not the fasteners. The bending moment becomes too high for the outer layers to be able to cope with the stress. When observing the failed samples, the outer layers are broken while the inner layers are still intact.

The observed cracking discussed in Chapter 7 are an indication of small sections within the sample which start failing. The structural degradation further increases the load on the other parts, which explains why the displacement did not have to be further increased to obtain failure.

The fracture occurs at the location of the highest strain, as can be observed by comparing the figures of the fractures with the DIC images. For downwards bending this location is at the edge of the support plate. For upwards bending it is at the edge of the joint as shown in Figure 8.3. These locations are for both bending directions at the edge of the morphing area. Other joining methods would most likely also fail at the edge of the flexible skin. This may imply that selecting another joining method would not significantly improve static test results. Other methods would still need to be tested. Also, the fasteners outperformed the other joining methods on selection criteria such as maintainability. Therefore, the static test results do not support changing to another joining method.

8.2. Fatigue Test Results

During the investigation into the skin fatigue behaviour for four-point bending a S/N-curve has been generated. In this research two types of samples were tested. The first samples were in pristine condition. The second type of samples had BVID inflicted to them before testing. Two failure levels were created. At the first failure level, the sample was considered failed if the residual stiffness of a sample was 95% of its original stiffness. The second failure level allowed 10% stiffness reduction which means a residual stiffness level of 90%. Therefore the research had four types of results:

A started as pristine and considered failed at 95% residual stiffness

B started as pristine and considered failed at 90% residual stiffness

C started with a BVID and considered failed at 95% residual stiffness

D started with a BVID and considered failed at 90% residual stiffness

These four results are plotted and a logarithmic fit has been applied to them. This has resulted in a S/N-curve which is shown in Figure 8.4.

In Section 7.2 the results are shown of a fatigue test on the skin when it is connected using the riveted joint. As the displacement remained constant during the test, the stress measurement can indicates stiffness variations of the samples. From the fatigue tests, the 95% residual stiffness was calculated. These results are also shown in Figure 8.4 and must be compared to the solid black line in this Figure.

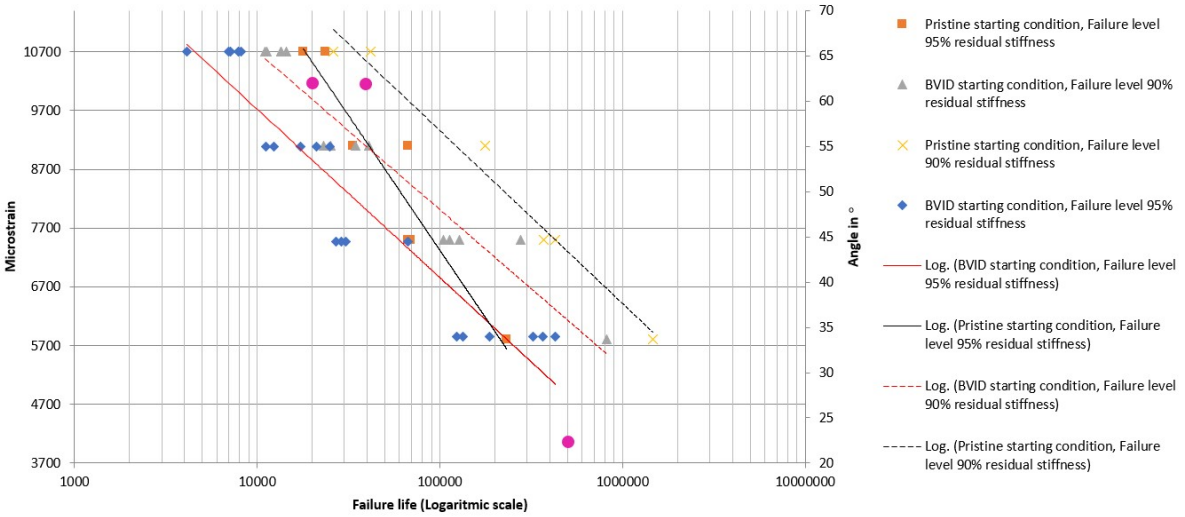

Figure 8.4: S/N curves for pure skin bending

8.2.1. Fatigue A 3x05 3

Sample 'A 3x05 3' was tested with an amplitude of 3500 micro-strain. The lowest amplitude of the four-point bend tests, shown in Figure 8.4, was 5500 micro-strain. To compare these tests, the solid black line in this figure must be considered. If this line is elongated, it would almost intersect the pink dot at the 22^o deflection angle which indicates the failure life of Sample 'A 3x05 3'. The solid line has a different trend compared to the other samples which indicates that the line might be a poor indication. But with all information currently available, the test performed on Sample 'A 3x05 3' matches the skin data. This skin data is assumed to meet the required fatigue life of 1,000,000 cycles for a deflection angle of 10^o in both directions [9].

8.2.2. Fatigue B 3x06 1 and C 4x05 1

Samples 'B 3x06 1' and 'C 4x05 1' experienced repeated strain levels of about 1% during the tests. This corresponds to the 10,000 micro-strain level on the graph and the 62^o deflection angle. The samples are able to withstand these situations for respectively 42,000 and 17,500 cycles. The graph of the skin test intersects with the 10,000 micro-strain level at a fatigue life of about 25,000 cycles. This once again is empirical evidence which cannot confirm the match to a high level of certainty. The fatigue tests performed are of the same order of magnitude compared to the skin. The skin has been shown to be able to carry the fatigue load. Therefore, the fatigue tests in this thesis might be sufficient.

9

Conclusion

The research question of this thesis is: *"What is the best method to connect a thin flexible skin element undergoing a peel-like motion to a rigid structure without disturbing the aerodynamic surface at the outside of the skin?"*. This research question was supported by several sub-questions. In this Chapter, these sub-questions are answered based on the results and discussion. This will subsequently create a basis on which the main research question can be answered.

The first sub-question was: *Are state-of-the-art joining methods available for peel dominated load situations?* To answer this question the literature study has been performed [10]. This has led to six categories of possible joining methods which have the potential to carry a peel dominated load situation as it is formulated in the research sub-question. These have been evaluated in a trade-off by nine criteria with sub-criteria. These criteria are the result of the second sub-question: *"What makes a connection a good fit for a peel dominated load situation?"* The result of this trade-off is that the most promising connection method for the Morphing Tab Concept is a Mechanical Fastener. Based on the sensitivity study it must be ascertained that Welding would also have been a good solution. But after a careful consideration, Mechanical Fastening was still selected as the joining method. It will specifically be Rivets which are used as mechanical fasteners due to their aerodynamic smoothness, one-sided placement and reliability.

Based on the outcome of the trade-off, a riveted connection is designed which is able to carry the loads. This is analysed by comparing the failure limits of the rivets to the load conditions. This resulted in a maximum pitch distance between the fasteners. Furthermore, design criteria were used in order to design other aspects of the connection such as edge distance. This design process yielded to a feasible design. To analyse this, a test had to be created.

The creation of the test resulted in an answer on the third sub-question: *"How will the joining method be evaluated?"* This question requires a segmented answer. In the literature study it was concluded that there are no standardised tests which form a representative loading condition. Therefore, a new test is created in Chapter 5. The test presented in this design is the answer to the third sub-question. Also, Chapter 6 must be considered for the answer as the measurements of the tests are discussed in that chapter. The essence of these chapters is that the connection is tested by applying a representative bending moment on the connection and measuring the stress and strain at the connection. The purpose of the tests is to show that the implementation of the joining method does not interfere with the functionality of the skin.

The results of these tests should be able to answer the last sub-question: *"Does the joining method meet all the requirements?* The answer of this sub-question is somewhat complex as multiple requirements are tested. To be as complete as possible with the answer, the results will be discussed in three separate conclusions of the test results. The combination of these three conclusions should be able to answer the sub-question.

The Aerodynamic Profile is only influenced to a limited extent by the presence of the fasteners. The strain measurements did not show uniform skin deflection but remained within the 1 mm contour limit at nominal load. This indicates that the skin bending is in not significantly effected negatively by the presence of the mechanical fasteners. The fasteners however do still interrupt the skin surface. But the amount of surface interruption is acceptable. It can therefore be concluded that the riveted connection meets the aerodynamic surface requirements.

The static strength analysis and the failure mode analysis have shown that the occurring failures are caused by skin bending. What can be concluded from the discussion in Section 8.1 is that the fasteners do not contribute to a lower failure level. A second conclusion is that the failure level is higher than the skin buckling limit, which means that the requirements under static loading conditions are met.

Similar to the static strength, the joint did not effect the performance of the skin significantly. This is the best result possible. The stiffness reduction as a consequence of the fatigue in the test samples has been measured to match the skin stiffness reduction. This means that the fasteners stiffness does not only degrade at the same rate as the skin, but it means that it does not contribute to the stiffness reduction in a significant manner. The sub-conclusion is therefore that also regarding the dynamic behaviour the requirements are met. One potential limitation of this area of research is the limited amount of dynamic tests.

As the tests were intended to examine the three mentioned requirements, the sub-question *"Does the joining method meet all the requirements?"* can be answered positively.

The overall conclusion can be made as all sub-questions are answered. From the Trade-off shown in Table 3.8, it can be seen that the 'mechanical fastener' had the best overall score. The mechanical fastener also outperformed or matched the score of other connections in four of the seven main categories. In the other and most important three categories it scored slightly lower than some other connections. Those three categories are: The Aerodynamics, the Static Strength and the Dynamic Strength. The tests have shown that the requirements for these aspects are met. Therefore, the trade-off conclusion is confirmed and it can be reasonably assumed that other joining methods would not result in a better performing joint for these loading conditions. By formulating the overall conclusion the main objective of the thesis is met and the main research question is answered. The overall conclusion of this thesis is: A riveted connection is the best method to connect a thin flexible skin element undergoing a peel-like motion to a rigid structure without disturbing the aerodynamic surface at the outside of the skin. The connection design created during in this thesis can be applied in further investigations in the Morphing Tab Concept.

10

Recommendations

In this chapter four recommendations are suggested based on the results and conclusions of this thesis. There are two main takeaways formulated in the conclusion. The first takeaway is the answer to the research question. The answer states that the riveted connection is the best method to connect a thin flexible skin element undergoing a peel-like motion to a rigid structure without disturbing the aerodynamic surface at the outside of the skin. This overall conclusion is based on the second takeaway, which concludes that the different analyses have proven that the functionality of the skin as a morphing skin component is not compromised by the use of the rivets as connection method.

As a component of the Morphing winglet tab, it is proven to a reasonable extend that the connection does not effect the skin functionality. The aerodynamic profile analysis, the static strength analysis and the dynamic strength analysis have all consistently shown no interference by the rivets. For other applications this may lack statistical depth. For instance, if the interest is only directed towards the fatigue behaviour of the connection, the amount of tests may be a problem. Three tests which are all performed with a different fatigue profile have been done. As they matched the fatigue behaviour of the skin alone, they have been accepted as evidence. It is however not sufficient to create an S/N-curve of this connection in this project. The research would potentially be more relevant for other projects if the statistical relevance is increased. It is therefore recommended for further research to increase the number of fatigue tests on the joint.

Another recommendation directed towards the Morphing Tab Concepts. The Skin and the Connection have been tested in a calculated load case. This load case combines the morphing loads and the aerodynamic loads. Within the Morphing Tab Concept development, a test has been created which applies these loads separately [7]. It would be interesting to confirm the structural abilities of the skin and the connection under a variety of loads using this test. Additionally, the connection and the skin can be tested in a higher development level. This means that the joint would be tested as part of a winglet tab (section) rather than separately. This can be done when the winglet tab as a whole or a segment of this tab is tested. Analysis resources should be attributed to the connection method during such tests in order to investigate effects which cannot be tested in smaller set-ups. Two such examples are twist and spanwise bending.

A third recommendation stems from the fact that it would be desirable to determine the precise origin of the bending failure within the skin. This might be found by investigating a few samples just before they fail. From a machine displacement level of 170 mm, cracking could be observed. From 200 mm displacement, a reduced Young's modulus was measured. If the test is stopped somewhere after these points, initial failure might be observable under the electron microscope. It would be recommended to do this as it would benefit the understanding of the failure. If the failure is understood well, it might be postponed even further or detection methods for this failure may be designed. Both these results would be desirable if the skin and connection would be implemented in aeroplanes.

The last recommendation has to do with the recovery of material properties. Thermoplastic materials

have the benefit that they can be heated and reshaped repeatedly. This might form the basis of material restoration in case of property degradation. During the test, property degradation has been observed in two different circumstances. The first is when static failure is about to occur. This effect is described in the paragraph above. The effect can probably be attributed to fibre fracture which cannot be fixed by restoring the matrix material. If the previous recommendation is executed and a different failure origin is found, the restoring of this material degradation should be revised. The second material degradation measured during the tests occurred during the fatigue testing. Repeated bending of the samples leads to a stiffness reduction. This may be caused by a form of matrix failure such as matrix cracking. If the matrix would be heated, the material properties may be restored. It would be recommended to investigate this. The Morphing Winglet Concept may be usable for applications demanding larger cycle counts, such as Gust Load Alleviation. Restoration of fatigue induced matrix degradation might help realise such applications.

A

Appendix

In this appendix, the motivations for grading a joining method with a certain score is explained. For each criterion, the scoring guidelines have been explained in Chapter 3. Tables 3.1 to 3.7 show reasons to appoint a score between one and five for seven overall criterion categories. These were: Aerodynamics, Static strength, Dynamic strength, Mass, Manufacturability, Maintainability and Cost. In the Trade-off, shown in Table 3.8, the motivation for each score is given in a code. These codes are references to this chapter where the motivations are further elaborated. These are ordered per joining method beginning with the Integral structure and following the Trade-off order.

A.1. Integral structure

I-A-1	Material completely integrated in rest of the design.
I-A-2	Connection does not interact with skin as such to shape the skin differently.
I-S-1	No stress concentration. Resistant against both load types.
I-S-2	Connection does not interact with skin with regards to stiffness.
I-D-1	No material disruption to cause effect.
I-D-2	No material disruption to cause effect.
I-D-3	Can handle both fatigue regiments, no indication to doubt handling of combined load.
I-W-1	No material added.
I-W-2	Requires the winglet and tab to be C/PPS as well. May induce added mass, however this will be limited as C/PPS is not extensively heavy.
I-Mn-1.1	Very complex manufacturing process. All parts must be constructed at ones and placed properly while they are still difficult to handle. One-off production is feasible.
I-Mn-1.2	This is a combined structure and skin, therefore the same logic applies for the structure as for the skin.
I-Mn-2.1	A very elaborate manufacturing system must be designed in order to make this possible for up-scaled production.
I-Mn-2.2	This is a combined structure and skin, therefore the same logic applies for the structure as for the skin.
I-Mi-1	The connection is not expected to require maintenance. If this is however the case, or the elements behind the skin do require maintenance, this connection denies all accessibility. Separating and restoring the skin requires a new joining technique.
I-Mi-2.1	The connection is not expected to require much maintenance. This is however not excluded as damage occurs during operations. If this is however the case, or the

elements behind the skin do require maintenance, this connection denies all accessibility. Access must be obtained via the back. Separating and restoring the skin requires a new joining technique.

I-Mi-2.2 The connection is not expected to require much maintenance. This is however not excluded as damage occurs during operations. If this is however the case, or the elements behind the skin do require maintenance, can only be replaced as a whole. Meaning, the entire part which is produced as one.

I-C-1 No material added. however the requirement for the structure to be of C/PPS adds material cost. This might be quite a large expense.

A.2. Bonded

B-A-1 Material interruption between structure and skin, flush and smooth.

B-A-2 Connection does not interact with skin as such to shape the skin differently.

B-S-1 Stress concentration at edge of adhesive (mainly under peel). Adhesives are not very good at handling these stress concentrations in out-of-plain loading.

B-S-2 Connection does not interact with skin with regards to stiffness.

B-D-1 Adhesive may experience some influence of fatigue, expected to handle this fatigue profile well.

B-D-2 Adhesive may experience some influence of fatigue, expected to handle this fatigue profile well.

B-D-3 No clear reason to expect worse fatigue handling due to combined loading.

B-W-1 Small added weight due to adhesive.

B-W-2 No change in structure.

B-Mn-1.1 Boding is a very simple procedure. Possible with one sided access.

B-Mn-1.2 No extra demands on structure.

B-Mn-2.1 Same explanation for large production as for test.

B-Mn-2.2 Same explanation for large production as for test.

B-Mi-1 The connection is not expected to require maintenance. If this is however the case, or the elements behind the skin do require maintenance, this connection denies all accessibility. Separating and restoring the skin will likely lead to damage.

B-Mi-2.1 The connection is not expected to require much maintenance. This is however not excluded as damage occurs during operations. If this is however the case, or the elements behind the skin do require maintenance, this connection denies all accessibility. Access must be obtained via the back. Separating and restoring the skin will likely lead to damage.

B-Mi-2.2 The connection is not expected to require much maintenance. This is however not excluded as damage occurs during operations. If this is however the case, or the elements behind the skin do require maintenance, can only be replaced as a whole. Meaning, the entire part which is produced as one.

B-C-1 Adhesives are not cheap but this is by no means an expensive solution with regards to material.

A.3. Welded

W-A-1 Material interruption between structure and skin, flush and smooth.

W-A-2 Connection does not interact with skin as such to shape the skin differently.

W-S-1 No stress concentration and no real connection. The material will be able to handle loads in both in- and out-of-plain direction.

W-S-2	Connection does not interact with skin with regards to stiffness.
W-D-1	No material disruption to cause effect.
W-D-2	No material disruption to cause effect.
W-D-3	Can handle both fatigue regiments, no indication to doubt handling of combined load.
W-W-1	No material added.
W-W-2	Requires the winglet and tab to be C/PPS as well. May induce added mass, however this will be limited as C/PPS is not extensively heavy.
W-Mn-1.1	Relatively easy systems available for welding with one sided access.
W-Mn-1.2	Must be a C/PPS structure. For small numbers this is not all to much of an obstacle.
W-Mn-2.1	Scale-up to large production is not complex
W-Mn-2.2	Demands C/PPS material to be used on structure. This may be a deviation from the original manufacturing plan and make manufacturing more complex.
W-Mi-1	The connection is not expected to require maintenance. If this is however the case, or the elements behind the skin do require maintenance, this connection denies all accessibility. Separating and restoring the skin will likely lead to damage.
W-Mi-2.1	The connection is not expected to require much maintenance. This is however not excluded as damage occurs during operations. If this is however the case, or the elements behind the skin do require maintenance, this connection denies all accessibility. Access must be obtained via the back. Separating and restoring the skin will likely lead to damage.
W-Mi-2.2	The connection is not expected to require much maintenance. This is however not excluded as damage occurs during operations. If this is however the case, or the elements behind the skin do require maintenance, can only be replaced as a whole. Meaning, the entire part which is produced as one.
W-C-1	No material added. however the requirement for the structure to be of C/PPS adds material cost. This might be quite a large expense.

A.4. Mechanical fasteners

R-A-1	Material interruption between structure and skin and by mechanical fasteners, flush and smooth.
R-A-2	Connection does not interact with skin as such to shape the skin differently.
R-S-1	Stress concentration due to uneven load distribution. Fasteners are very well able to carry both in- and out-of-plain loading.
R-S-2	Connection does not interact with skin with regards to stiffness.
R-D-1	Material around mechanical fastener may experience some influence of fatigue, expected to handle this fatigue profile well.
R-D-2	Material around mechanical fastener may experience some influence of fatigue, expected to handle this fatigue profile well.
R-D-3	No clear reason to expect worse fatigue handling due to combined loading.
R-W-1	Small added weight due to adhesive.
R-W-2	No change in structure.
R-Mn-1.1	Mechanical fastening is a very simple procedure. Possible with one sided access.
R-Mn-1.2	No extra demands on structure.
R-Mn-2.1	Same explanation for large production as for test.
R-Mn-2.2	Same explanation for large production as for test.

R-Mi-1 The connection is not expected to require much maintenance. This is however not excluded as damage occurs during operations. Maintenance is very easy. The mechanical fastener can be removed, potentially via drilling, and later be replaced by another fastener.

R-Mi-2.1 The connection is not expected to require much maintenance. This is however not excluded as damage occurs during operations. Maintenance is very easy. The mechanical fastener can be removed, potentially via drilling, and later be replaced by another fastener. This allows all access which can be desired.

R-Mi-2.2 The connection is not expected to require much maintenance. However, maintenance is very easy. The mechanical fastener can be removed, potentially via drilling, and later be replaced by another fastener.

R-C-1 Cost of mechanical fasteners is limited. No other material costs induced by the system.

A.5. Piano hinge

P-A-1 Material interruption between structure and skin and piano hinge connections, flush and smooth.

P-A-2 Piano hinge connection to surface can influence skin bending at that location.

P-S-1 Stress concentrations due to load path change into hinge. A hinge is able to carry the loads in both in- and out-of-plain direction.

P-S-2 Piano hinge connection to surface can influence stiffness leading to an increased actuation load.

P-D-1 Hinge itself is not expected to experience any problems as it designed for repeated deflection. Material surrounding the hinge may experience some influence of fatigue. The fatigue profile is expected not to form a problem.

P-D-2 Hinge itself is not expected to experience any problems as it designed for repeated deflection. Material surrounding the hinge may experience some influence of fatigue. The fatigue profile is expected not to form a problem.

P-D-3 No clear reason to expect worse fatigue handling due to combined loading.

P-W-1 Added mass of hinge expected between 10% and 40% of flexible skin mass.

P-W-2 Requires redesign of structure with less efficient load load path. Expected weight addition.

P-Mn-1.1 Connecting the skin and the structure via one long hing is cumbersome but certainly possible for small numbers.

P-Mn-1.2 Requires a design change of the structure which is somewhat more difficult to produce. Still very feasible though.

P-Mn-2.1 Rather labour intensive as explained for small numbers. Upscale is therefore not ideal.

P-Mn-2.2 Requires a design change of the structure which is somewhat more difficult to produce. Still very feasible though also for larger numbers.

P-Mi-1 This connection is expected to require just a bit more maintenance due to the movable part. However this will still be very limited. The system allows maintenance fairly easy as well. The flexible skin can be removed by a combination of the fastener removal and disassembly of the hinge. This might be some work but it is straight forward. This allows all access which can be desired.

P-Mi-2.1 This connection is expected to require just a bit more maintenance due to the movable part. However this will still be very limited. The system allows maintenance fairly easy as well. The flexible skin can be removed by a combination of the fastener removal

and disassembly of the hinge. This might be some work but it is straight forward. This allows all access which can be desired.

P-Mi-2.2 This connection is expected to require just a bit more maintenance due to the movable part. However this will still be very limited. The system allows maintenance fairly easy as well. The flexible skin can be removed by a combination of the fastener removal and disassembly of the hinge. This might be some work but it is straight forward. This allows for easy replacement

P-C-1 The hinge will not be very cheap in order to have one approved for aerospace. The material cost is not all to excessive though.

A.6. Flexible element

F-A-1 Material interruption between structure and skin and by flexible element connection, flush and smooth.

F-A-2 Flexible element connection to surface can influence skin bending at that location.

F-S-1 Stress concentrations due to load path change into flexible element. Might have difficulties to cope with high out-of-plain loads as it is designed for in-plain loads.

F-S-2 Flexible element connection to surface can influence stiffness leading to an increased actuation load.

F-D-1 The small flexible element may experience worse fatigue behaviour for larger stains at critical areas in the element. For small amplitudes the effect is expected to be well within limits.

F-D-2 The small flexible element may experience worse fatigue behaviour for larger stains at critical areas in the element. Larger amplitudes induce larger strains. Fatigue failure cannot be excluded for this fatigue regiment.

F-D-3 Combined loading will experience the same problems as the high amplitude fatigue regiment. No further problems expected due to the combined loading.

F-W-1 Added mass of multiple flexible element expected between 40% and 70% of flexible skin mass.

F-W-2 Requires redesign of structure with less efficient load load path. Expected weight addition.

F-Mn-1.1 The flexible elements are probably relatively hard to produce if high quality is required. Also there are quite some elements required to divide the load evenly along the tab. This combination makes it rather not ideal.

F-Mn-1.2 Requires a design change of the structure which is somewhat more difficult to produce. Still very feasible though.

F-Mn-2.1 Up-scaling an already labour intensive method is even worse. However, potential manufacture engineering might help increase the production rate and quality.

F-Mn-2.2 Requires a design change of the structure which is somewhat more difficult to produce. Still very feasible though also for larger numbers.

F-Mi-1 This connection is expected to require just a bit more maintenance due to the movable part. However this will still be very limited. The system allows maintenance fairly easy as well. The flexible skin can be removed by removing the flexible element from the structure. This will be fairly difficult and can only be performed with access from the rear.

F-Mi-2.1 This connection is expected to require just a bit more maintenance due to the movable part. However this will still be very limited. The system allows maintenance fairly easy as well. The flexible skin can be removed by removing the flexible element from the structure. This will be fairly difficult and can only be performed with access from the

	rear. Once the flexible element is removed, accessibility is good. However access via this side alone is not possible.
F-Mi-2.2	This connection is expected to require just a bit more maintenance due to the movable part. However this will still be very limited. The system allows maintenance fairly easy as well. The flexible skin can be removed by removing the flexible element from the structure. This will be fairly difficult and can only be performed with access from the rear. This allows for replaceability.
F-C-1	the cost will mainly be in the production of the samples. This is incorporated in the manufacturing criterion. The expense of the material for the flexible elements will be considerable but will not be excessive.

B

Appendix

This appendix supports the rivet pitch distance calculations shown in Chapter 4. Equations 4.1 to 4.6 have been written using variables which change for different rivets. In this appendix, these equations are calculated for the three potential fasteners. The relevant information for the calculations is shown in Table B.1. For more information on the fasteners, Figure 4.4 and Table 4.1 should be checked.

Table B.1: Dimensions and Buckling stress [1][35]

Rivet type	Thickness t mm	Diameter rivet d mm	Diameter head D mm	Ultimate load σ_{peak} MPa
EN6122C05	1.86	4.14	7.52	350
EN6122C06	1.86	5.03	8.81	350
EN6122C07	1.86	5.74	9.47	350

In Table B.2, the outcomes of Equations 4.1, 4.2 and 4.3 are shown. The first equation calculates the internal moment which is caused by the ultimate load condition which is discussed in Chapter 2. The second equation is used to calculate the out-of-plain load from the internal moment. Equation 4.3 calculates the in-plain load in the outer layer of the skin based on the internal moment. All results are shown per meter of the spanwise length.

Table B.2: Internal Moment and Loads on first fastener row corresponding to buckling stress

Rivet type	Internal bending moment M_i Nm/m	Out-of-plain load F_1 N/m	In-plain load in the outer layer F_{2_6} N/m
EN6122C05	201.8	48747	24261
EN6122C06	201.8	40122	24261
EN6122C07	201.8	35159	24261

Table B.2, shows the loads which are experienced by the joint per meter of the spanwise length. By checking what the individual load is which a fastener can carry, the amount of fasteners per meter can be calculated. To do so, five failure mechanisms have been defined: rivet failure in tension, rivet shear failure, hole bearing failure, pull through due to shear of the skin and pull through due to compression failure of the skin. The failure loads of the first two failure mechanisms are rivet properties and do not have to be calculated [1]. The failure loads for these two failure mechanisms are shown in Table B.4. The latter three failure mechanisms must be calculated. The calculations are shown in Equations 4.4, 4.6 and 4.5. To calculate these failure loads, the shear strength, compressive strength out-of-plain and bearing strength in-plain of the skin are required. These material properties are shown in Table B.3. The failure levels for hole bearing failure, pull through due to shear of the skin and pull through due to compression failure of the skin, are also shown in Table B.4.

Table B.3: Skin strength for different failure types

Rivet type	Shear strength τ_s MPa	Compressive strength out-of-plain σ_{s_c} MPa	Bearing strength in-plain σ_{s_b} MPa
All fasteners	111	41	511

Table B.4: Failure loads per fastener for five failure types

Rivet type	Rivet failure in tension F_t kN	Rivet shear failure level F_s kN	
EN6122C05	4761	8807	
EN6122C06	6673	13011	
EN6122C07	8851	17036	
Rivet type	Hole bearing failure level F_i N	Pull through, shear failure level F_o N	Pull through, compression failure level F_o N
EN6122C05	655	4877	5076
EN6122C06	796	5714	6738
EN6122C07	909	6142	7307

Failure levels of the rivet failure in tension, pull through due to shear of the skin and pull through due to compression failure of the skin are failure levels due to out-of-plain loads. Their failure loads should therefore be compared to the out-of-plain load shown in Table B.2. By dividing the out-of-plain load F_1 by the failure loads, the number of fasteners per meter are known to cope with the applied load per failure mechanism. The rivet shear and hole bearing failure modes must be compared to the in-plain load in the outer layer of the skin F_{2_6}. From the number of fasteners per meter, the pitch distance per failure mechanism can be calculated. These pitch distances are shown in Table 4.3.

C

Appendix

In this appendix, the strain measurements using Measurement Methods A, B, C and D are shown. The results of a representative sample are shown and discussed in Chapters 7 and 8. The results presented in this Chapter are an addition to that measurement. In Section C.9, the reasons for not incorporating the stress measurements and Measurement Method E in this appendix are discussed. Table C.1 shows all tests and measurements performed in the thesis. It supports the legends of Figures C.1 to C.8.

C.1. Strain Measurements of Sample A 3x05 2

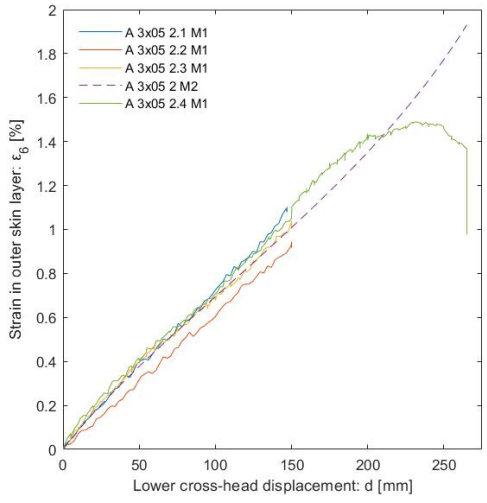

(a) Strain A 3x05 2 using Measurement Methods A and B

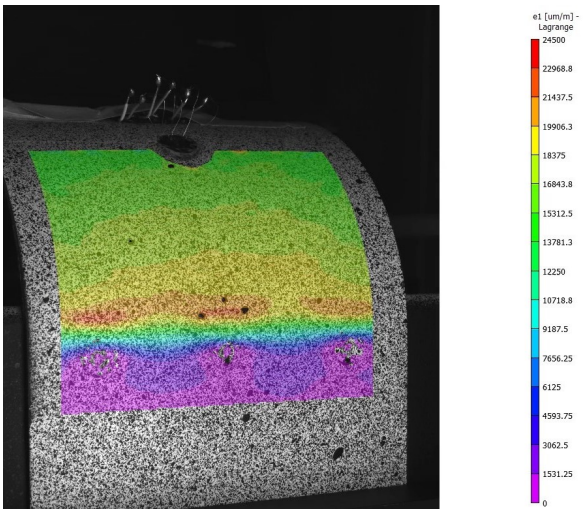

(b) Strain A 3x05 2 using Measurement Method C

Figure C.1: Strain measurements A 3x05 2

Table C.1: Test and Measurement details / Legend support for Figures C.1 to C.8

Legend code	Lay-out (Figure 5.1)	Sample	Test	Measurement Method	Section	Lines
A 3x05 2.1 M1	1	2	1	A: force and disp.	6.1	solid
A 3x05 2.2 M1	1	2	2	A: force and disp.	6.1	solid
A 3x05 2.3 M1	1	2	3	A: force and disp.	6.1	solid
A 3x05 2 M2	1	2	1,2,3,4	B: displacement	6.2	dashed
A 3x05 2.4 M1	1	2	4	A: force and disp.	6.1	solid
A 3x05 3 M2	1	3	1,2,3	B: displacement	6.2	dashed
A 3x05 3.1 M1	1	3	1	A: force and disp.	6.1	solid
A 3x05 3.2 M1	1	3	2	A: force and disp.	6.1	solid
A 3x05 3.2 M3	1	3	3	D: strain gauges	6.4	dotted
B 3x06 1 M2	2	1	1,2	B: displacement	6.2	dashed
B 3x06 1.1 M1	2	1	1	A: force and disp.	6.1	solid
B 3x06 1.2 M1	2	1	2	A: force and disp.	6.1	solid
B 3x06 2 M2	2	2	1,2,3	B: displacement	6.2	dashed
B 3x06 2.1 M1	2	2	1	A: force and disp.	6.1	solid
B 3x06 2.2 M1	2	2	2	A: force and disp.	6.1	solid
B 3x06 2.3 M1	2	2	3	A: force and disp.	6.1	solid
B 3x06 2.3 M3	2	2	3	D: strain gauges	6.4	dotted
B 3x06 3 M2	2	3	1	B: displacement	6.2	dashed
B 3x06 3 M1	2	3	1	A: force and disp.	6.1	solid
B 3x06 3 M3	2	3	1	D: strain gauges	6.4	dotted
C 4x05 1 M2	3	1	1,2,3	B: displacement	6.2	dashed
C 4x05 1.1 M1	3	1	1	A: force and disp.	6.1	solid
C 4x05 1.2 M1	3	1	2	A: force and disp.	6.1	solid
C 4x05 1.3 M1	3	1	3	A: force and disp.	6.1	solid
C 4x05 1.3 M3	3	1	3	D: strain gauges	6.4	dotted
C 4x05 2.1 M2	3	2	1	B: displacement	6.2	dashed
C 4x05 2.1 M1	3	2	1	A: force and disp.	6.1	solid
C 4x05 2.2 M2	3	2	2	B: displacement	6.2	dashed
C 4x05 2.2 M1	3	2	2	A: force and disp.	6.1	solid
C 4x05 2.2 M3	3	2	2	D: strain gauges	6.4	dotted
C 4x05 3.1 M2	3	3	1	B: displacement	6.2	dashed
C 4x05 3.1 M1	3	3	1	A: force and disp.	6.1	solid
C 4x05 3.2 M2	3	3	3	B: displacement	6.2	dashed
C 4x05 3.2 M1	3	3	3	A: force and disp.	6.1	solid
C 4x05 3.2 M3	3	3	2	D: strain gauges	6.4	dotted
C 4x05 3.2 M3	3	3	2	D: strain gauges	6.4	dotted
C 4x05 3.3 M3	3	3	3	D: strain gauges	6.4	dotted

C.2. Strain Measurements of Sample A 3x05 3

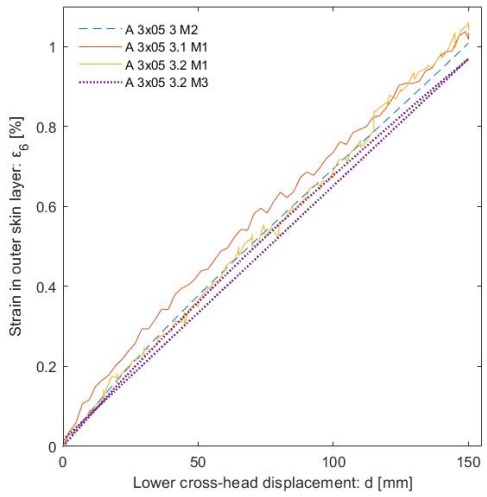

(a) Strain A 3x05 3 using Measurement Methods A, B and D

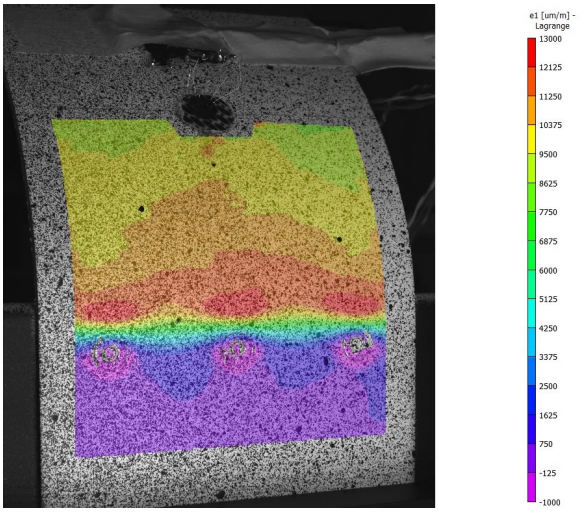

(b) Strain A 3x05 3 using Measurement Method C

Figure C.2: Strain measurements A 3x05 3

C.3. Strain Measurements of Sample B 3x06 1

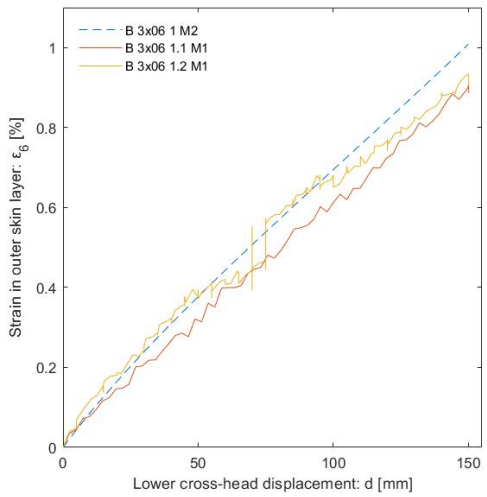

(a) Strain B 3x06 1 using Measurement Methods A and B

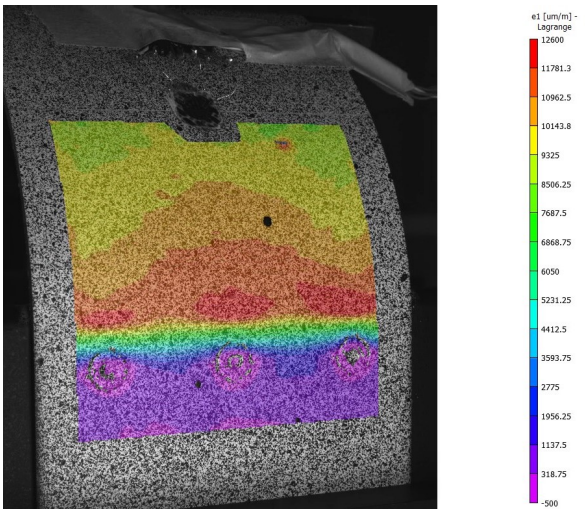

(b) Strain B 3x06 1 using Measurement Method C

Figure C.3: Strain measurements B 3x06 1

C.4. Strain Measurements of Sample B 3x06 2

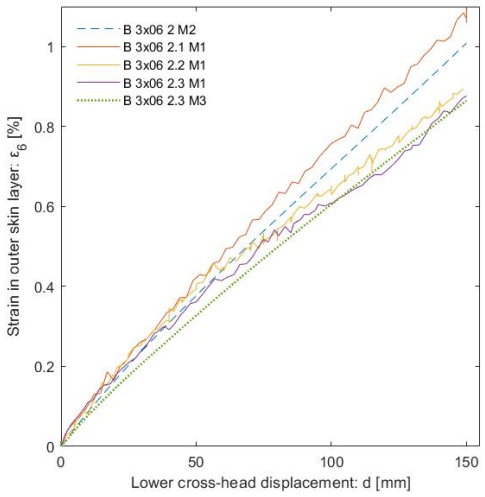

(a) Strain B 3x06 2 using Measurement Methods A, B and D

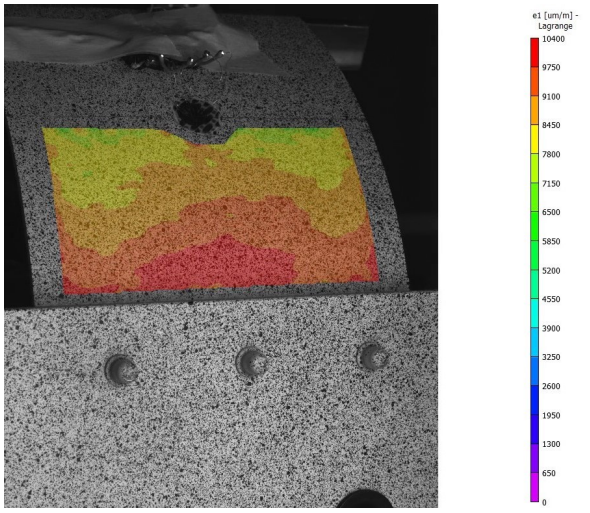

(b) Strain B 3x06 2 using Measurement Method C

Figure C.4: Strain measurements B 3x06 2

C.5. Strain Measurements of Sample B 3x06 3

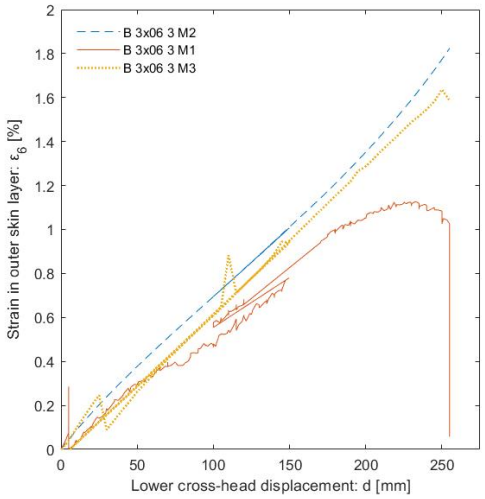

(a) Strain B 3x06 3 using Measurement Methods A, B and D

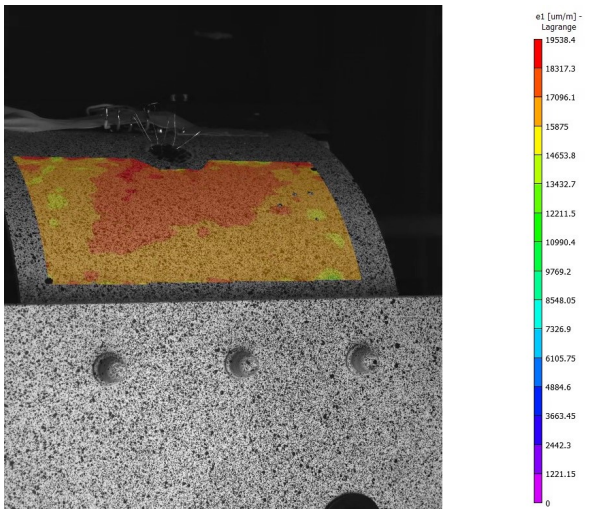

(b) Strain B 3x06 3 using Measurement Method C

Figure C.5: Strain measurements B 3x06 3

C.6. Strain Measurements of Sample C 4x05 1

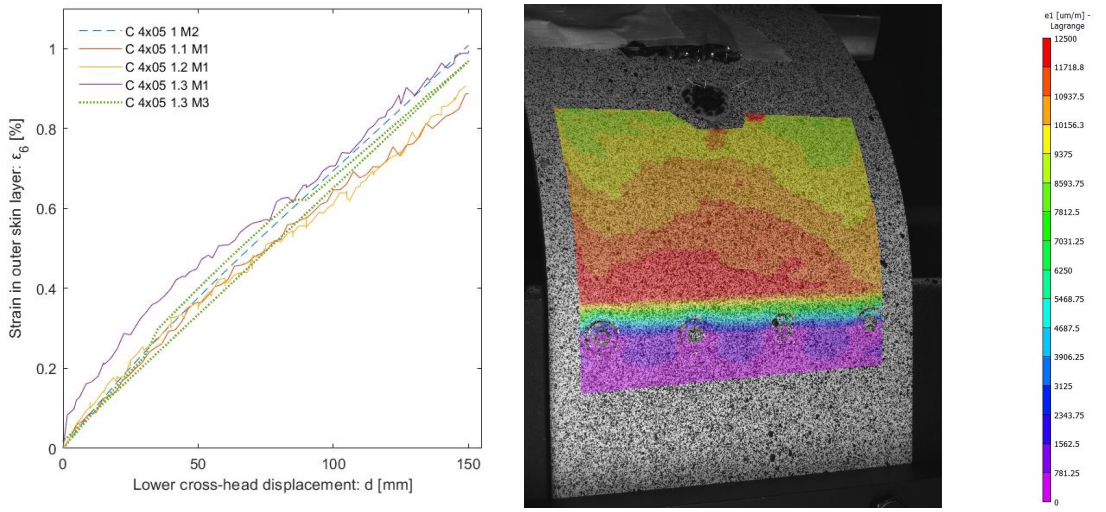

(a) Strain C 4x05 1 using Measurement Methods A, B and D (b) Strain C 4x05 1 using Measurement Method C

Figure C.6: Strain measurements C 4x05 1

C.7. Strain Measurements of Sample C 4x05 2

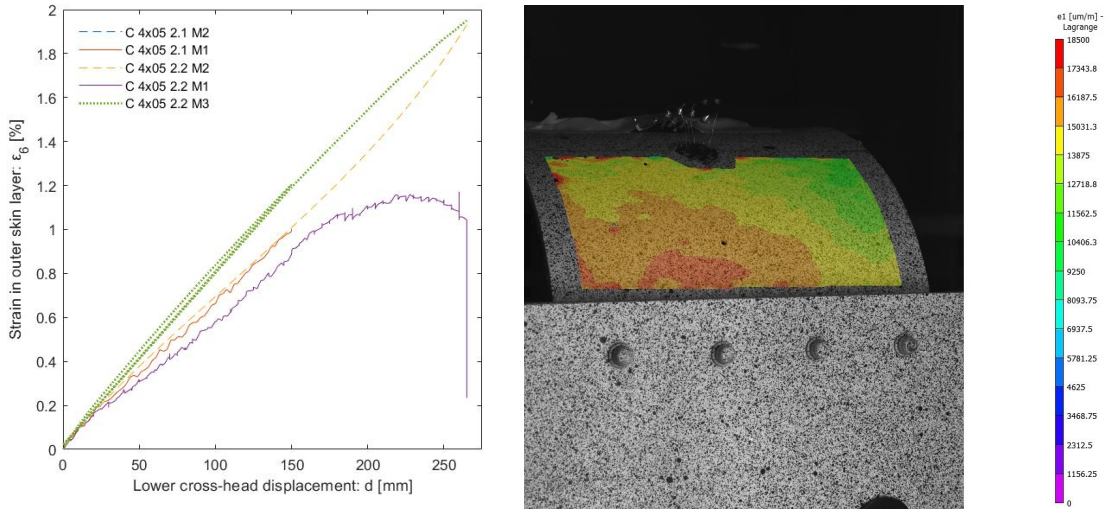

(a) Strain C 4x05 2 using Measurement Methods A, B and D (b) Strain C 4x05 2 using Measurement Method C

Figure C.7: Strain measurements C 4x05 2

C.8. Strain Measurements of Sample C 4x05 3

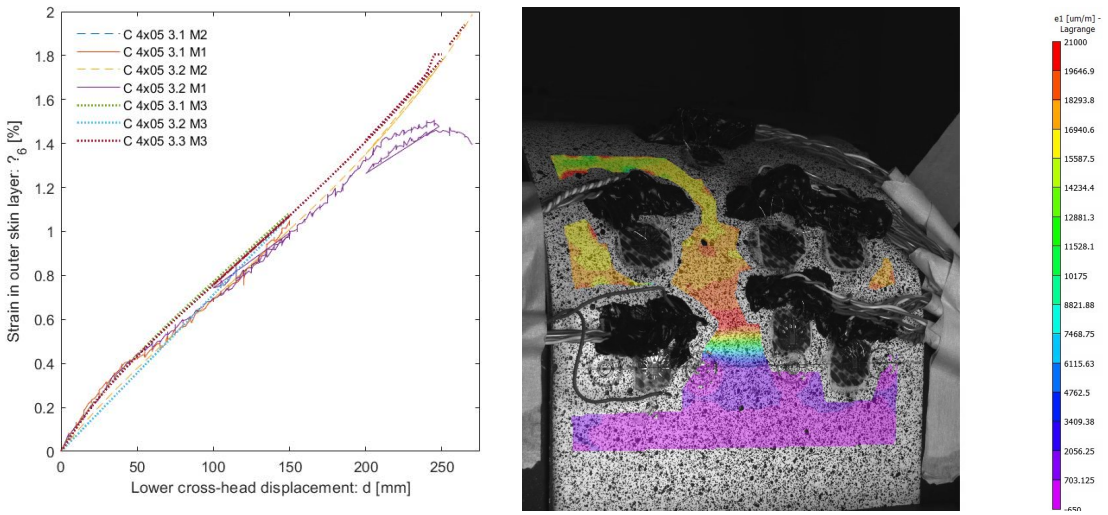

(a) Strain C 4x05 3 using Measurement Methods A, B and D

(b) Strain C 4x05 3 using Measurement Method C

Figure C.8: Strain measurements C 4x05 3

C.9. Stress and Measurement Method E

The stress measurements are not displayed separately as the they are based on the same measurements as the strain and therefore have the same trends. This has been explained in Chapter 7 and is further discussed in Chapter 8.

Also Measurement Method E is not shown for all the samples. There is a lot of video material which is used to verify different aspects such as contour, deflection angle and damage. These images without the data which they must verify do not contribute to the report.

Bibliography

[1] GKN Aerospace / Fokker aerostructures b.v. Gkn aerospace / fokker aerostructures b.v. handbook th & fon. Technical guidelines, GKN Aerospace / Fokker aerostructures b.v., 2021. Internal documentation.

[2] Silvestro Barbarino, Onur Bilgen, Rafic M. Ajaj, Michael I. Friswell, and Daniel J. Inman. A review of morphing aircraft. *Journal of Intelligent Material Systems and Structures*, 22(9):823–877, 2011. doi: 10.1177/1045389X11414084. URL https://journals-sagepub-com.tudelft.idm.oclc.org/doi/pdf/10.1177/1045389X11414084.

[3] Dennis L. Carter, Russell F. Osborn, Joel A.Hetrick, and Sridhar Kota. The quest for efficient transonic cruise. *AIAA Aviation Technology*, 7, 2007. ISSN 2007-7812. URL https://arc.aiaa.org/doi/pdfplus/10.2514/6.2007-7812.

[4] Toray Cetex. Toray cetex tc1100 pps. Product data sheet, Toray Cetex, 2020. URL https://www.toraytac.com/media/221a4fcf-6a4d-49f3-837f-9d85c3c34f74/smphpw/TAC/Documents/Data_sheets/Thermoplastic/.

[5] European Commission. Flightpath 2050 europe's vision for aviation. *Publications Office of the European Union*, 2011. doi: 10.2777/50266. URL https://ec.europa.eu/transport/sites/default/files/modes/air/doc/flightpath2050.pdf.

[6] Jesse Daniels, Paul W. Werner, and A. Terry Bahill. Quantitative methods for tradeoff analyses. *System Engineering*, 2001. doi: 10.1002/sys.1016. URL https://www.researchgate.net/publication/227500145_Quantitative_Methods_for_Tradeoff_Analysis.

[7] Mauryn G. de Graaf. Towards the application of morphing movables in a new winglet design. M.sc. thesis, University of Twente, 2021.

[8] Clive L. Dym and Irving H. Shames. *Solid Mechanics*. Springer, Dordrecht, 2013. ISBN 978-1-4614-6034-3. doi: 10.1007/978-1-4614-6034-3. Augmented edition.

[9] Adri Van Eemeren. Fatigue behaviour in thin composites kin under bending. Internship report, GKN Aerospace - Fokker Aerostructures B.V., 2020.

[10] Adri Van Eemeren. Literature study: What is the best method to connect a thin flexible skin element undergoing a peel-like motion to a rigid structure without disturbing the aerodynamic surface at the outside of the skin? Literature study, Delft University of Technology / GKN Aerospace - Fokker Aerostructures B.V., 2021.

[11] Raja A.R. Ghazilla, Zahari Taha, Sumiani Yusoff, Salwa H.A. Rashid, and Novita Sakundarini. Development of decision support system for fastener selection in product recovery oriented design. *The International Journal of Advanced Manufacturing Technology*, 70:1403–1413, 2014. doi: 10.1007/s00170-013-5373-3.

[12] Jonas Grünewald, Patricia Parlevliet, and Volker Altstädt. Manufacturing of thermoplastic composite sandwich structures: A review of literature. *Journal of Thermoplastic Composite Materials*, 30(4):437–464, 2015. doi: 10.1177/0892705715604681.

[13] Vega Handojo, Paul Lancelot, and Roeland De Breuker. Implementation of active and passive loads alleviation methods on a generic mid-range aircraft configuration. *AIAA Aviation Forum*, 2018. doi: 10.2514/6.2018-3573. URL https://arc.aiaa.org/doi/pdf/10.2514/6.2018-3573.

[14] J. Hofstede. Bolt, blind, 130° flush head, high strength, pulltype. Fastener sizing sheet and details FoN02-1225 – Issue 8, GKN Aerospace - Fokker Aerostructures B.V., 2009.

[15] Róbert Huňady, Martin Hagara, and František Trebuňa. The measurement of standing wave patterns by using high-speed digital image correlation. *American Journal of Mechanical Engineering*, 2(7), 2014. doi: 10.12691/ajme-2-7-15. URL http://pubs.sciepub.com/ajme/2/7/15/index.html#Figure1.

[16] T.G. Ivanco, R.C. Scott, M.H. Love, S. Zink, and T.A. Weisshaar. Novel folding methods for deterministic deployment of common space structures. *3rd AIAA Spacecraft Structures Conference*, 2016. doi: 10.2514/6.2016-2168.

[17] R.Hilbig J.Szodruch. Variable wing camber for transport aircraft. *Progress in Aerospace Sciences*, 25(3):297–328, 1988. ISSN 0376-0421. doi: 10.1016/0376. URL https://www.sciencedirect.com/science/article/pii/0376042188900036.

[18] Paul Lancelot. Manta – wp4 aerodynamic load analysis for the control surfaces ground demonstrators. Technical report, Clean Sky 2 (TUD), 2020. AIR-A-4.1.2.2-XX.

[19] LaVision. Digital image correlation (dic), 2021. URL https://www.lavision.de/en/techniques/dic-dvc/.

[20] J.E.J Maseland, J. Aalbers, H. Timmermans, M. Titze, O. Bertram, M. Schäfer, M. Medaikkar, H. van Goozen, R. Kapper, and M.N. Roelofs. Manta – synthesis on feasibility and impact of outer wing concepts. Technical report, Clean Sky 2 (NLR, DLR, FAE, TUD), 2019. AIR-A-4.1.2.2-1.

[21] Chris Megens. Kalibierschein, kraft nr.: 154810 - 04.02.2019. Calibration report, ZwickRoell GmbH & Co. KG, 2019.

[22] T.H.G Megson. *Aircraft structures for engineering students*. Butterworth Heinemann, Elsevier Science & Technology, Linacre House, Jordan Hill, Oxford OX2 8DP, UK, 1999. ISBN 978-0-75066-7395. 6th edition.

[23] Haibin Ning, Uday Vaidya, and George Husman. Design, manufacture and analysis of a thermoplastic composite frame structure for mass transit. *Composite Structures*, 80(1):105–116, 2007. doi: 10.1016/j.compstruct.2006.04.036.

[24] S. Andrew Ning and Ilan Kroo. Multidisciplinary considerations in the design of wings and wing tip devices. *Journal of Aircraft*, 47(2), 2010. doi: 10.2514/1.41833. URL https://arc.aiaa.org/doi/10.2514/1.41833.

[25] Kevin N. Otto and Erik K. Antonsson. Trade-off strategies in engineering design. *Research in Engineering Design*, 3(2):87–104, 1991. URL https://www.researchgate.net/publication/2852102_Trade-Off_Strategies_In_Engineering_Design/link/0046353156b4789b58000000/download.

[26] Daniël Peeters, Gearóid Clancy, Vincenzo Oliveri, Ronan O'Higgins, David Jones, and Paul M. Weaver. Concurrent design and manufacture of a thermoplastic composite stiffener. *Composite Structures*, 212:271–280, 2019. doi: 10.1016/j.compstruct.2006.04.036.

[27] Jaap Schijve. *Fatigue of Structures and Materials*. Springer Science+Business, Dordrecht, 2009. ISBN 978-1-4020-6807-2.

[28] M.J. Siclari, W. Van Nostrand, and F. Austin. The design of transonic airfoil sections for an adaptive wing concept using a stochastic optimization method. *34th AIAA Aerospace Sciences Meeting and Exhibit*, 1996.

[29] Stephen B. Smith and David W. Nelson. Determination of the aerodynamic characteristics of the mission adaptive wing. *Journal of Aircraft*, 27:950–958, 1990. doi: 10.2514/3.45965. URL https://arc-aiaa-org.tudelft.idm.oclc.org/doi/10.2514/3.45965.

[30] Vijay K. Stokes. Joining methods for plastics and plastic composites: An overview. *Polymer Engineering & Science*, 29(19), 1989. doi: 10.1002/pen.760291903. URL https://onlinelibrary-wiley-com.tudelft.idm.oclc.org/doi/abs/10.1002/pen.760291903?casa_token=U5yXZj2WuQgAAAAA:8JNZUgkShdbVVAwpjJURtgv_mmwK3vmGR9mv9Zp8Yf7tBnaiG-ltdEJiQbX8pjDwkAm-04CCoCyYBSmH.

[31] N.S. Taylor, S.B. Jones, and M. Weld. The feasibility of welding thermoplastic composite materials. *Construction and Building Materials*, 3(4):213–219, 1989. doi: 10.1016/0950-0618(89)90016-0. URL https://www-sciencedirect-com.tudelft.idm.oclc.org/science/article/pii/0950061889900160.

[32] S.V. Thornton. Reduction of structural loads using maneuver load control on the advanced fighter technology integration (afti)/f-111 mission adaptive wing. *NASA TM 4526*, 1993.

[33] Alexander Uithol. Keithley data acquisition. Manual, Delft University of Technology, 2020.

[34] G. Vaessen and J. Koning. Joints for solid rivets and blind rivets. Detailed design guidelines FE-0043 – Issue 2, GKN Aerospace - Fokker Aerostructures B.V., 2003.

[35] Wouter van der Eijk and Hans van Goozen. Manta – v3 requirements fse in relation to v-plan 3. Technical report, Clean Sky 2 (FAE), 2021. TYG03-WP4-REP-210113.

[36] Hans van Goozen. Manta – development plan for winglet with morphing tab. Technical report, Clean Sky 2 (FAE), 2019. AIR-3-FAE-DEL-0001.

[37] Hans van Goozen. Catia model. Technical report, GKN Aerospace - Fokker Aerostructures B.V., 2020.

[38] Ronald J. White. Improving the airplane efficiency by use of wing maneuver load alleviation. *Journal of Aircraft*, 8(10), 1971. doi: 10.2514/3.59169. URL https://arc.aiaa.org/doi/10.2514/3.59169.

[39] Dan Mihai Ştefănescu. Strain gauges and wheatstone bridges — basic instrumentation and new applications for electrical measurement of non-electrical quantities. In *Eighth International Multi-Conference on Systems, Signals Devices*, pages 1–5, 2011. doi: 10.1109/SSD.2011.5767428.